

**GAZIANTEP UNIVERSITY GRADUATE  
SCHOOL OF NATURAL & APPLIED SCIENCES**

**ANALYSIS OF FRACTURE MECHANICS  
VIA FINITE ELEMENTS  
AND ARTIFICIAL INTELLIGENCE**

**Ph.D THESIS  
IN  
MECHANICAL ENGINEERING**

**BY  
Nihat ATMACA  
JUNE 2007**

**Analysis of Fracture Mechanics via Finite Elements and  
Artificial Intelligence**

**PhD Thesis  
in  
Mechanical Engineering  
University of Gaziantep**

**Supervisor  
Prof. Dr. İBRAHİM H. GÜZELBEY**

**by  
Nihat ATMACA**

**June 2007**

T.C.  
GAZİANTEP UNIVERSITY  
GRADUATE SCHOOL OF  
NATURAL & APPLIED SCIENCES  
MECHANICAL ENGINEERING DEPARTMENT

Name of the thesis: Analysis of Fracture Mechanics via Finite Elements and Artificial Intelligence

Name of the student: Nihat ATMACA

Exam date:21.06.2007

Approval of the Graduate School of Natural and Applied Sciences

Prof. Dr. Sadettin ÖZYAZICI  
Director

I certify that this thesis satisfies all the requirements as a thesis for the degree of Doctor of Philosophy.

Prof. Dr. Sedat BAYSEÇ  
Head of Department

This is to certify that we have read this thesis and that in our opinion it is fully adequate, in scope and quality, as a thesis for the degree of Doctor of Philosophy.

Prof. Dr. İbrahim H. GÜZELBEY  
Supervisor

Examining Committee Members

signature

Prof. Dr. İ. Hüseyin FİLİZ

\_\_\_\_\_

Prof. Dr. Naki TÜTÜNCÜ

\_\_\_\_\_

Prof. Dr. Mustafa ÖZAKÇA

\_\_\_\_\_

Prof. Dr. İbrahim H. GÜZELBEY

\_\_\_\_\_

Assist. Prof. Dr. Bahattin KANBER

\_\_\_\_\_

## **ACKNOWLEDGEMENTS**

I express sincere appreciation to my supervisor Prof. Dr. İbrahim H. Güzelbey for his guidance and great help and to my family.

I would like to thank Dr. Abdülkadir Çevik, Dr. M. Akif Kütük, Dr. Bahattin Kanber and Dr. Ahmet Erklig for their support.

Finally, I wish to express my heartfelt gratitude to my beloved family. First of all, I owe everything to my parents, Kemal and Elif, who raised me to respect certain universal moral values. I also thank to my wife Gönül and my sons Kemal and Enes and my brothers Yusuf, Murat, and Adem and my sisters Aynur and Medine for all their love and support.

## ABSTRACT

### ANALYSIS OF FRACTURE MECHANICS VIA FINITE ELEMENTS AND ARTIFICIAL INTELLIGENCE

ATMACA, Nihat  
PhD in Mechanical Engineering  
Supervisor: Prof. Dr. İbrahim H. GÜZELBEY  
June 2007, 122 pages

In this thesis, a finite element analysis has been carried out for accurate calculation and evaluation of the Stress Intensity Factor (SIF) in Linear Elastic Fracture Mechanics (LEFM) and J-integral in elasto-plastic Fracture Mechanics (EPFM). The direct relations between the parameters and some guide lines for future works have been investigated. This study also presents the influence of mesh refinement on the SIF and J-integral values of Mixed Mode (Mode I and Mode II) loading. Furthermore, the prediction of crack path has been performed numerically using maximum circumferential stress criterion. Finally, explicit formulations have been obtained in the evaluation of SIF and J-integral parameters using Neural Networks (NN's) and Genetic Programming (GP).

**Keywords:** Stress Intensity Factor, J-integral, Crack Path Prediction, Displacement Extrapolation Method, Finite Element Method, Artificial Intelligence, Neural Networks and Genetic Programming.

## ÖZET

### SONLU ELEMANLAR VE YAPAY ZEKA İLE KIRILMA MEKANIĞI ANALİZİ

ATMACA, Nihat  
Doktora Tezi, Makine Mühendisliği  
Tez Yöneticisi: Prof. Dr. İbrahim H. GÜZELBEY  
Haziran 2007, 121 sayfa

Bu tezde, Lineer Elastik Kırılma Mekaniği (LEKM) problemleri için Gerilme Şiddet Faktörü (GŞF) ve Elasto-Plastik Kırılma Mekaniği (EPKM) problemleri için ise J-integral parametrelerinin doğru bir şekilde hesap edilebilmesi ve değerlendirilmesi için bir sonlu eleman analizi yapılmıştır. Bu parametreler arasındaki direk ilişkiler kullanılarak bir inceleme gerçekleştirilmiş ve ilerideki çalışmalar için bazı kılavuz bilgiler önerilmiştir. Bu çalışmada ayrıca karışık mod (Mod I ve Mod II) yüklemeleri altında ağ yoğunluk yapısının, GŞF ve J-integral değerleri üzerindeki etkileri gösterilmektedir. Ayrıca çatlak yayılımının tahmini, maksimum halka gerilme kriteri yardımı ile yapılmıştır. Son olarak, Sınır Ağları (SA) ve Genetik Programlama (GP) kullanılarak, GŞF ve J-integral parametrelerinin değerlendirilmesi için açık formüller elde edilmiştir.

**Anahtar Kelimeler:** Gerilme Şiddet Faktörü, J-integral, Çatlak Yolu Tahmini, Deplasman Ekstrapolasyon Yöntemi, Sonlu Eleman Yöntemi, Yapay Zeka, Sınır Ağları ve Genetik Programlama

## CONTENT

ACKNOWLEDGEMENT.....	iv
ABSTRACT.....	v
ÖZ.....	vi
LIST OF FIGURES.....	ix
LIST OF TABLES.....	xii
LIST OF SYMBOLS.....	xiii
CHAPTER 1 INTRODUCTION.....	1
1.1 Research Objectives and Tasks.....	2
1.2 Thesis Layout.....	3
CHAPTER 2 LITERATURE REVIEW.....	4
2.1 Introduction.....	4
2.2 Linear elastic fracture mechanics .....	4
2.2.1 Stress intensity factor.....	6
2.2.2 Energy release rate .....	8
2.3 Elasto-plastic fracture mechanics .....	9
2.3.1 J-Integral.....	11
2.3.2 Crack tip opening displacement.....	11
2.4 Crack initiation and propagation.....	12
2.5 Artificial Intelligence.....	13
2.6. Conclusions.....	15
CHAPTER 3 LINEAR ELASTIC FRACTURE MECHANICS.....	16
3.1 Introduction.....	16
3.2 Determination of SIF's.....	18
3.2.1 FEM for SIF calculations.....	19
3.2.1.1 Displacement Extrapolation Method .....	21
3.2.1.2 Stress Extrapolation Method.....	24
3.2.2 Artificial intelligence for SIF calculation.....	25
3.2.2.1 Neural networks.....	25
3.2.2.2 Genetic Programming .....	28
3.3 FEM for Crack Path Prediction.....	31
3.3.1 Fracture criteria for unstable crack growth.....	32
3.3.2 Maximum circumferential stress criteria.....	34
3.3.3 Maximum energy release rate criteria.....	35
3.3.4 Simulation of crack path prediction.....	36
CHAPTER 4 ELASTO-PLASTIC FRACTURE MECHANICS.....	41
4.1 Introduction.....	41
4.2 J- Integral.....	43
4.2.1 Path Independence of J-integral.....	44
4.3 Artificial intelligence for J-Integral calculation.....	46
4.3.1 Neural Networks .....	46
4.3.2 Genetic programming .....	47

CHAPTER 5 CASE STUDIES.....	48
5.1 Introduction.....	48
5.2 SIF calculations.....	48
5.2.1 Mode I loading geometric models.....	48
5.2.1.1 Center cracked model.....	49
5.2.1.2 Double edge cracked model.....	51
5.2.1.3 Single edge cracked model.....	54
5.2.2 Mixed mode loading geometric models.....	57
5.2.2.1 Single edge cracked model with mixed mode loading.....	57
5.2.2.2 Off- center cracked model.....	65
5.3 J-Integral calculations.....	68
5.3.1 Center cracked model.....	69
5.3.1.1 Influence of the shape of the paths with center crack example.....	69
5.3.2 Single edge cracked mode.....	72
5.3.2.1 Influence of the node numbers on paths with single edge crack example.....	73
5.3.3 Three point bending beam.....	76
5.3.4 Compact tension specimen.....	77
5.3.5. J-Integral path effect on the test calculations.....	78
5.4. SIF formulations using artificial intelligence techniques.....	79
5.4.1 Neural Networks formulation of SIF.....	82
5.4.2 Genetic Programming formulation of SIF.....	85
5.4.3 Conclusions for SIF with Neural Networks .....	86
5.4.4 Conclusions for SIF with Genetic programming .....	88
5.5. J-integral formulations using artificial intelligence techniques.....	89
5.5.1 Neural Networks formulation of J-integral.....	90
5.5.1.1 Parametric studies on J-integral calculations.....	92
5.5.2 Genetic Programming formulation of J-integral.....	94
5.5.3 Conclusions for J-integral with Neural Networks .....	95
5.5.4 Conclusions for J-integral with Genetic programming .....	96
5.5.5 General Conclusions.....	97
5.6. The crack path prediction.....	98
CHAPTER 6 CONCLUSIONS.....	101
RECOMMENDATIONS FOR FUTURE WORK.....	103
REFERENCES.....	104
APPENDIX.....	112
CURRICULUM VITAE.....	121



## LIST OF FIGURES

Fig 2.1 Modes of Fracture.....	4
Fig 3.1 Cylindrical-polar coordinates of a crack.....	20
Fig.3.2 A quadratic quadrilateral element with mid-side nodes shifted to the quarter-points nearest the crack tip.....	20
Fig. 3.3 Distribution of stresses in vicinity of crack tip.....	22
Fig 3.4 Basic elements of an artificial neuron.....	26
Fig 3.5 Backpropagation algorithm.....	27
Fig 3.6 Genetic Programming Flowchart.....	29
Fig 3.7 Expression tree (ET) .....	31
Fig. 3.8 2D crack under mixed-mode loading.....	33
Fig. 3.9 Crack path prediction flow-chart.....	36
Fig.3.10 The critical elements area and crack tip node.....	37
Fig.3.11 The parts of the critical elements area.....	37
Fig.3.12 The neighboring elements.....	38
Fig.3.13 The crack tip and quarter point nodes.....	39
Fig. 3.14 Intersection point on vertical boundary of the element.....	39
Fig. 3.15 Intersection point on horizontal boundary of the element.....	39
Fig 4.1 J-integral definition around a crack .....	43
Fig 4.2 Closed contours for proof of J-integral path independence.....	45
Fig.4.3 NN Model for J-integral calculation .....	46
Fig.5.1 Center cracked full geometry.....	49
Fig 5.2 Center cracked quarter geometry.....	50
Fig 5.3 Comparison of correction factors for the center cracked model.....	50
Fig 5.4 Center cracked model SIF analysis.....	51
Fig 5.5 Double edge cracked full geometry.....	52
Fig 5.6 Double edge cracked quarter geometry.....	52
Fig 5.7.Comparison of correction factors for the double edge cracked model.....	53
Fig 5.8 Double edge cracked model SIF analysis.....	54
Fig 5.9 Single edge cracked full geometry.....	55
Fig 5.10. Single edge cracked half geometry.....	55
Fig 5.11 Comparison of correction factors for the single edge cracked model.....	56
Fig 5.12 Single edge cracked model SIF analysis.....	57
Fig 5.13 Single edge cracked with mixed mode loading.....	58
Fig 5.14 Single edge cracked deformed FE mesh for $a=3.5$ , (1240 nodes & 499 elements).....	58
Fig 5.15 Crack-tip modeling for single edge cracked model.....	59
Fig 5.16 Percent difference of $K_{I1}$ values for single-edge cracked model as a function of $n=8, 12, 16$ and $20$ .....	60
Fig 5.17 Percent difference of $K_{I1}$ values for single-edge cracked model with the equation 5 as a function of $n= 12$ .....	61
Fig 5.18 Percent difference of $K_{II1}$ values for single-edge cracked model. with the Eq.8.6 as a function of $n =8, 12, 16$ and $20$ .....	61
Fig 5.19 Percent difference of $K_{II1}$ values for single-edge cracked model with the equation 8 as a function of $n =8, 12, 16$ and $20$ .....	62

Fig 5.20 Percent difference of $K_{II}$ values for single-edge cracked model with the Eq. 10 as a function of $n = 8, 12, 16$ and $20$ .....	62
Fig 5.21 Percent difference of $K_I$ values for single-edge cracked model as a function of Poisson's ratio and <i>plane stress</i> state ( $n = 8 \& 12$ elements around the crack tip).....	64
Fig 5.22 Percent difference of $K_{II}$ values for single-edge cracked model as a function of Poisson's ratio and <i>plane stress</i> state ( $n = 8 \& 12$ elements around the crack tip).....	64
Fig 5.23 Percent difference of $K_I$ values for single-edge cracked model as a function of Poisson's ratio and <i>plane strain</i> state ( $n = 8 \& 12$ elements around the crack tip).....	65
Fig 5.24 Percent difference of $K_{II}$ values for single-edge cracked model as a function of Poisson's ratio and <i>plane strain</i> state ( $n = 8 \& 12$ elements around the crack tip).....	65
Fig 5.25 Effect of stress state and poisson's ratio on numerical SIF values .....	66
Fig 5.26 Off-center crack model.....	67
Fig 5.27 Some FE mesh configurations of off-center crack geometry for $a=0.5$ .....	67
Fig 5.28 $K_I$ and $K_{II}$ values for off-center cracked model as a function of angle $\theta$ ( $0^\circ, 30^\circ, 60^\circ$ ).....	68
Fig 5.29 Circular paths for center crack example with $a/w = 0.5$ .....	70
Fig 5.30 Rectangular paths for center crack example with $a/w = 0.5$ .....	70
Fig 5.31 Triangular paths for center crack example with $a/w = 0.5$ .....	71
Fig 5.32 Number of nodes used in circular paths.....	73
Fig 5.33 Number of nodes used in rectangular paths.....	74
Fig 5.34 Number of nodes used in triangular paths .....	74
Fig 5.35 Percent error of J-Integral for circular path.....	75
Fig 5.36 Percent error of J-Integral for rectangular path .....	75
Fig 5.37 Percent error of J-Integral for triangular path .....	75
Fig 5.38 Three point bending beam full model.....	76
Fig 5.39 Three point bending beam half model.....	76
Fig 5.40. Compact tension specimen model .....	77
Fig 5.41 Compact tension specimen half model.....	78
Fig 5.42 Types of the crack geometries.....	79
Fig 5.43. Center cracked model geometry.....	80
Fig 5.44 Double edge cracked model geometry.....	81
Fig 5.45 Single cracked model geometry .....	81
Fig 5.46 Performance of NN results vs. FE results.....	83
Fig 5.47 NN Model for $K_I$ calculation.....	83
Fig 5.48 Center cracked model analysis.....	87
Fig 5.49 Double cracked model analysis.....	87
Fig 5.50 Single cracked model analysis.....	88
Fig 5.51 Performance of GP results vs. FE results .....	89
Fig 5.52 NN Model for J-integral calculation.....	90
Fig 5.53 Trend of J-integral vs $\sigma$ ( $a=10$ mm, $w=40$ mm) .....	93
Fig 5.54 Trend of J-integral vs $a$ ( $\sigma =25$ MPa, $w=40$ mm) .....	93
Fig 5.55 Trend of J-integral vs $w$ ( $\sigma =25$ MPa, $a=10$ mm) .....	94
Fig 5.56 Performance of GP results vs. FE results .....	97
Fig 5.57 Crack path predictions of center edge cracked model.....	98
Fig 5.58 Crack path predictions of single edge cracked model.....	99

Fig 5.59 Crack path predictions of single edge cracked with  
mixed mode loading model ..... 99  
Fig 5.60 Crack path predictions of off-center cracked model..... 100

## LIST OF TABLES

Table 5.1 Percent error of PATH 1 J-Integral values with different paths .....	71
Table 5.2 Percent error of PATH 2 J-Integral values with different paths.....	71
Table 5.3 Percent error of PATH 3 J-Integral values with different paths.....	71
Table 5.4 Percent error of PATH 4 J-Integral values with different paths.....	72
Table 5.5 Percent error of PATH 5 J-Integral values with different paths.....	72
Table 5.6 Compact tension specimen.....	78
Table 5.7 Three point bending specimen.....	78
Table 5.8 Statistical parameters of the NN used for $K_I$ .....	82
Table 5.9 Statistical parameters of the GP Model used for $K_I$ .....	85
Table 5.10 Statistical parameters of the GP Model used for J-integral.....	96

## LIST OF SYMBOLS

$E$	: Young's modulus
$E_t$	: Tangential modulus
$\mu$	: Shear modulus
$\nu$	: Poisson's ratio
$\kappa$	: Kolosov constant
$G$	: Elastic energy release rate
$G_c$	: Critical elastic energy release rate
$a$	: Crack length
$da$	: Crack increment
$K$	: Stress intensity factor
$K_c$	: Critical value of the stress intensity factor
$K_I$	: Stress intensity factor for Mode I
$K_{Ic}$	: Fracture toughness
$K_{II}$	: Stress intensity factor for Mode II
$K_{III}$	: Stress intensity factor for Mode III
$u, v$	: Displacement components
$x, y$	: Cartesian coordinates
$\zeta, \eta$	: Natural coordinates
$r, \theta$	: Cylindrical polar co-ordinates
$f(a/w)$	: Correction factor
$w$	: Plate width
$\sigma$	: Direct stress
$\sigma_{yld}$	: Yield stress
$P$	: Point load
$\delta$	: Crack opening displacement
$J$	: J-integral
$w$	: Strain energy density
$\Gamma$	: Closed contour followed counter-clockwise
$d\Gamma$	: Element of the arc along the path $\Gamma$
$T$	: Traction vector
$u$	: Displacement vector

## CHAPTER 1

### INTRODUCTION

Fracture mechanics (FM) is one of the important branches of mechanics. FM can be defined as a quantitative analysis for evaluating structural behavior in terms of applied stress, crack length, and geometry of machine component.

Design of machine elements requires the considerations of fracture due to environmental and working conditions and defects in materials. In many machine elements, failures of loaded structures have been frequently caused by growth of cracks or crack - like flaws in the structures or machines.

Those defects may be in microscopic or macroscopic level. From a practical point of view, many cracks may be considered as harmless. If a crack reaches a certain size and situated in a highly stress concentration region, it is regarded as a potential cause of fracture and failure. Therefore, engineers must understand and characterize cracks and their effects, and try to predict if and when they may become unsafe during the structures and machines operational service life (**Wu, 2004**).

The identification of the mode of the failure and the application of a suitable failure criterion are the most important step in designing machine components. In the mechanical failure, the fracture can be characterized as the formation of new surfaces in the material. The essential feature of this process is breaking of interatomic bonds in the solid. However, fracture may be considered as the rupture separation of the structural component into two or more pieces due to the propagation of cracks from a macroscopic level.

In the macroscopic approach to fracture, it is generally assumed that the material contains some flaws which may act as fracture nuclei and that the medium is a homogeneous continuum in the sense that the size of a dominant flaw is large in comparison with the characteristic microstructural dimension of the material. The

problem is, then, to study the influence of the applied loads, the flaw geometry and material behavior on the fracture process in the solid (**Erdogan, 2000**).

In summary, fracture mechanics deals with the effect of a crack or flaw in a structure. The effect of the shape of a crack, working conditions and applied loads are the main interest of fracture mechanics.

### **1.1 Research Objectives and Tasks**

The subject of this thesis is to solve fracture mechanics problems using Finite Element Method and Artificial Intelligence. For this purpose, an attempt has been made to develop a computer program for the two-dimensional fracture problems based on Finite Element Methods. The basic research tasks have been carried out through a number of phases, which are summarized as follows.

- i A comprehensive literature review on fracture mechanics has been carried out.
- ii Understanding previously developed FEM program by **Guzelbey (1992)** on the linear elastic, elastoplastic, finite strain and related programs. The program is capable of handling linear elastic and finite strain elasto-plastic analysis.
- iii Derivation of crack tip elements and related equations.
- iv Calculation of Stress Intensity Factor (SIF) and J-integral.
- v Application of Neural Network (NN) and Genetic Programming (GP) for the evaluation of SIF and J-integral parameters.
- vi Prediction of crack path for linear elastic fracture mechanics.

It is essential for every developed program to be validated using cases with known solutions or comparing the results obtained from the developed programs with those obtained by means of commercial packages such as ANSYS finite element package.

The derivation of the SIF and J-integral parameters has been carried out using the direct and indirect relations between the linear elastic and elasto-plastic fracture mechanics parameters with known extrapolation and energy approaches and new approaches using artificial intelligence techniques. A flexible algorithm has been designed for this purpose. This algorithm should be applicable to further studies such as fatigue and impact analysis.

## **1.2 Thesis Layout**

A general literature review for linear elastic and elasto-plastic fracture mechanics, crack initiation and propagation analyses, numerical techniques and artificial intelligence in fracture mechanics is summarized in chapter 2.

Fundamental principles of linear elastic fracture mechanics theory are presented and finite element and artificial intelligence methods for stress intensity factor calculations, criteria for crack path prediction are given in chapter 3.

Basic concepts of elasto-plastic fracture mechanics and its common parameters of crack tip opening displacement method and J-integral method, artificial intelligence applications regarding J-integral calculations are given in chapter 4.

Case studies of fracture mechanics are presented in chapter 5.

In chapter 6 final conclusions and recommendations for future works are summarized.



## CHAPTER 2 LITERATURE REVIEW

### 2.1 Introduction

Fracture mechanics is a field of solid mechanics that deals with the mechanical behavior of cracked bodies. Fracture occurs due to various loading types. Those loading types are expressed in three modes as seen in Fig. 2.1.

In **Mode I**, also named as **Opening Mode**, the crack surfaces move directly apart under a tensile stress perpendicular to the surfaces. In **Mode II (Sliding Mode)**, the crack surfaces move normal to the crack front and remain in the crack plane under a shearing stress parallel to the plane. The mode is analogous to an edge dislocation. The crack surfaces move parallel to the crack front and remain in the crack plane under a shearing stress perpendicular to this plane in **Mode III (Tearing Mode)**. It is analogous to a screw dislocation (**Broek, 1986**).

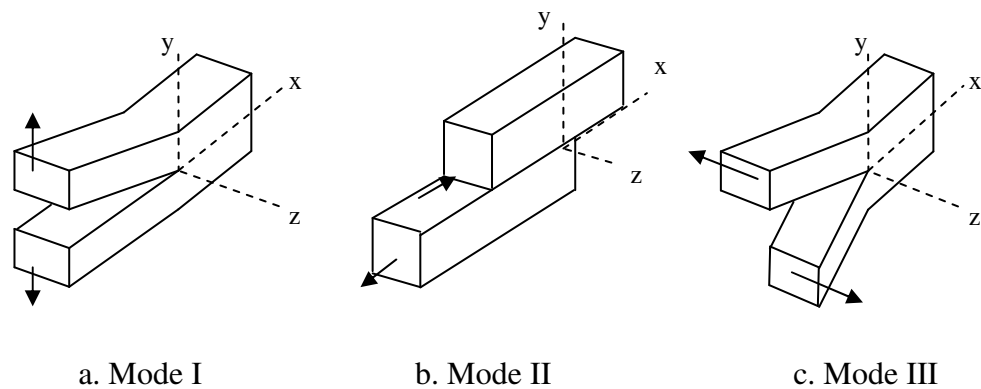


Fig. 2.1 Modes of fracture

### 2.2 Linear elastic fracture mechanics

The first approaches to fracture mechanics from a mathematical point of view had been started with the studies of **Inglis (1913)**, **Griffith (1921)** and **Westergaard (1939)**.

**Inglis (1913)** concentrated on the determination of the stress fields around an elliptical hole in a plate. Inglis claimed that his results are exact, and therefore it is applicable at the extreme limits of the elliptical form. **Griffith (1921)** assumed that growth of a crack requires creation of surface energy, which is supplied by the loss of strain energy accompanying the relaxation of local stresses as the crack advances. He developed a thermodynamic approach and proposed a theory assuming that there is a simple energy balance, consisting of a decrease in elastic strain energy within the stressed body as the crack extends, counteracted by the energy required to create new crack surfaces. This theory allows for the estimation of the theoretical strength of brittle solids and also gives the correct relationship between fracture strength and defect size. **Westergaard (1939)** used the complex variable technique to solve crack problems. A complex stress function, which satisfied the nominal requirement of compatibility, as demanded by the bi-harmonic governing equation, was used in order to determine displacements and stress levels in the immediate neighborhood of a crack in an infinite plate subjected to a remote bi-axial stress.

A design for materials containing flaws has been outlined (**Sih and McDonald, 1974**). LEFM was used on high strength-low toughness materials in-the analysis of a structure due to the influence of a crack under mixed mode loading, where the crack will grow in a curved fashion.

**Karami and Fenner (1986)** developed a multi-domain boundary integral equation method, employing an isoparametric quadratic representation of geometries and functions for the analysis of 2D LEFM problems. The multi-domain approach allows the two faces of a crack to be modeled in independent sub-regions of the body, thus avoiding singularity difficulties, and consequently making it possible to analyze crack closure problems with contact stresses over part of the cracked faces. The problems solved using the method, include slanted cracked plate under mixed-mode loading, and crack closure examples, also crack closure situations involving fully reversed bending of an edged cracked strip both with and without a superimposed tensile loading were analyzed.

**Banks-Sills (1991)** has shown the application of the finite element method to linear elastic fracture mechanics problems. **Pan (1997)** used single domain method for the

analysis of LEFM's in 2-D solids. Materials properties in the medium can be anisotropic as well as isotropic in Pan's study.

**Erdoğan (2000)**, gave a summary of the key engineering applications of fracture mechanics and its methods and presented some important contributions and areas of future research in his studies.

### **2.2.1 Stress intensity factor**

SIF is used in fracture mechanics to more accurately predict the stress state around a crack (crack tip) caused by a remote load or residual stresses. It has the symbol  $K$  which is a theoretical parameter applicable to a homogeneous elastic material. This parameter amplifies the magnitude of the applied stress that includes the geometrical parameter load types. The load types are categorized as Mode I, II or III given before in Fig.2.1. A crack can grow when the SIF reaches the fracture toughness of the material.

Fracture toughness is a material property used to evaluate the ability of a material to resist a fracture resulting from crack growth. Materials with low fracture toughness value will probably experience brittle fracture and materials with large fracture toughness value will apparently experience ductile fracture.

**Tracey (1971)** used the finite element method with inverse square root singularity elements to calculate the SIF's. He showed that by using the above elements neighborhood of the crack tip in two typical crack configurations, SIF's within 5% of the accepted values had been obtained.

**Cartwright and Rooke (1976)** developed a "compounding" method for determining SIF's at the tips of cracks in structures having complex geometrical configurations. This method is based on the systematic evaluation of the effects on one particular crack tip in the presence of other cracks, holes or other structural boundaries.

**Vainshtok (1980)** used a virtual crack variation technique based on curvilinear crack theory to calculate the SIF's for mixed mode crack problems and concluded that the results obtained from the method satisfactory with results obtained using the energy method.

**Rook and Hutchins (1984)** used an integral transform to calculate the SIF's for a crack at the edge of a hole, which was loaded on its perimeter by a localized radial or tangential force. The calculated SIF's can be used as numerical Green's functions to obtain Mode I and Mode II SIF's. It was concluded that this Green's function technique allowed simple summation methods to be employed and avoided costly computer computation time. The method has been used successfully for crack growth in components subject to fretting.

A predicted stiffness matrix was proposed which shortened CPU times by one third, and also raised the accuracy of the solutions. Analytic solutions to Mode III crack problems for elastic materials were investigated (**Hsu-I-Min, 1989**). Basic assumptions of infinitesimal deformations, homogeneous and isotropic material with linear-elastic and power-law hardening plastic constitutive relationship, and deformation plasticity are employed. Three crack problems are formulated and solved, namely, semi-infinite crack in an infinite strip, an edge crack in a semi-infinite body, and an edge crack in a semi-infinite strip.

**Richard and Kuna (1990)** presented an all-fracture mode specimen with which it is possible to conduct tests for pure Mode I, pure Mode II, pure Mode III as well as all possible combinations of all the modes of fracture as stated above. An FE analysis of this specimen was conducted where the stress intensity factors,  $K_I$ ,  $K_{II}$ , and  $K_{III}$  were determined. The results showed that  $K_{II}$  and  $K_{III}$  are coupled for in-plane shear and anti-plane shear loading. Fracture experiments under mixed-mode loading, using this new specimen, demonstrated the influence of the loading type on the orientation and on the structure of the fracture surface.

**Barsoum (1974) and Hensell and Shaw (1975)** are used quarter-point isoparametric elements to obtain a good representation of the crack-tip field. The  $r^{-1/2}$  linear-elastic singularity for stresses and strains is obtained by shifting a quarter to the crack tip the

midside nodes of all surrounding elements. The original quarter point element has been extended and refined in some ways (**Horvath, 1994**). He used higher order singular isoparametric elements for crack problems.

**Guinea et al. (2000)** evaluated Mode I SIF values using the displacement extrapolation technique. They showed the influences of element size, element shape and mesh arrangement on numerical Mode I SIF values.

**Gray et al. (2003)** presented a modification to the quarter-point crack tip element and employed this element in 2-D boundary integral fracture analysis. They showed that the modified quarter point crack tip element produced highly accurate SIF's.

**Xie et al. (2004)** proposed an exact and very simple method based on a new concept of crack surface widening energy release rate to determine SIF's for cracked structural rectangular thin-walled tubes.

### **2.2.2 Energy release rate**

The Griffith energy criterion for fracture states that crack growth can occur if the energy required to form an additional crack can be delivered by the system. This parameter can be defined also as the rate of energy absorbed by the growth of the crack.

**Zenner and Holman (1944)** concerned Griffith's concept to brittle fracture of metals. Later, **Irwin (1957)** showed that the energy approach is equivalent to the stress intensity approach, where fracture is seemed to have occurred when a critical stress distribution ahead of the crack tip is reached. Fracture may therefore be governed by a material property  $K_c$ , the critical stress intensity factor, or  $G_c$  the critical energy release rate. LEFM is based upon the equivalence of  $G$  and  $K$ , because the stress distribution around and close to the crack tip is always the same.

**Walsh and Pipes (1985)** used the FEM and other energy release rate principles to determine Mode I SIF values for selected crack configurations. The method relates

the change in strain energy resulting from crack growth, to the change in the stiffness matrix of the structure containing the crack.

**Banks-Sills and Sherman (1986)** made a comparison between three methods of calculating SIF's, i.e. displacement extrapolation, the J-integral and Griffiths energy calculations, and the stiffness derivative technique. It was observed that the stiffness derivative method yields the most accurate results, whereas displacement extrapolation was the easiest method to implement for special cases.

### **2.3 Elasto plastic fracture mechanics**

When the plastic zone of the crack tip becomes large and spreads through the whole cracked section then the fracture stress can not be determined by means of LEFM. If the plastic zone is large compared to the crack size the EPFM calculations has to be applied on crack tip stress calculations.

**Zienkiewicz et al. (1969)** prescribed a general elasto-plastic matrix formulation for the evaluation of incremental stress values for any surface with an associated flow rule. Computation of an "initial stress" was also given which, as it was claimed, gave convergence quicker than existing methods, and which allowed large load increments without violation of the yield criteria. Both Von Mises and Coulomb yield criteria were tested and stress distribution with strain and growth of the plastic regions shown.

An incremental plasticity finite element formulation for the analysis of a complete field problem including the plastic region near the crack tip was presented by **Tracey (1976)**. General applicability of the formulation was claimed and that it can be used for small scale yielding with material hardening. The distribution of the crack tip opening displacement (CTOD) at the crack tip was presented as a function of the elastic stress intensity factor and material properties.

An elasto-plastic finite element analysis of a centrally cracked plate was conducted by **Miller and Kfoury (1979)**. Comparison of features such as the crack tip zone,

plastic strain near the crack tip, CTOD, principal stresses in the crack tip region, and the J-Integral values, was made corresponding to different biaxial stress states.

**Aoki et al (1981)**, showed that the energy release rates associated with the translation, rotation, self-similar expansion and distortion of the fracture process region, are expressed by the newly introduced integrals J, L, M, and I. These integrals can be defined even if there exists plastic deformation, thermal strains, body forces or inertial forces.

An Experimental and numerical investigations of the relationships between fracture toughness parameters (CTOD, K, and J) was carried out by **Pilcer and Ohlson (1983)**. It was found that by using certain factors, taking account of strain hardening, the relations in the elastic range could be extended to the elasto-plastic range.

**Ahmad et al (1983)** presented a program of integrated experimental finite element analysis for understanding crack growth initiation, propagation, and arrest under initial combined-mode dynamic loading conditions. **Zien (1983)**, developed a finite element post processor to calculate an incremental plasticity-based J-integral for fracture mechanics evaluation.

**Atluri and Nishioka (1984)** considered the relevance of certain path independent integrals in the presence of cracks and inelastic solids. The constitutive material properties considered include: (i) finite and infinitesimal elasticity, (ii) rate-independent incremental flow theory of elasto-plasticity, and (iii) rate-sensitive behaviour including elasto-viscoplasticity and creep. In each case finite deformations are considered along with the effects of body forces, material acceleration, and arbitrary traction and displacement conditions on the crack face. Physical interpretation of each of the integrals, either in terms of crack tip energy release rates or simply energy-rate differences in the comparison of two cracked-bodies are considered.

The modeling of an elasto-plastic crack tip using Green's function formulation for 2D problems was carried out by **Cruse (1986)**. The work shows how even a crude model of the plastic strains can adequately represent the singular strain distribution.

### 2.3.1 J-Integral

Using a path independent line integral known as the J-integral which describes the fracture conditions in a component experiencing both elastic and plastic deformation has been developed by **Rice (1968)**. It is related to the energy available in the vicinity of a crack and Rice solved 2D crack problems in the presence of plastic deformation.

The J-Integral as the energy release rate during crack extension has been presented by **Sakata et al (1979)** where the usefulness of the J-integral in fracture mechanics problems and in particular in the presence of body forces, inertial effects, thermal strains and preloadings has been shown and evaluated using FEM.

A method for estimating the dynamic stress intensity factor by using the FEM and the path independent J-integral was developed by **Kishimoto et al (1982)**. The formula allowed for mixed mode analysis where the SIF's for pure and mixed modes were shown to agree well with published analytical results. This method was recommended because neither a refined crack tip mesh nor a special crack tip element was required. The J-integral method will be used in our optimum path calculations.

**Nguyen et al. (1990)** proposed a coupled displacement crack length rate analysis based on path integrals derived from the expression of the J-integral.

**Courtin et al. (2005)** showed the advantages of the J-integral approach for calculating the SIF's when using the commercial finite element software ABAQUS.

### 2.3.2 Crack tip opening displacement

The CTOD parameter can be considered as strain based estimation of fracture toughness. However it can be separated into elastic and plastic components. The elastic part of the CTOD can be derived from the SIF and the plastic component can be obtained by assuming the specimen rotates about a plastic hinge.



The CTOD approach was first introduced by **Wells (1962)**. The method proposes that crack extension can take place when the material at the crack tip has reached a permissible strain, and that the stresses and strains in the vicinity of a crack or defect are responsible of failure.

In practice, the stresses at the crack tip always exceed the yield strength of the material, resulting in a localized plastic region around the crack tip. Failure is the progression of this plastic region through the structure. Dugdale's strip yield model was utilized by **Burdekin and Stone (1966)**, to find an expression for the CTOD. This method provided an improved rationale for the method.

**Turner (1975)** concluded that either the CTOD ( $\delta$ ), or the J-integral method offers a reasonable one term description of the conditions at the tip of an elasto-plastic crack.

#### **2.4 Crack initiation and propagation**

Crack initiation and propagation are essential to fracture. The manner through which the crack propagates through the material gives great insight into the mode of fracture. The modes of fracture have been explained in introduction section and the related figure can be seen from Fig. 2.1.

Cracks usually initiate at some point of stress concentration. Examples of these common areas include scratches, fillets, threads, and dents. Crack propagation in a critical component or structure can determine whether failure fatal (catastrophic) or not (safe).

**Shanyi and Lee (1982)** presented an FE analysis of slow crack growth for a centre cracked plate subject to monotonically increasing load until the point of fast fracture is reached. The formulation is based on an incremental theory of plasticity with isotropic hardening. Numerical results were compared with experimental data, where good correlation was shown to exist.

**Broberg (1984)** determined the crack growth properties of the process region. The conclusion of this paper was that the upper limit for the propagation velocity of a healing region is the velocity of irrotational waves.

**Saouma and Zatz (1984)** determined the crack path and fatigue life using interactive computer graphics and the FEM in LEFM for a given problem. Automatic remeshing was also catered for.

An analytical model based on crack closure which can account for the influence of initial residual stresses on crack growth and vice-versa was presented (**Keyvanfar, 1985**).

A comparison of the effects of crack tip plasticity on crack growth retardation through residual stresses ahead of the crack tip and through crack closure were investigated (**Cruse and Raveendra, 1988**). A comparison of elasto-plastic crack-opening for long and short cracks in plane stress and plane strain was also investigated. Also a comparison of elasto-plastic crack-opening for long and short cracks in plane stress and plane strain was investigated.

Four kinds of cracked specimens of brittle material were tested under all possible combinations of modes I,II, and III (**Yishu, 1989**). From the measured experimental data an empirical criterion of mixed-mode crack propagation was suggested. The test results indicated that the higher the  $K_{Ic}$  value, the higher was the susceptibility to the coupling effect of  $K_I$  and  $K_{III}$ , therefore the more the fracture toughness can be increased.

**Richard et al. (2005)** presented theoretical crack prediction of the mixed mode loading conditions. The hypotheses and concepts described the superposition of Mode I and Mode II as well as the superposition of all three modes ( Mode I, II, III) for spatial loading conditions in the study.

## **2.5 Artificial Intelligence**

Artificial Intelligence (AI) is a combination of computer science, physiology and philosophy. This inter-discipliner science area is focusing on creating machines that

can mimic human thought, understand speech and engage on behaviours that humans consider intelligent. Artificial Neural Networks (ANN) and Genetic Algorithm (GA) are the most popular AI techniques used by lots of researchers.

The first step toward ANN came in 1943 when Warren McCulloch, a neurophysiologist, and a young mathematician, Walter Pitts, wrote a paper on how neurons might work. They modeled a simple neural network with electrical circuits.

**Hebb (1949)** proposed 'Hebb rule' which states that nets can learn from their experience in a training environment. 'Hebb rule' has always played a striking role in the field of ANN studies.

Throughout 1950s scientists implemented models called perceptrons based on the work of McCulloch and Pitts. **Rosenblatt (1958)** invented the *Perceptron* which has been a milestone in ANN studies.

**Widrow and Hoff (1960)** developed the models called ADALINE and MADALINE which was the first neural network to be applied to a real world problem. Then **Marvin and Seymour (1969)** published some intrinsic limitations of neural Networks which slowed down the implementations of ANN drastically.

The studies in the field ANN almost stopped for more than a decade until **Hopfield (1982)** invented The Hopfield network whose dynamics were guaranteed to converge. After this novel invention ANN studies have raised again.

**Rumelhart et al., (1986)** were invented *Backpropagation* which opened a new era in ANN applications.

Genetic algorithm (GA) is an optimization and search technique based on the principles of genetics and natural selection. A GA allows a population composed of many individuals to evolve under specified selection rules to a state that maximizes the "fitness" (i.e., minimizes the cost function).

GA method was developed by **Holland (1975)** and finally popularized by one of his students, David **Goldberg (1989)**, solved a difficult problem involving the control of gas-pipeline transmission for his dissertation (**Haupt and Haupt 2004**).

Genetic programming (GP) is an extension to Genetic Algorithms proposed by **Koza (1992)**. Koza defined GP as a domain-independent problem-solving approach in which computer programs were evolved to solve the problems based on the Darwinian principle of reproduction and survival of the fittest and analogs of naturally occurring genetic operations such as crossover and mutation.

The fitness of each individual in a genetic algorithm is the measure the individual has been adapted to the problem that is solved employing this individual. It means that fitness is the measure of optimality of the solution offered, as represented by an individual from the genetic algorithm. The basis of genetic algorithms is the selection of individuals in accordance with their fitness; thus, fitness is obviously a critical criterion for optimization (**Chambers, 2001**).

## **2.6 Conclusions**

It is clear from the literature review that a large amount of work has been carried out in the LEFM regime, mainly using finite element analysis. A variety of approaches and methods have developed to estimate or to find valid relations, which can describe or relate certain fracture mechanics parameters such as stress intensity factors, J-integrals, crack-opening displacements, and fracture toughness.

It is also clear that there is no general relation, criterion, or method which is valid for all regimes of fracture problems. This is so because of other factors, such as plasticity, yielding, loading conditions, crack configurations, and material behavior, influencing the fracture process.

A limited work has been done in the non-linear EPFM area. Additional 3-D non-linear analysis of fracture of structures is quite rare in the literature. Furthermore few studies are available on the application of NN and GP to fracture mechanics.

## CHAPTER 3

### LINEAR ELASTIC FRACTURE MECHANICS

#### 3.1 Introduction

The stress intensity factor  $K$  which describes the magnitude of the elastic crack tip stress field, can be used to correlate the crack growth and fracture behavior of materials, provided that the crack tip stress field remains predominantly elastic. This makes the SIF an extremely important parameter for the Linear Elastic Fracture Mechanics (LEFM) problems .

There are basically three modes of fracture state (Fig 2.1). The three modes are: Opening, sliding and tearing modes (Modes I, II and III). All stress systems in the vicinity of a crack tip may be derived from the three modes of loading. Most materials are more susceptible to fracture by normal tensile stresses than by shear stresses (**Guinea et al., 2000**).

There are generally two approaches in LEFM for the determination of SIF; energy balance approach and the stress intensity approach.

**Griffith (1921)** is the pioneer in **the energy balance approach**. He stated that the crack propagation would occur if the energy released upon crack growth was sufficient to provide all the energy that is required for crack growth. **Irwin (1957)** showed that the energy balance postulated by Griffith should exist between the stored strain energy and the surface energy plus the work done in plastic deformation. He further concluded that the energy required to form new crack surfaces was significantly less than the work done in plastic deformation for ductile materials. So he defined the parameter  $G$ , which is the total stored energy absorbed during cracking per unit increase in crack length and per unit thickness. This parameter was called “the energy release rate” or “crack driving force”.

The alternative approach is **the stress intensity approach**. The stress intensity approach depends on the SIF which is used in fracture mechanics to more accurately predict the stress state (stress intensity) around the tip of a crack. When this stress state becomes critical a small crack grows and the material fails. The load at which this failure occurs is referred to as the fracture strength. Some large cracks seen in the materials were the result of small cracks and internal residual stresses not known at the time.

**Irwin (1960)** showed that the stresses in the vicinity of a crack tip take the form:

$$K = c\sigma\sqrt{\pi a}f\left(\frac{a}{w}\right) \quad (3.1)$$

where  $K$  is a constant, which gives the magnitude of the elastic stress field, and is called the stress intensity factor. The  $c$  and  $f(a/w)$  are dimensionless parameters that depend on the geometries of the specimen and the crack. These parameters can be determined from numerical approximation or experimental methods. Similar expressions may be obtained for all modes of loading,  $K_I$ ,  $K_{II}$ , and  $K_{III}$ .

The parameter, which governs fracture, may then be expressed as a critical value of the stress intensity factor ie:  $K_c$ , instead of the critical energy release rate  $G_c$ . The relationship between  $K_c$  and  $G_c$  for tensile loading conditions is given by:

$$G_c = \frac{K_c^2}{E'} \quad (3.2)$$

Where

$$E' = E \quad \text{for plane stress} \quad (3.3)$$

$$E' = \frac{E}{1-\nu^2} \quad \text{for plane strain} \quad (3.4)$$

When the material is predominantly in plane strain and under maximum constraint, the value of  $K_c$  tends to a limiting constant value. This value is called the plane strain fracture toughness,  $K_{IC}$ , and may be considered a material property. If Mode I is

predominant and the other modes insignificant, and since  $K_{IC}$  is a material constant, the sign of  $\frac{dK_I}{da}$  determines the stability of fracture propagation.

### 3.2 Determination of SIF's

The behaviors of a crack can be determined by the stress field of the near crack-tip region and this quantified by the  $K$ . Thus an accurate knowledge of this fracture parameter can give useful data for future life of the component under investigation. There are mainly three types of methods for the determination of the SIF; analytical, numerical and experimental methods.

**The analytical methods** for the derivation of the SIF have been the bases for the development of fracture mechanics. They have delivered the basic equations for the crack tip stress and displacement fields, which still serve as the starting point for many other solutions. The knowledge that the stress and displacements fields for either fracture mode always take the same form offers the possibility to determine the SIF in an indirect way.

However, the analytical methods are the least interesting from an engineering point of view. In general, they try to satisfy the boundary conditions exactly. Usually this is possible only in the case of an infinite plate or solid. In the analytical solutions it is tried to find an Airy stress function to solve the problem under consideration.

Various **numerical methods** have been developed to derive SIF. These are finite difference, finite element and boundary element methods. An effective method among these is the FEM. The application of the finite element method to determine crack-tip stress fields has seen rapid progress. The method has great versatility: it allows the analysis of complicated engineering geometries (bolted and welded structures), it enables treatment of 3-D problems, and it permits the use of elastic-plastic elements to include crack tip plasticity. FE approximations are very promising for extensive use in engineering crack problems.

**Experimental determination** of the SIF is sometimes useful to obtain an approximate value. The SIF can not be measured directly in an experiment, but it can be found through the relations between  $K$  and a measurable quantity, such as strain, compliance, and displacement. Some methods are applicable only in laboratory experiments, but a few may have a limited use under service conditions, provided the load on the structure can be measured also. This would enable an appreciation of the danger involved in an unexpected service crack, pending a more elaborate analysis. A typical laboratory technique is the use of photoelasticity. Three dimensional problems can be investigated by employing the frozen-stress technique. In principle, any technique that can measure stresses or displacements can be applied for an experimental determination of the SIF. One of these techniques can be applied using the electrical resistance strain gauges (**Broek, 1986**).

### 3.2.1 FEM for SIF calculations

Numerical methods are extremely powerful tools for engineering analyses. With the advent of computers, there has been a tremendous explosion in the development and use of numerical methods. Of these, the FEM and its variants are the most commonly used methods in the analysis of practical engineering problems. The technique is based on the discretisation of an assembly into structural elements interconnected at a finite number of nodes. Forces can only be transmitted via these nodal points which are displaced appropriately. The nodal displacements for each element are evaluated and the resulting solutions are assembled into a matrix. Stress-strain relationships together with the minimum energy theorem are then applied which will reveal expressions relating forces, displacements and stiffness (**Reddy, 2004**).

In the FE models, the crack region must be modeled with very fine meshes in order to obtain accurate stress values near crack tip. This can also be done considering special crack tip elements at crack tip. Although a number of special types of elements have been developed for use at the tips of cracks, one of the simplest approaches for linear elastic problems involves modifications to the isoparametric elements in the neighbourhood of the crack. The purpose of these modifications is to impose the  $r^{-1/2}$  stress and strain singularity which is known to exist near the tip of a



crack in an elastic material where  $r$  and  $\theta$  are cylindrical polar co-ordinates of a point with respect to the crack (Fig. 3.1).

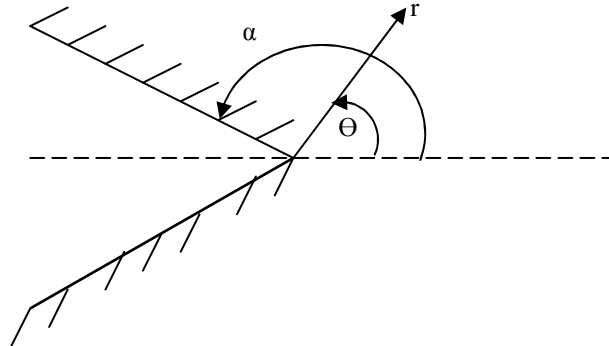


Fig. 3.1 Cylindrical-polar coordinates of a crack (Fenner, 1986).

The method of modification is only applicable to isoparametric elements employing polynomial shape functions of quadratic or higher degree. The mid-side nodes must be displaced to a point at a quarter of the element length from the node at which the singularity is to occur after this modification method. In other words, node shifting must be applied all elements which meet at the crack tip which is shown in Fig. 3.2.

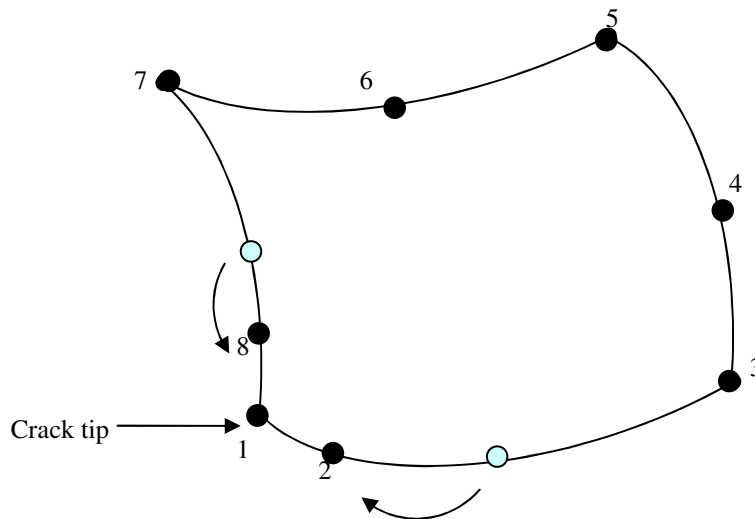


Fig. 3.2 A quadratic quadrilateral element with mid-side nodes shifted to the quarter-points nearest the crack tip (Fenner, 1986)

The techniques for determining SIF using extrapolation methods the displacement and stress extrapolation methods are widely used in literature after application of crack tip element. In these techniques, values of displacements and stresses very close to the crack tip must be known. After determining the required stresses and displacements, the extrapolation techniques can be used to determine accurate SIF values.

### 3.2.1.1 Displacement extrapolation method

The DEM is based on the nodal displacements around the crack tip. To obtain a good representation of the crack-tip field, quarter-point isoparametric elements are used as suggested by **Barsoum (1974) and Hensell and Shaw (1975)**. The  $r^{-1/2}$  linear-elastic singularity for stresses and strains is obtained by shifting a quarter to the crack tip the midside nodes of all surrounding elements.

The stress distributions (Fig. 3.3) near the crack tip can be written in terms of the two stress intensity factors (**Fenner, 1986**) as

$$\sigma_{rr} = \frac{K_I}{\sqrt{2\pi r}} \cos\left(\frac{\theta}{2}\right) \left(\frac{3}{2} - \frac{1}{2} \cos \theta\right) + \frac{K_{II}}{\sqrt{2\pi r}} \sin\left(\frac{\theta}{2}\right) \left(\frac{3}{2} \cos \theta - \frac{1}{2}\right) \quad (3.5)$$

$$\sigma_{\theta\theta} = \frac{K_I}{\sqrt{2\pi r}} \cos\left(\frac{\theta}{2}\right) \left(\frac{1}{2} + \frac{1}{2} \cos \theta\right) - \frac{K_{II}}{\sqrt{2\pi r}} \sin\left(\frac{\theta}{2}\right) \left(\frac{3}{2} + \frac{3}{2} \cos \theta\right) \quad (3.6)$$

$$\sigma_{r\theta} = \frac{K_I}{\sqrt{2\pi r}} \cos\left(\frac{\theta}{2}\right) \left(\frac{1}{2} \sin \theta\right) + \frac{K_{II}}{\sqrt{2\pi r}} \cos\left(\frac{\theta}{2}\right) \left(\frac{3}{2} \cos \theta - \frac{1}{2}\right) \quad (3.7)$$

Where  $K_I$  and  $K_{II}$  are SIF's and  $\theta$  is the angle between x-axis and radial line.

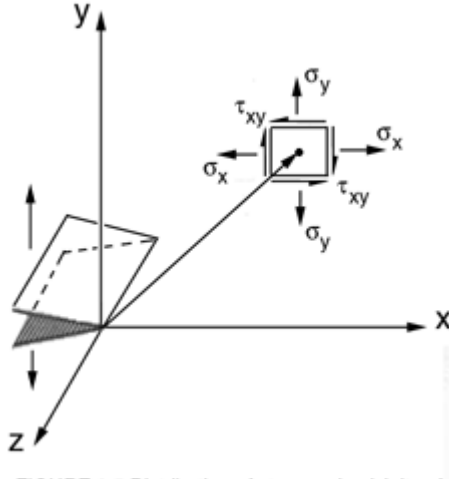


Fig. 3.3 Distribution of stresses in vicinity of crack tip (Hertzberg, 1996).

If the constitutive and compatibility equations are applied to Eqs. (3.5), (3.6) and (3.7), the strains and displacement distribution can be obtained. In these equations  $\theta$  depends on geometry,  $K_I$  and  $K_{II}$  depend on the loading condition and  $r$  is a small distance. The stress intensity factor for Mode I, II and mixture mode can be obtained by stress and displacement extrapolation when the distance  $r$  approaches zero.

However, the asymptotic expression of the displacement normal to the crack plane has been calculated for a bi-dimensional crack, under Mode I loading :

$$v = K_I \frac{1+\nu}{4E} \sqrt{\frac{2r}{\pi}} \left\{ (2\kappa+1) \sin \frac{\theta}{2} - \sin \frac{3\theta}{2} \right\} + \frac{A_1(1+\nu)r}{E} (\kappa-3) \sin \theta + \frac{A_2(1+\nu)r^{3/2}}{E} \left\{ \frac{(2\kappa-1)}{3} \sin \frac{3\theta}{2} - \sin \frac{\theta}{2} \right\} + \dots \quad (3.8)$$

The displacement  $v$  normal to the crack plane is also given by Guinea et al (2000), Fenner (1986), Dechaumpai et al (2003) and Gray et al. (2003). In this formulation, parameters are;  $E$ , the modulus of elasticity,  $\nu$ , the Poisson's ratio,  $\kappa$ , an elastic parameter which is equivalent to  $3-4\nu$  for plane strain and  $(3-4\nu)/(1+\nu)$  for plane stress.  $A_i$  is the parameters on the geometry and load on the specimen, and  $r$  and  $\theta$  are the polar coordinates, defined before in Fig 3.1. The normal displacement at crack tip,  $v(r=0)$ , is seen to be zero as prescribed by the symmetry of Mode I.

When the displacement  $v$  is evaluated along the crack faces ( $\theta = \pm\pi$ ), Eq. (3.8) only contains terms in  $r^{1/2}$ ,  $r^{3/2}$ ,  $r^{5/2}$  etc. making the extrapolation with using Eq. (3.8) and ignoring higher order terms a set of approximate equation has been obtained by **Guinea et al. (2000)** for Mode I loading. The approximate equations:

$$K_I = \frac{E'}{12} \sqrt{\frac{2\pi}{1}} (8v_A - v_B) \quad (3.9)$$

$$K_I = \frac{E'}{2} \sqrt{\frac{2\pi}{1}} v_A \quad (3.10)$$

$$K_I = \frac{E'}{4} \sqrt{\frac{2\pi}{1}} (4v_A - v_C) \quad (3.11)$$

where  $E'$  is the effective elastic modulus defined as equal to  $E$  for plane stress and  $E/(1 - \nu^2)$  for plane strain.

Eqs. (3.9), (3.10) and (3.11) are based on the series expansion of displacements along the crack faces. Eq. (3.9) is a second order approximation with  $r^{1/2}$  and  $r^{3/2}$  terms while Eq. (3.10) is a first order with  $r^{1/2}$  term. The 4<sup>th</sup> equation is produced by matching the term  $r^{1/2}$  with corresponding term of the element interpolation function of Eq. (3.8).

Eqs. (3.9), (3.10) and (3.11) are estimations of  $K_I$  with the nodal displacements of the quarter point elements located on the upper face of the crack. Due to symmetry, similar results would be obtained for the lower face of the element. Now SIFs may be determined for a full model for Mode I and Mode II for Eq.(3.9) (**Dechaumpai et al, 2003**):

$$K_I = \frac{E}{3(1+\nu)(1+\kappa)} \sqrt{\frac{2\pi}{1}} \left( 4(v_A - v_C) - \frac{(v_B - v_D)}{2} \right) \quad (3.12)$$

$$K_{II} = \frac{E}{3(1+\nu)(1+\kappa)} \sqrt{\frac{2\pi}{1}} \left( 4(u_A - u_C) - \frac{(u_B - u_D)}{2} \right) \quad (3.13)$$

If the similar approach is applied to the Eqs. (3.10) and (3.11), a new set of equations is obtained as follows:

$$K_I = \frac{E}{(1+\nu)(1+\kappa)} \sqrt{\frac{2\pi}{l}} (v_A - v_C) \quad (3.14)$$

$$K_{II} = \frac{E}{(1+\nu)(1+\kappa)} \sqrt{\frac{2\pi}{l}} (u_A - u_C) \quad (3.15)$$

$$K_I = \frac{E}{2(1+\nu)(1+\kappa)} \sqrt{\frac{2\pi}{l}} (4(v_A - v_C) - (v_B - v_D)) \quad (3.16)$$

$$K_{II} = \frac{E}{2(1+\nu)(1+\kappa)} \sqrt{\frac{2\pi}{l}} (4(u_A - u_C) - (u_B - u_D)) \quad (3.17)$$

For full model applications, Eqs. (3.14 - 3.15) and Eqs. (3.16-3.17) have been used in place of Eq. (3.12) and Eq. (3.13) respectively. In those equations,  $u$  and  $v$  are the displacement components in the  $x$  and  $y$  directions and their subscripts indicate the position of the nodes.

Eqs. (3.12-3.17) are the different estimates of  $K_I$  and  $K_{II}$ . The performance of the  $K_I$  and  $K_{II}$  estimations has been done using some numerical analysis.

### 3.2.1.2 Stress extrapolation method

It is basically the same procedure as the displacement approach except the stress expressions are correlated with the stresses from the finite element analysis. Thus, the stress intensity factor can be obtained as:

$$K_I = \frac{\sqrt{2\pi r}}{f_{ij}(\theta)} \sigma_{ij}^* \quad (3.18)$$

where  $\sigma_{ij}^*$  are the stresses of a node with coordinates  $r$  and  $\theta$  given before in Fig. 3.1.

### 3.2.2 Artificial Intelligence for SIF calculations

In recent years, AI methods have been widely used in engineering problems. However the calculation of SIF parameters of fracture mechanic problems with AI methods has not been used so common. The future life estimation of a component or structure under investigation mostly depends on the accurate knowledge of SIF. Although there are numerous analytical formulations in literature for the prediction of SIF parameter for common geometries, no unified analytical expression being valid for varying geometries has been proposed in literature so far.

#### 3.2.2.1 Neural Networks

A neural network (NN's) can be defined as a massively parallel distributed processor that has a natural propensity for storing experimental knowledge and making it available for use (**Haykin, 2000**).

The basic element of a neural network is the artificial neuron as shown in Fig. 3.4 which consists of three main components namely as weights, bias, and an activation function. Each neuron receives inputs  $x_1, x_2, \dots, x_n$ , attached with a weight  $w_i$  which shows the connection strength for that input for each connection. Each input is then multiplied by the corresponding weight of the neuron connection. A bias  $b_i$  can be defined as a type of connection weight with a constant nonzero value added to the summation of inputs and corresponding weights  $u$ , given in Eq. (3.19).

$$u_i = \sum_{j=1}^H w_{ij} x_j + b_i \quad (3.19)$$

The summation  $u_i$  is transformed using a scalar-to-scalar function called an "activation or transfer function",  $F(u_i)$  yielding a value called the unit's "activation", given in Eq. (3.20).

$$Y_i = f(u_i) \quad (3.20)$$

Activation functions serve to introduce nonlinearity into neural networks which makes NN's so powerful.

Neural networks are commonly classified by their network topology, (i.e. feedback , feedforward) and learning or training algorithms (i.e. Supervised , Unsupervised). For example a multilayer feedforward neural network with backpropagation indicates the architecture and learning algorithm of the neural network.

Back propagation algorithm is one of the most widely used supervised training methods for training multilayer neural Networks due to its simplicity and applicability. It is based on the generalized delta rule and was popularized by Rumelhart and coworkers (**Rumelhart et al. 1986**). As it is a supervised learning algorithm, there is a pair of inputs and corresponding output. The algorithm is simply based on a weight. It consists of two passes: a forward pass and a backward pass. In the forward pass, first, the weights of the network are randomly initialized and an output set is obtained for a given input set where weights are kept as fixed. The error between the output of the network and the target value is propagated backward during the backward pass and used to update the weights of the previous layers as shown in Fig.3.5. (**Haykin 2000, Hebb 1949, Minsky and Seymour 1969, Rumelhart et al. 1986 and Zupan and Gasteiger 1993**).

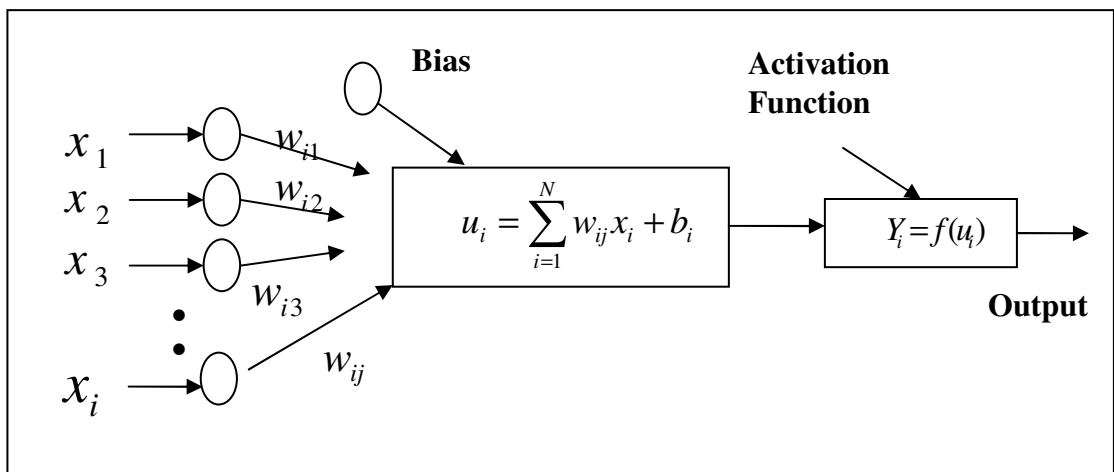


Fig. 3.4 Basic elements of an artificial neuron

The performance of a NN model mainly depends on the network architecture and parameter settings. One of the most difficult tasks in NN studies is to find this optimal Network architecture which is based on determination of numbers of optimal

layers and neurons in the hidden layers by trial and error approach. The assignment of initial weights and other related parameters may also influence the performance of the NN in a great extent. However there is no well defined rule or procedure to have optimal network architecture and parameter settings where trial and error method still remains valid. This process is very time consuming.

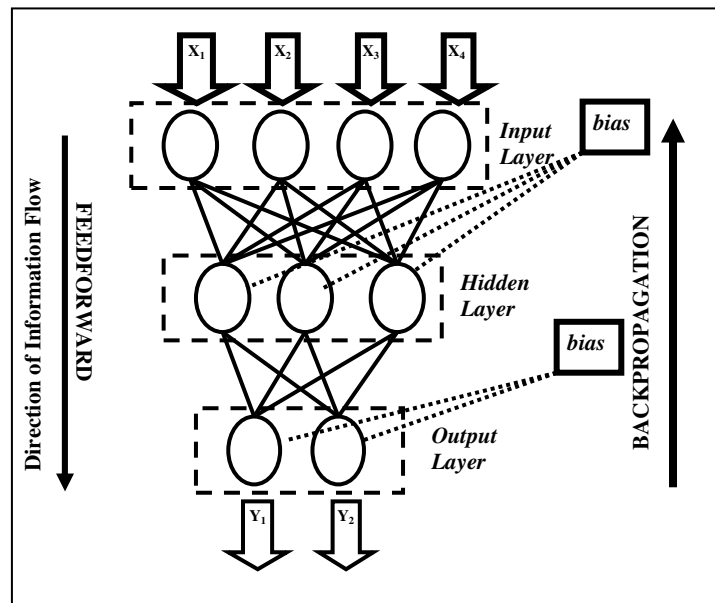


Fig.3.5. Backpropagation algorithm

In this thesis Matlab NN toolbox is used for NN applications. The prediction and formulation of Mode I and Mode II SIF values for varying geometries using NNs has been carried out. The case studies have been applied on the three well known fracture geometries: the center cracked, the double edge cracked and the single edge cracked models.

FE results are divided into train and test sets where patterns in test set are randomly selected among the experimental database shown in bold characters given in Table A1. The training patterns for NNs have been obtained using ANSYS FE software package. The optimal NN architecture was found to be 4-11-1 architecture with hyperbolic tangent sigmoid transfer function (tansig). The training algorithm was quasi-Newton backpropagation (BFGS). All necessary neural procedures are performed by MATLAB NN Toolbox.



Explicit formulation of Mode I SIF value is obtained as a function of stress, crack width, plate width and crack type.

The explicit formula is obtained using the weights of the trained network as follows:

$$\text{Net}_j = \sum_{i=1}^n w_{ij} x_i \quad (3.21)$$

where  $\text{Net}_j$  is the weighted sum of the  $j$ th neuron for the input received from the preceding layer with  $n$  neurons,  $w_{ij}$  is the weight between the  $j$ th neuron and the  $i$ th neuron in the preceding layer,  $x_i$  is the output of the  $i$ th neuron in the preceding layer. The output of the  $j$ th neuron  $\text{out}_j$  is calculated with a sigmoid function as follows:

$$\text{out}_j = f(\text{Net}_j) = \frac{1}{1 + \exp(-k\text{Net}_j)} \quad (3.22)$$

where,  $k$  is a constant used to control the slope of the semi-linear region.

Recalling Eqs. (3.20) and (3.21) the explicit formula is obtained by using the weights of the trained network given step by step as follows:

$$u_i = \sum_{i=1}^N w_{ij} x_i + b_i \quad \text{and} \quad Y_i = f(u_i) \quad (3.23)$$

where  $u_i$  is the summation of the  $i$ th node and  $Y_i$  the output of transfer function of this summation.

### 3.2.2.2 Genetic Programming

GP is an extension to Genetic Algorithms proposed by **Koza (1992)**. GP reproduces computer programs to solve problems by executing the following steps (Fig. 3.6):

- 1) Generate an initial population of random compositions of the functions and terminals of the problem (computer programs).
- 2) Execute each program in the population and assign it a fitness value according to how well it solves the problem.
- 3) Create a new population of computer programs.

- i) Copy the best existing programs (Reproduction)
  - ii) Create new computer programs by mutation.
  - iii) Create new computer programs by crossover (sexual reproduction).
  - iv) Select an architecture-altering operation from the programs stored so far.
- 4) The best computer program that appeared in any generation, the best-so-far solution, is designated as the result of genetic programming (**Koza, 1992**).

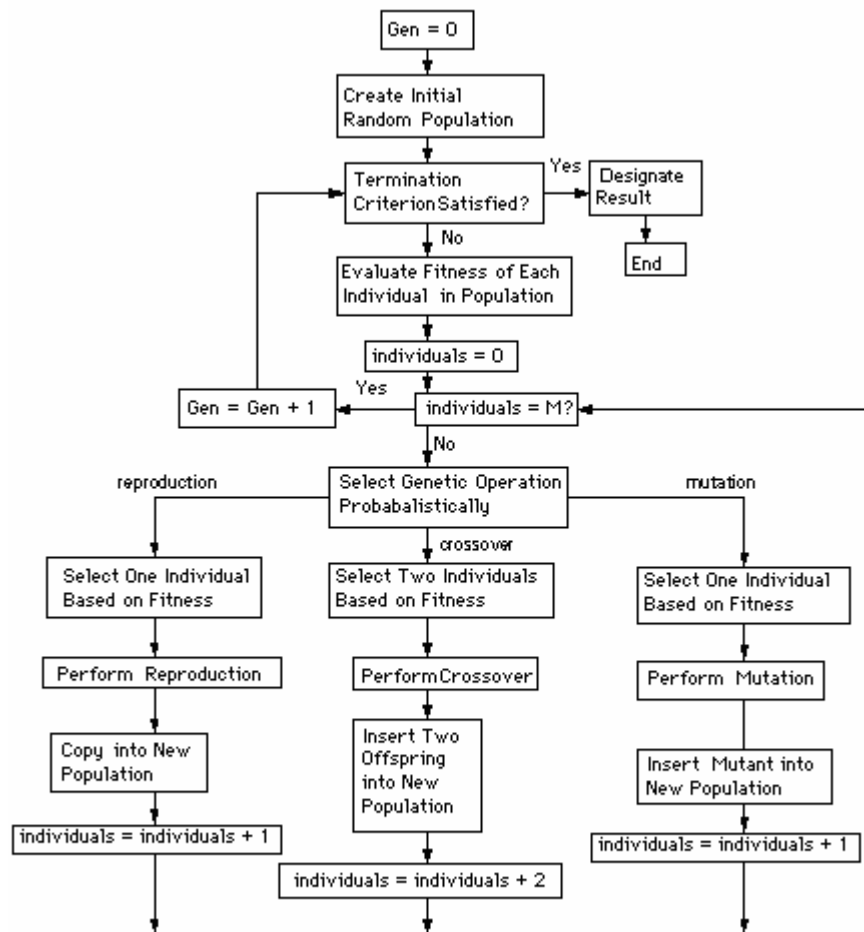


Fig. 3.6 Genetic Programming Flowchart (**Koza,1992**)

Gene expression programming (GEP) software which is used in the present study is an extension to GP that evolves computer programs of different sizes and shapes encoded in linear chromosomes of fixed length. The chromosomes are composed of multiple genes, each gene encoding a smaller sub-program. Furthermore, the structural and functional organization of the linear chromosomes allows the unconstrained operation of important genetic operators such as mutation, transposition, and recombination. One strength of the GEP approach is that the

creation of genetic diversity is extremely simplified as genetic operators work at the chromosome level. Another strength of GEP consists of its unique, multigenic nature which allows the evolution of more complex programs composed of several sub-programs. As a result GEP surpasses the old GP system in 100-10,000 times (**Ferreira 2001, 2002**). **APS 3.0** (<http://www.gepsoft.com/>), a GEP software developed by Candida Ferreira is used in this study.

The fundamental difference between GA, GP and GEP is due to the nature of the individuals: in GAs the individuals are linear strings of fixed length (chromosomes); in GP the individuals are nonlinear entities of different sizes and shapes (parse trees); and in GEP the individuals are encoded as linear strings of fixed length (the genome or chromosomes) which are afterwards expressed as nonlinear entities of different sizes and shapes (i.e., simple diagram representations or expression trees). Thus the two main parameters GEP are the chromosomes and expression trees (ETs). The process of information decoding (from the chromosomes to the ETs) is called translation which is based on a set of rules. The genetic code is very simple where there exist one-to-one relationships between the symbols of the chromosome and the functions or terminals they represent. The rules which are also very simple determine the spatial organization of the functions and terminals in the ETs and the type of interaction between sub-ETs (**Ferreira 2001, 2002**).

That's why two languages are utilized in GEP: the language of the genes and the language of ETs. A significant advantage of GEP is that it enables to infer exactly the phenotype given the sequence of a gene, and *vice versa* which is termed as *Karva* language. Consider, for example, the algebraic expression

$(d4 * \sqrt{(d3 - d0 + d1 * d4)}) - d4$  can be represented by a diagram (Fig. 3.7) which is the expression tree:

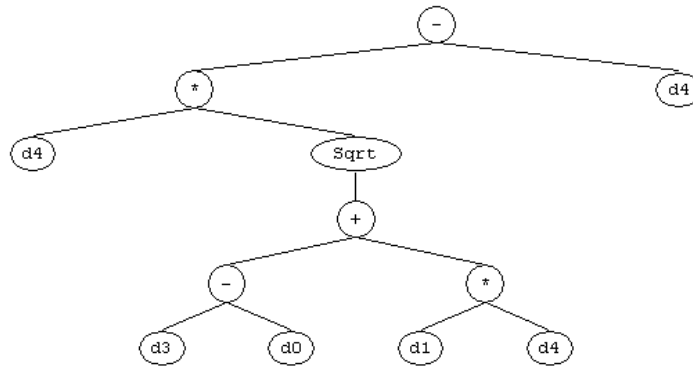


Fig. 3.7 Expression tree (ET)

FE results are divided into train and test sets where patterns in test set are randomly selected among the experimental database shown in bold characters given in Table A2. The training patterns for GP formulation have been obtained using ANSYS FE software package. A wide range of variables are chosen to represent a general model for GP.

Explicit formulation of Mode I SIF is obtained as a function of stress, crack width, plate width and crack.

### 3.3 FEM for Crack Path Prediction

The prediction not only of when and how far a crack will grow, but of its path is important analysis of potential failures.

The crack path prediction can be done numerically or experimentally. The calculation of crack tip field stress values becomes more important for the prediction of crack path while using the numerical methods. The resolution of the stress field around the crack tip and the prediction of crack path are the essential requirements for the numerical methods. The traditional FEM have been improved with these requirements (Zehnder A.T., 2007).

Some criteria are explained briefly below but it is not important which criteria one uses because of the crack propagation criteria come in different characteristic

parameters but all lead to similar end results for fractures. The determination of  $K_I$  and  $K_{II}$  values has to be done using numerical solutions in domain. The domain form of the interaction integral is well-suited to extract the mixed-mode SIFs. The domain form of this interaction integral can be reduced to the Rice's J-integral form in pure Mode I problems. However it is too difficult to separate  $K_I$  and  $K_{II}$  values in Mixed Mode problems with the Rice's J-integral method. In this case we need to use extrapolation techniques around the crack tip.

The crack growth may be stable or unstable. It depends on the rate of change in driving force, fracture energy and crack size. The conditions for stable crack can be expressed as follows:

$$G = R \quad (3.24)$$

and

$$\frac{dG}{da} \leq \frac{dR}{da} \quad (3.25)$$

Unstable crack growth occurs when

$$\frac{dG}{da} > \frac{dR}{da} \quad (3.26)$$

where  $G$  is the elastic energy release rate,  $R$  is the resistance to crack extension and  $a$  is the crack width.

### 3.3.1 Fracture criteria for unstable crack growth

The unstable crack growth deals especially with the following questions:

- When does the crack growth become unstable?
- In which direction does the unstable crack grow?
- At what loading level or at what crack length does a structure fail?
- What is the magnitude safety versus unstable crack growth/fracture in a structure?

These questions can be answered by so-called fracture criteria for plane mixed mode problems. For pure Mode I loading unstable crack growth occurs if the Mode I stress intensity  $K_I$  reaches the fracture toughness  $K_{IC}$ .

$$K_I \leq K_{IC} \quad (3.27)$$

The application of this criterion to a mixed-mode situation would result in a non-conservative estimation for the risk of fracture. For a plane mixed-mode loading of a crack, besides the  $K_I$  also  $K_{II}$  has an influence on the beginning of unstable crack growth, and thus on the fracture of components and structures (**Richard H.A. et al., 2005**).

If a crack is subjected to a combination of Mode-I and Mode-II loadings (Fig. 3.8), the crack will generally not propagate straight ahead. Direction of next step of crack growth is shown in Fig. 3.8 as dashed line on right with direction  $\theta^*$  from the crack line.

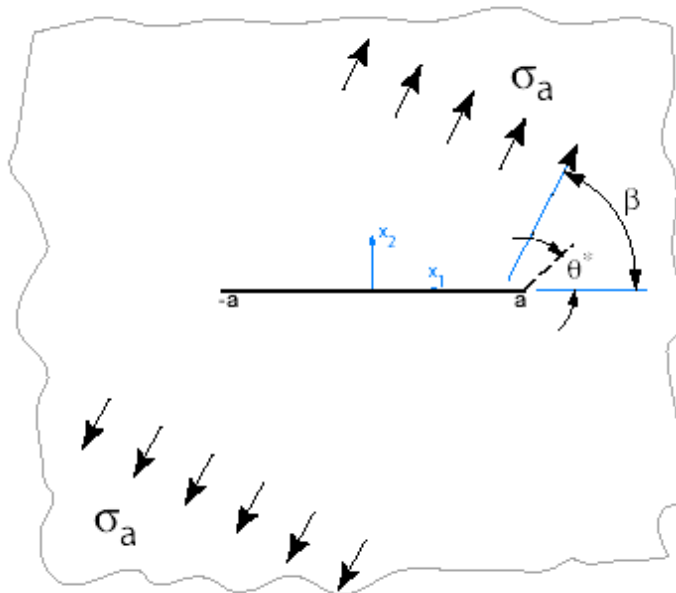


Fig. 3.8 2D crack under mixed-mode loading

Far away from the crack the stress is  $\sigma_{22} = \sigma_a \sin^2 \beta$ ,  $\sigma_{12} = \sigma_a \sin \beta \cos \beta$ ,  $\sigma_{11} = \sigma_a \cos^2 \beta$ . The resulting stress intensity factors are  $K_I = \sigma_a \sqrt{\pi a} \sin^2 \beta$ ,  $K_{II} = \sigma_a \sqrt{\pi a} \sin \beta \cos \beta$ . At what stress level,  $\sigma_a$  will the crack begin to grow and in what direction?

Mixed-mode fracture theories include:

- (1) Maximum circumferential stress theory,

- (2) Maximum energy release rate theory and
- (3) Minimum strain energy density theory,
- (4) Local symmetry.

Only the theory of maximum circumferential stress, and of maximum energy release rate will be given here. We used the maximum circumferential stress criteria due to its simple applicability on mixed mode loading crack problems in crack propagation angle.

### 3.3.2 Maximum circumferential stress criteria

The maximum circumferential stress theory postulates that a crack will grow in the direction,  $\theta^*$ , of maximum circumferential stress,  $\sigma_{\theta\theta}$ , when  $\sqrt{r}\sigma_{\theta\theta}(r, \theta^*) \geq \text{Const.}$  Assuming that the constant is the same for mixed-mode loading as for pure Mode-I loading, from the Mode-I criterion  $K_I \geq K_{IC}$ , the mixed-mode criterion can be written as

$$\sqrt{r}\sigma_{\theta\theta}(r, \theta^*) \geq \frac{K_{IC}}{\sqrt{2\pi}} \quad (3.28)$$

The directional criterion is that the crack will grow in the direction  $\theta^*$  that satisfies

$$\frac{\partial \sigma_{\theta\theta}}{\partial \theta} = 0, \frac{\partial^2 \sigma_{\theta\theta}}{\partial \theta^2} < 0 \quad (3.29)$$

Combining the stress equations and re-arranging, the circumferential stress can be written as

$$\sigma_{\theta\theta}(r, \theta^*) = \frac{1}{\sqrt{2\pi r}} \left( K_I \cos \frac{\theta}{2} \frac{(1 + \cos \theta)}{2} - K_{II} \frac{3}{2} \sin \theta \cos \frac{\theta}{2} \right) \quad (3.30)$$

which yields

$$K_I \sin \theta + K_{II} (3 \cos \theta - 1) = 0 \quad (3.31)$$

and

$$\theta = -\arccos\left(\frac{3K_{II}^2 + K_I\sqrt{K_I^2 + 8K_{II}^2}}{K_I^2 + 9K_{II}^2}\right) \quad (3.32)$$

Comparison of this theory with experimental results shows that the maximum circumferential stress theory predicts the angle of crack growth well but somewhat underestimates the envelope of failure. Nonetheless, at least for crack growth angle the maximum circumferential stress theory is quite accurate and is easily implemented in fracture simulations.

### 3.3.3 Maximum energy release rate criteria

The maximum energy release rate criterion states that the crack will propagate so as to maximize the energy release. Since  $G = -\frac{\partial\Pi}{\partial s}$ , this criterion is equivalent to saying that the crack grows so as to minimize the potential energy of the body, corresponding to the thermodynamic idea equilibrium systems seek their local energy minima (**Zehnder A.T., 2007**).

**Wu W.L. (2004)** studied this problem for 2D cracks under Mode I and Mode II loading. He considers a straight crack that extends with a kink of length  $\epsilon$  and angle  $\theta$  from the pre-existing crack tip. The criterion can be stated as the crack will kink at the angle  $\theta^*$  such that

$$\frac{\partial G(\theta^*)}{\partial \theta} = 0, \frac{\partial^2 G(\theta^*)}{\partial \theta^2} < 0 \text{ and } G(\theta^*) \geq G_c \quad (3.33)$$

where  $G(\theta) \equiv \lim_{\epsilon \rightarrow 0} \frac{1}{\epsilon} (\Pi_z - \Pi)$ , and  $\Pi_z$  is the potential energy for the kinked crack and  $\Pi$  is the potential energy for the original crack.  $G_\theta$  cannot be calculated in closed-form, however an excellent approximation can be obtained.

Both of the above criteria predict that a crack under pure Mode-I loading will continue to propagate straight ahead. In this case  $K_I = f\left(\frac{a}{w}\right)\sigma\sqrt{\pi a}$  and



$K_{II} = 0$  and the above theories predict that the crack will grow straight ahead, i.e. in the -x direction.

### 3.3.4 Simulation of crack path prediction

The flow chart of the used procedure for the crack path prediction is displayed and explained in Fig. 3.9.

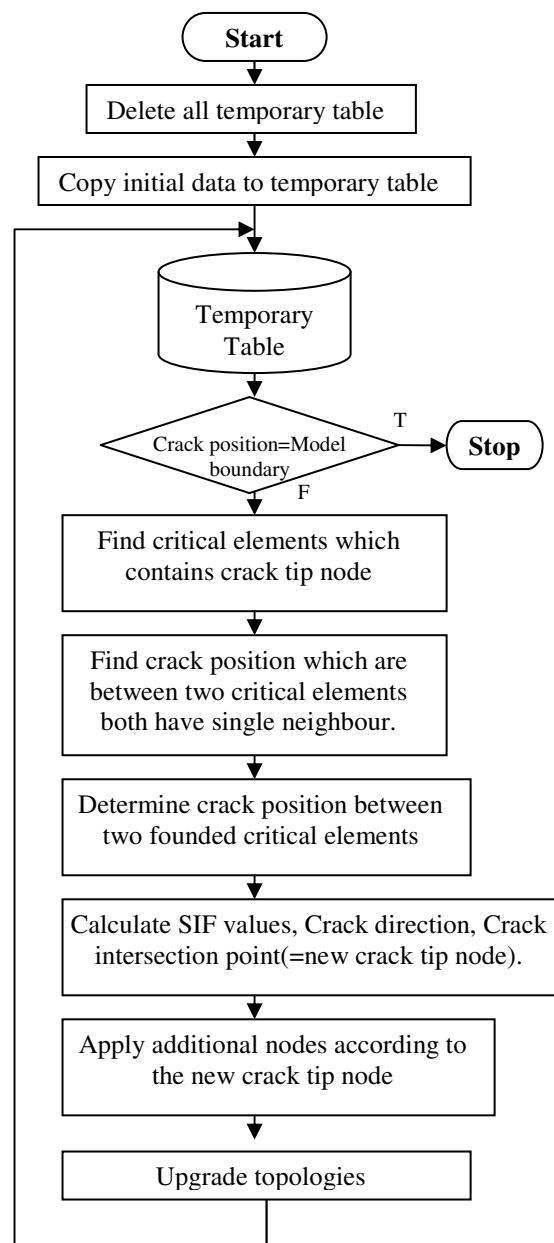


Fig. 3.9 Crack path prediction flow-chart

The crack tip node and the initial nodes located upper and lower part of the crack have been defined initially in data file of the FEM program. A critical area has been stated around the crack tip to find the crack path. The element topologies that consist of crack tip nodes are investigated for the critical elements area. This critical area can be seen from Fig. 3.10.

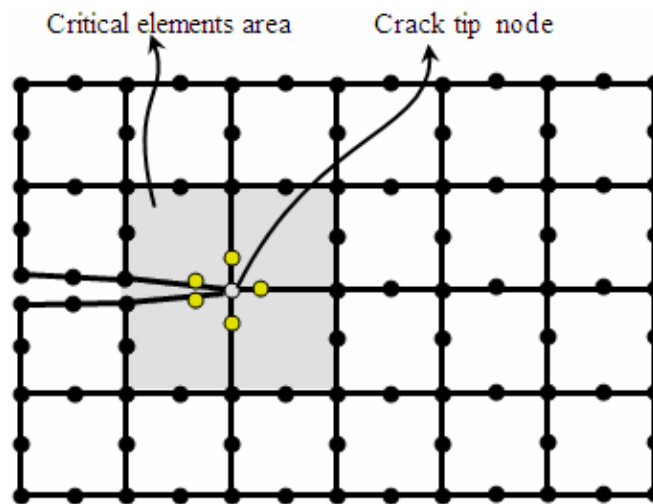


Fig.3.10 The critical elements area and crack tip node.

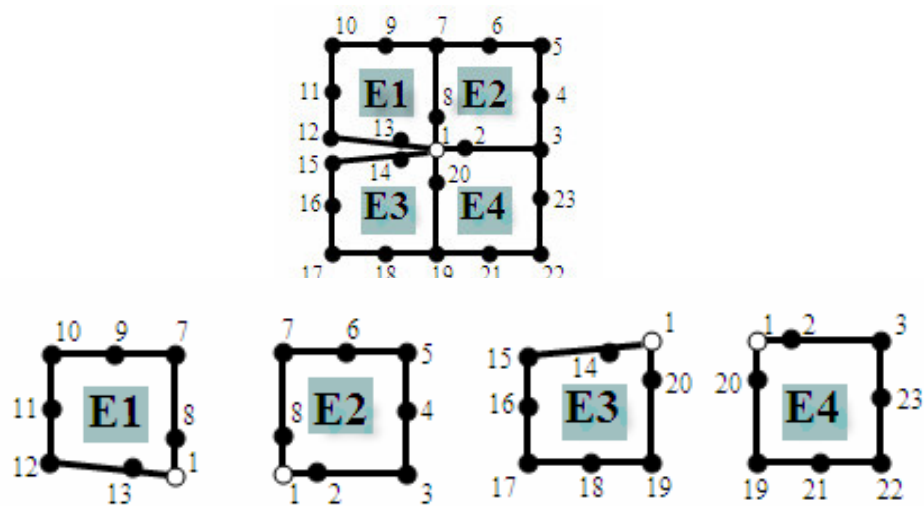


Fig.3.11 The parts of the critical elements area

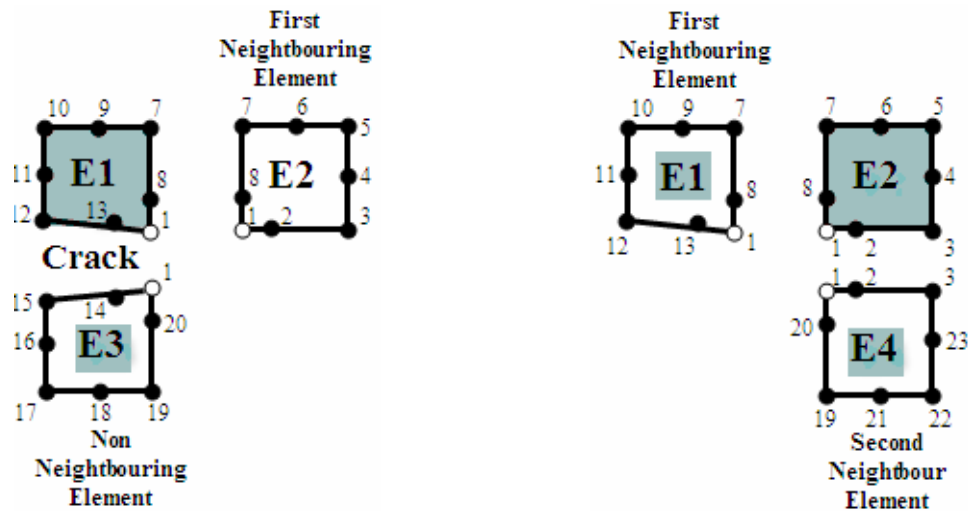


Fig.3.12 The neighbouring elements

Node numbers 1-13-14-12-15 of Fig. 3.11 are chosen for the crack path. It is obvious from Fig.3.11 node 1 is the crack tip node. E1, E2, E3 and E4 element topologies contains this crack tip node 1. All element topologies are compared with each other horizontally and vertically two by two in order to find the crack location. In these comparisons it is important to find the number of overlapping nodes. If these number of overlapping nodes is greater than one than it means that these two topologies compose a neighbouring elements. If the number of overlapping elements are equal to one, it represents the other neighbouring element which actually shows the crack region (Figs.3.12 and 3.13).

As a result two elements with one neighbouring element remain where both are the neighbouring elements around the crack. It is now possible to find the potential crack direction. The initial upper and lower nodes and the crack tip node of the crack has been defined in the first statement of the data file. The  $K_I$  and  $K_{II}$  can be calculated using the quarter point nearest the crack tip nodes given in the data file and after finding the SIF values, the crack trajectory prediction angle  $\theta$  can be computed by Maximum Circumferential Stress Criterion (Eq. 3.32). The related formulas have given before in Eqs. (3.12-3.17) for the calculation of  $K_I$  and  $K_{II}$  values.

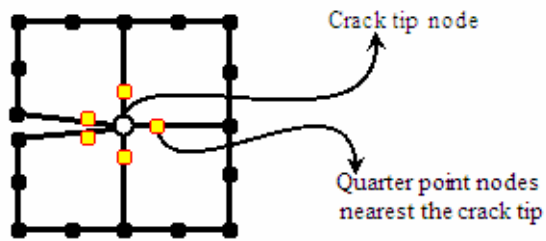


Fig.3.13 The crack tip and quarter point nodes

The new crack tip can be found using the crack path angle  $\theta$  in neighbouring element boundaries. The old crack tip has to be divided into two nodes and the new element topologies have to be redefined in another file. In the developed program we have this file with the same input name but a different extension name called .TPL.

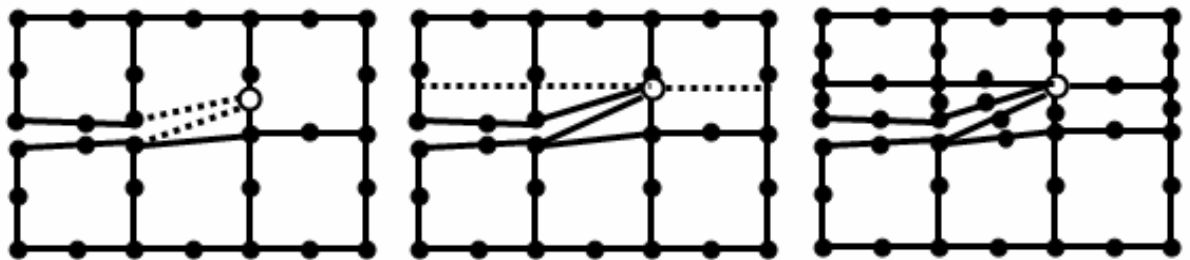


Fig. 3.14 Intersection point on vertical boundary of the element

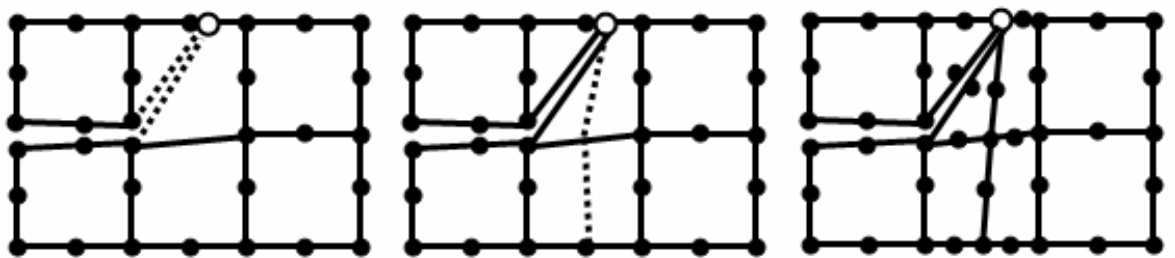


Fig. 3.15 Intersection point on horizontal boundary of the element

If the intersection point is on vertical boundary of the element, one needs to define a horizontal line for the new element topologies. If the intersection point is on horizontal boundary of the element, one needs to define a vertical line for the new element topologies (Figs. 3.14 and 3.15).

The crack path prediction procedure will be used to simulate the crack growth trajectory of center edge, single edge crack model cases under Mode I and Mode II loading.

## CHAPTER 4

### ELASTO-PLASTIC FRACTURE MECHANICS

#### 4.1 Introduction

Linear elastic fracture mechanics is only valid as long as nonlinear material deformation is confined to a small region surrounding the crack tip. All materials have a finite strength, thus there will always be a small plasticized zone around the crack tip. If this zone is small compared to the crack size, then linear elastic assumptions are correct; if not, LEFM is not applicable (thus it would be incorrect to use a  $K$  or  $G$  criterion) and a nonlinear model must be used. In this cases there are two approaches in Elasto Plastic Fracture Mechanics (EPFM) for the calculation of fracture parameters. The first one is a local criterion based on the crack tip opening displacement (CTOD). The second one is a global criterion based on the quasi-strain energy release rate J- integral.

Under LEFM the crack tip opening displacement is clearly zero. However, when the material is allowed to yield, then the crack tip will blunt resulting in a non-zero crack tip opening displacement (CTOD).

There are two approaches to determine the CTOD: First-order approximation based on a fictitious crack and a second-order approximation based on Dugdale's model.

The first-order approximation depends on the Irwin's solutions (**Irwin,1960**). In this approximation the vertical displacement of a point next to the crack tip due to Mode I loading is given by Eq. (4.1).

$$v = \frac{K_I}{2\mu} \left[ \frac{r}{2\pi} \right]^{\frac{1}{2}} \sin \frac{\theta}{2} \left[ \kappa + 1 - 2 \cos^2 \frac{\theta}{2} \right] \quad (4.1)$$

If we substitute  $\theta = \pm\pi$  we obtain the upper and lower displacements of the crack face, and due to symmetry their sum corresponds to the crack opening displacement. Hence the crack opening is given by

$$\text{CTOD} = 2v = \frac{\kappa+1}{\mu} K_I \sqrt{\frac{r}{2\pi}} \quad (4.2)$$

If we determine the crack tip opening displacement a distance  $r_p^*$  away from the crack tip using Irwin's plastic zone correction.

$$r_p^* = \frac{1}{2\pi} \frac{K_I^2}{\sigma_{\text{yld}}^2} \quad (4.3)$$

and using  $\kappa = \frac{3-\nu}{1+\nu}$  for plane stress we obtain

$$\text{CTOD} = \frac{4}{\pi} \frac{K_I^2}{E \sigma_{\text{yld}}} \quad (4.4)$$

The second-order approximation is based on Dugdale's model. **Kanninen (1985)** has shown that the crack opening along the crack using Dugdale's solution:

$$\text{CTOD} = 2v = \frac{8}{\pi} \frac{a \sigma_{\text{yld}}}{E} \log \left[ \sec \frac{\pi \sigma}{2 \sigma_{\text{yld}}} \right] \quad (4.5)$$

using the series expansion of  $\log \sec$ :

$$\text{CTOD} = \frac{8}{\pi} \frac{a \sigma_{\text{yld}}}{E} \left[ \frac{1}{2} \left( \frac{\pi \sigma}{2 \sigma_{\text{yld}}} \right)^2 + \frac{1}{12} \left( \frac{\pi \sigma}{2 \sigma_{\text{yld}}} \right)^4 + \dots \right] \quad (4.6)$$

or

$$\text{CTOD} = \frac{K^2}{E \sigma_{\text{yld}}} \left[ 1 + \frac{\pi^2}{24} \frac{\sigma^2}{\sigma_{\text{yld}}^2} + \dots \right] \quad (4.7)$$

note that for small  $\sigma/\sigma_{\text{yld}}$ , the CTOD can be approximated by  $\text{CTOD} = K^2/E\sigma_{\text{yld}}$ .

## 4.2 J- Integral

**Eshelby (1969)** has defined a number of contour integrals that are path independent by virtue of the theorem of energy conservation. The two-dimensional form of one of these integrals can be written as:

$$J = \oint_{\Gamma} \left( w dy - t \frac{\partial u}{\partial x} d\Gamma \right) \quad (4.8)$$

with

$$w = \int_0^{\varepsilon} \sigma_{ij} d\varepsilon_{ij} \quad (4.9)$$

where;

$w$  is the strain energy density;  $\Gamma$  is a closed contour followed counter-clockwise, as shown in Fig. 4.1;

$t$  is the traction vector on a plane defined by the outward drawn normal  $n$  and

$t = \sigma n$ ;  $u$  the displacement vector, and  $d\Gamma$  is the element of the arc along the path  $\Gamma$ .

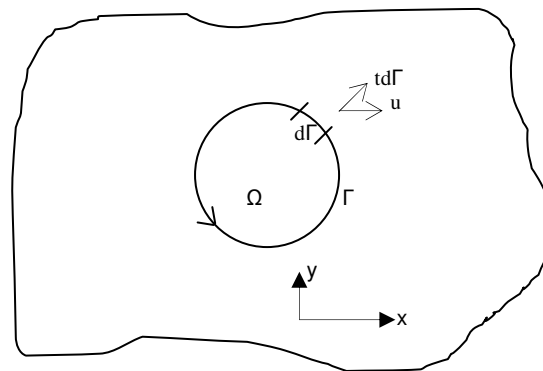


Fig. 4.1 J-integral definition around a crack (**Anderson, 1986**)

Although **Eshelby (1969)** had defined a number of similar path independent contour integrals, he had not assigned to them a particular physical meaning.



#### 4.2.1 Path independence of J-Integral

It must be shown that the former is indeed equal to zero for a closed path before establishing of the connection between **Eshelby's (1969)** expression for J-Integral and the energy release rate G.

$$J = \oint_{\Gamma} \left( w dy - t_i \frac{\partial u_i}{\partial x} d\Gamma \right) \quad (4.10)$$

assuming  $\Gamma$  to be defined counterclockwise, then  $d_x = -n_y d\Gamma$ , and  $d_y = n_x d\Gamma$  and  $t_i = n_j \sigma_{ij}$  where  $n_x$ ,  $n_y$  and  $n_j$  are direction cosines. Substituting in Eq. (4.10);

$$J = \oint_{\Gamma} \left( w n_x - n_j \sigma_{ij} \frac{\partial u_i}{\partial x} \right) d\Gamma \quad (4.11)$$

and invoking Green's theorem;

$$\oint_{\Gamma} v_i n_i d\Gamma = \int_{\Omega} v_{i,i} d\Omega \quad (4.12)$$

we obtain:

$$J = \int_{\Omega} \left[ \frac{\partial w}{\partial x} - \frac{\partial}{\partial x_j} \left( \sigma_{ij} \frac{\partial u_i}{\partial x} \right) \right] dx dy \quad (4.13)$$

Substituting the strain energy density, Eq. (4.8), the first term in the square bracket becomes;

$$\frac{\partial w}{\partial x} = \frac{\partial w}{\partial \epsilon_{ij}} \frac{\partial \epsilon_{ij}}{\partial x} = \sigma_{ij} \frac{\partial \epsilon_{ij}}{\partial x} \quad (4.14)$$

The strain is given by

$$\epsilon_{ij} = \frac{1}{2} (u_{i,j} + u_{j,i}) \quad (4.15)$$

Substituting in Eq. (4.15) given

$$\frac{\partial w}{\partial x} = \frac{1}{2} \sigma_{ij} \left[ \frac{\partial}{\partial x} \left( \frac{\partial u_i}{\partial x_j} \right) + \frac{\partial}{\partial x} \left( \frac{\partial u_j}{\partial x_i} \right) \right] = \sigma_{ij} \frac{\partial}{\partial x_j} \left( \frac{\partial u_i}{\partial x} \right) \quad (4.16)$$

On the other hand, we have

$$\frac{\partial}{\partial x_j} \left( \sigma_{ij} \frac{\partial u_i}{\partial x} \right) = \sigma_{ij} \frac{\partial}{\partial x_j} \left( \frac{\partial u_i}{\partial x} \right) + \frac{\partial \sigma_{ij}}{\partial x_j} + \frac{\partial u_i}{\partial x} \quad (4.17)$$

hence

$$\frac{\partial w}{\partial x} = \sigma_{ij} \frac{\partial}{\partial x_j} \left( \frac{\partial u_i}{\partial x} \right) \quad (4.18)$$

which is identical to the second term of Eq. (4.13).

Thus the integrand of Eq. (4.10) vanishes and  $J = 0$  for any closed contour.

Having shown that indeed  $J = 0$ , this will be exploited to prove that around a crack,  $J$  is non-zero and is independent of the path.

With reference to Fig. 4.2 if we consider the closed path  $\Gamma = \Gamma_1 + \Gamma_2 + \Gamma_3 + \Gamma_4$  in which  $\Gamma_1$  and  $\Gamma_3$  are arbitrarily chosen contours. Obviously  $J = 0$  over  $\Gamma$  in order to satisfy compatibility conditions, provided that the stresses and displacement gradients are continuous. Along paths  $\Gamma_2$  and  $\Gamma_4$ , the traction vector  $t_i = 0$  and also  $dy = 0$ .

Consequently, the contributions to  $J$  from  $\Gamma_2$  and  $\Gamma_4$  vanish. Taking into account the difference sense of integration along paths  $\Gamma_1$  and  $\Gamma_3$  we arrive at the conclusion that the values of  $J$  integrated over paths  $\Gamma_1$  and  $\Gamma_3$  are identical. Because these two paths were arbitrarily chosen, the path independence of  $J$  is assured.

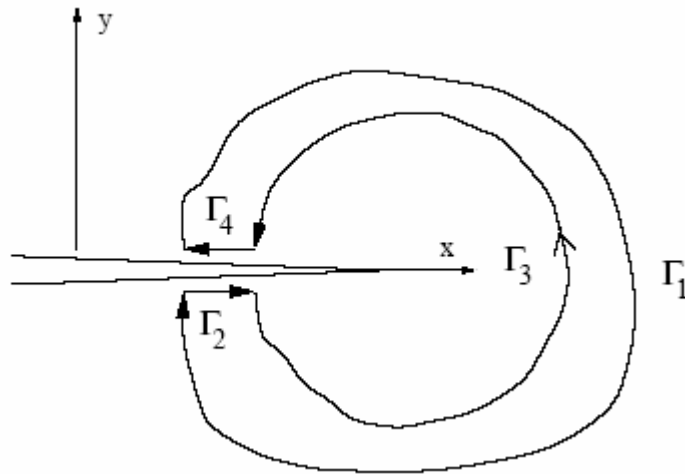


Fig 4.2 Closed contours for proof of J-integral path independence  
(Anderson, 1986)

### 4.3 Artificial intelligence for J-Integral calculation

The prediction and formulation of J-integral values for varying geometries using GP based FE (ANSYS) results in an interesting and new area in fracture mechanic problems.

J-Integral calculations have been done with an ANSYS macro in the present study. For this purpose, a Fortran subroutine has been developed for ANSYS which reads the results from stress analysis and computes the appropriate line integral along a path through the integration points. The obtained J-integral values using ANSYS have been used for GP training and formulation.

#### 4.3.1 Neural networks

The trained NN in this case study does not serve as a black box anymore as it is considered in most of the NN . It is an independent program to compute J-integral values for three different geometries for given set of  $\sigma_{applied}$  ,  $a$  ,  $w$  , and  $Type$  values as shown in Fig.4.3.

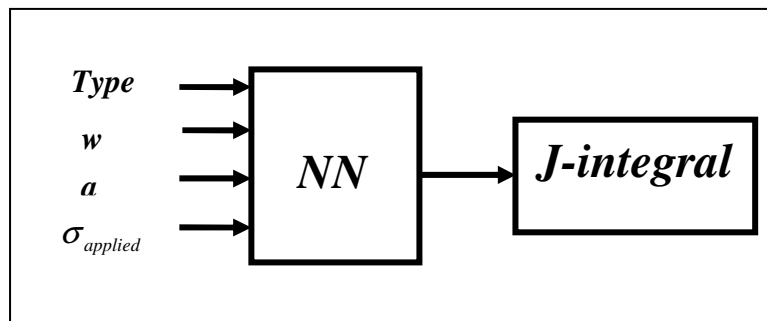


Fig.4.3 NN Model for J-integral calculation

Furthermore it is actually an explicit formulation that computes directly stress intensity factor for three different geometries which is given as a function of some fracture parameters:

$$\text{J-integral} = \mathbf{f}(\sigma_{\text{applied}}, a, w, \text{Type}) \quad (4.19)$$

where,  $\sigma_{\text{applied}}$  is the applied stress,  $a$  is the crack length,  $w$  is the plate width. Crack types will be given in Chapter 5.

### **4.3.2 Genetic Programming**

The training patterns for GP formulation have been obtained using ANSYS FE software package. A wide range of variables are chosen to represent a general model for GP

Explicit formulation of J-integral is obtained as a function of stress, crack width, plate width and crack type which is the expression tree of GP formulation given in MATLAB CODE.

## **CHAPTER 5**

### **CASE STUDIES**

#### **5.1 Introduction**

In this study, a FORTRAN computer program has been developed to validate some case studies. In these case studies, the well known fracture geometries have been used to compare the results of the developed FE program, with ANSYS, analytical solutions and related references for this purpose. A number of J-integral calculations have been done using a macro written in ANSYS and FORTRAN program. AI techniques are also used to calculate SIF and J-integral parameters of some specific case studies. Finally, the crack path prediction has been carried out with the developed program for linear elastic fracture mechanics.

The case studies are center cracked, double edge cracked, single edge cracked, three-point bending beam, compact tension specimen, off-center crack, single edge cracked model with mixed mode loading and U section model cases. They have been carried out and compared with literature and ANSYS.

#### **5.2 SIF calculations**

##### **5.2.1 Mode I loading geometric models**

The center, double and single edge cracked models have been chosen for pure Mode I loading calculations. These calculations have been done using numerical extrapolation techniques (DEM and SEM) explained in Sections 3.2.1.1 and 3.2.1.2. Furthermore comparisons with analytical formulations and ANSYS have been carried out. In these comparisons crack width and applied stress have been taken as:  $w = 40 \text{ mm}$ ,  $\sigma = 100 \text{ N/mm}^2$  for center, double edge and single edge cracked models respectively. All Mode I cases have been analyzed using developed FEM program and ANSYS and compared with the **Broek (1986)**'s analytical results. The

displacement and stress extrapolation methods have been used in the calculation of SIF values. The analytical formulas have also been compared in term of correction factors used in literature.

### 5.2.1.1 Center cracked model

The center cracked model geometry is shown in Fig.5.1. Due to symmetry, only a quarter of the model has been used (Fig.5.2) in the analysis. The analytical formulas for the SIF calculations are taken from **Broek (1986)**.

$$K_I = \sigma \sqrt{\pi a} f\left(\frac{a}{w}\right) \quad (5.1)$$

where

$$f\left(\frac{a}{w}\right) = \sqrt{\sec\left(\frac{\pi a}{w}\right)}$$

The other analytical formulas given in literature are applied for the graphical representation of  $f(a/w)$  correction factors with 2, 4, 6 and 8 mm crack lengths shown in Fig. 5.3 for the center cracked case.

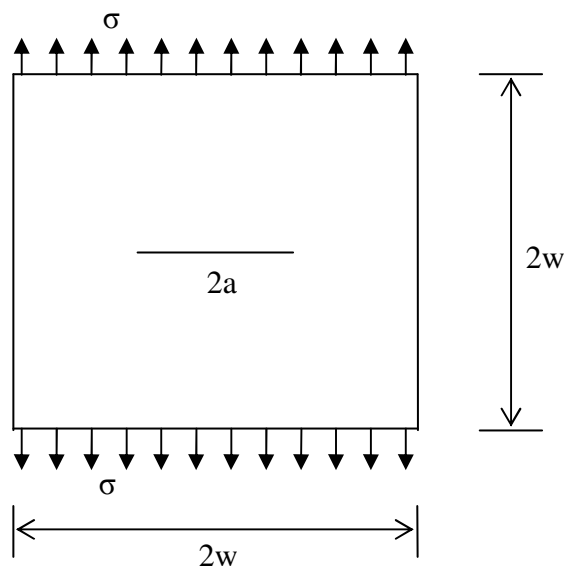


Fig. 5.1 Center cracked full geometry

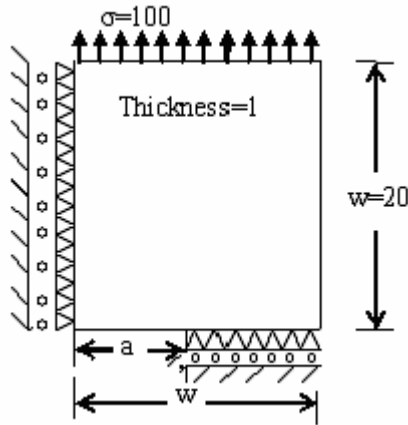


Fig. 5.2 Center cracked quarter geometry

**Comparison of correction factor conclusions**

A small deviation -as much as 1%- is observed with respect to the values given by Fedderson and Dixon (Ewalds and Wanhill 1986) for  $a/w$  ratio of 0.2 as seen in Fig. 5.3.

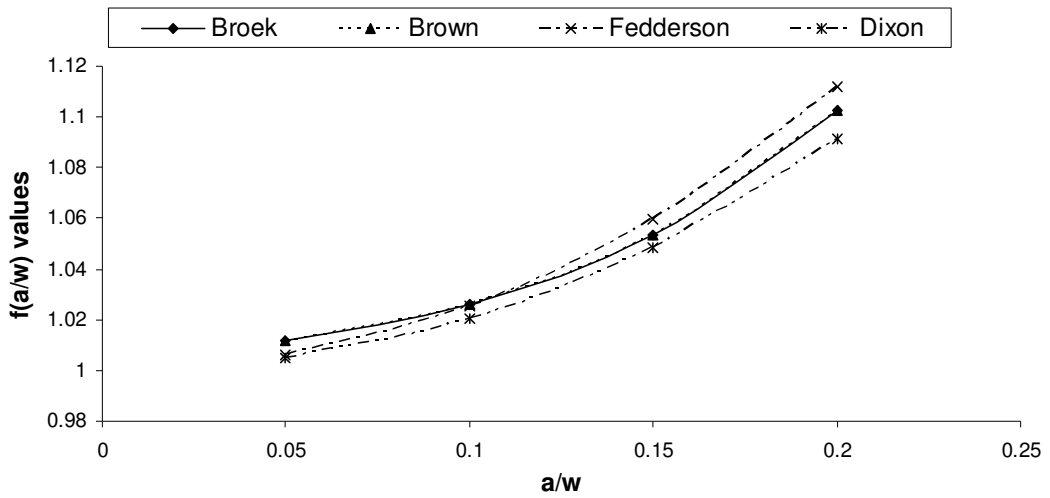


Fig. 5.3 Comparison of correction factors for the center cracked model

**Comparison of  $K_I$  values conclusions**

In the center cracked case following material properties are used:

- Young's modulus      $E = 80000 \text{ MPa}$
- Poisson's ratio      $\nu = 0.3$
- Applied stress        $\sigma = 100 \text{ MPa}$
- Plate width            $w = 20 \text{ mm}$

Crack length  $a=2, 4, 6$  and  $8$  mm.

The SIF's for the range of crack lengths analyzed as given above, were calculated using Eq. (5.1) and are referred to as the analytical solution of **Broek (1986)**. The numerically calculated SIF's were determined using the finite element program. The results for this case are displayed in Fig. 5.4; inspection of these graphs reveals that DEM, SEM and FE-ANSYS results are reasonably close to each other and to the analytical result for the mid range of crack lengths. The numerical results for short crack lengths are influenced by the plastic zone at the crack tip, and the analytical solution loses accuracy at larger crack lengths.

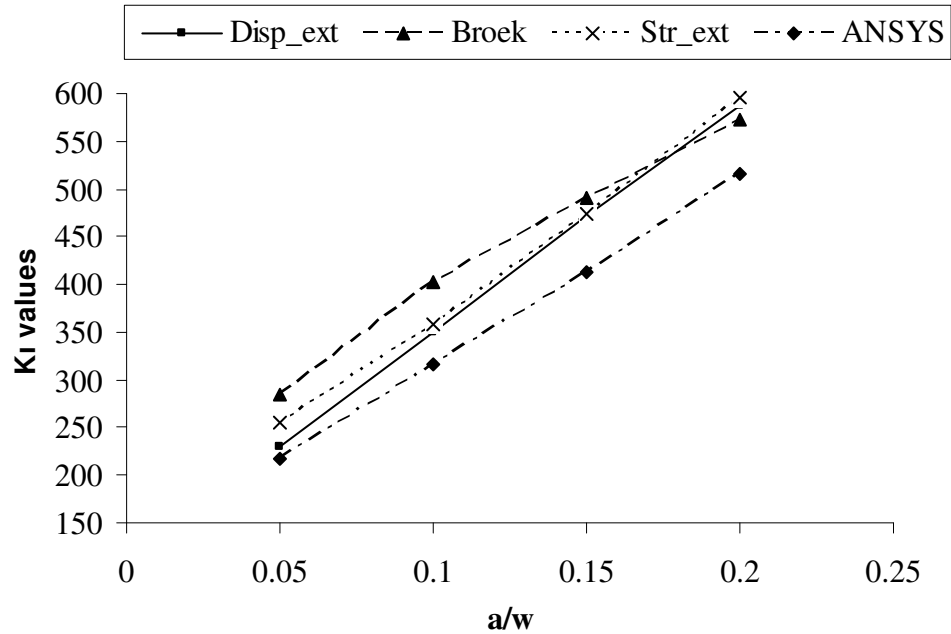


Fig. 5.4 Center cracked model SIF analysis

### 5.2.1.2 Double edge cracked model

The double edge cracked model geometry is shown in Fig.5.5. Due to symmetry, only a quarter of the model has been used (Fig.5.6) in the analysis. The SIF values can be calculated by **Broek (1986)** as:

$$K_I = \sigma \sqrt{\pi a f \left( \frac{a}{w} \right)} \quad (5.2)$$



where

$$f\left(\frac{a}{w}\right) = 1.99 + 0.76\frac{a}{w} - 8.48\left(\frac{a}{w}\right)^2 + 27.36\left(\frac{a}{w}\right)^3$$

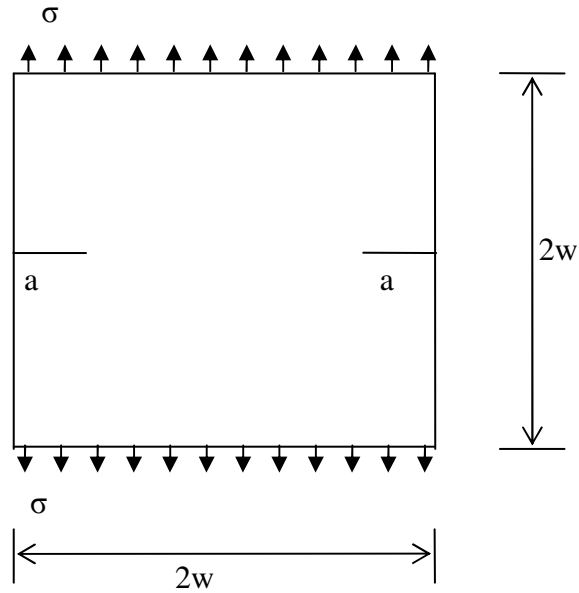


Fig. 5.5 Double edge cracked full geometry

Other analytical formulas given in literature are applied and a graphical representation of  $f(a/w)$  correction factors with 2, 4, 6, and 8 mm crack lengths shown in Fig. 5.7 for the double edge cracked case.

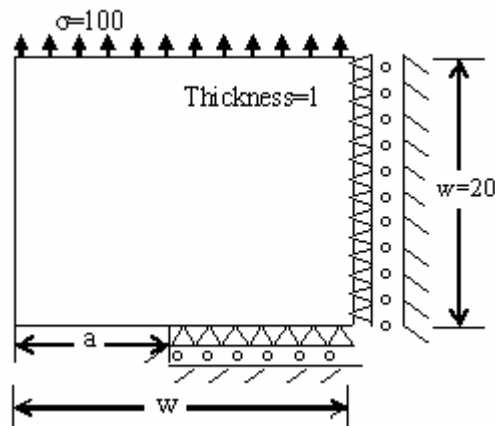


Fig. 5.6 Double edge cracked quarter geometry

### Comparison of correction factor conclusions

A very small deviation is observed for values of **Ewalds and Wanhill (1986)** for  $a/w$  ratio of 0.2 as seen in Fig. 5.7.

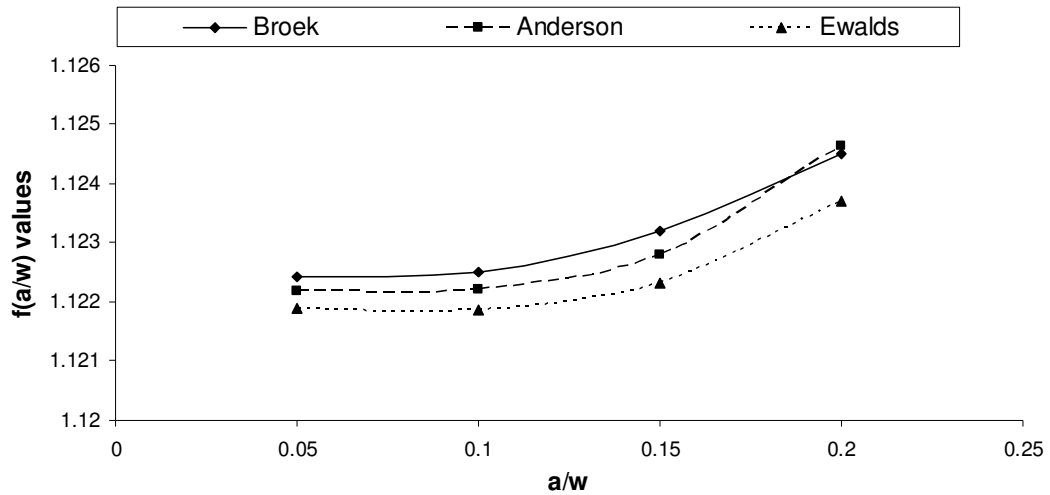


Fig. 5.7 Comparison of correction factors for the double edge cracked model

### Comparison of $K_I$ values conclusions

In the double edge cracked case following material properties are used:

Young's modulus	$E = 80000$ MPa
Poisson's ratio	$\nu = 0.3$
Applied stress	$\sigma = 100$ MPa
Plate width	$w = 20$ mm
Crack length	$a = 2, 4, 6$ and $8$ mm.

The SIF's for the range of crack lengths analyzed as given above, were calculated using Eq. (5.2) and are referred to as the analytical solution. The numerically calculated SIF's were determined using the finite element program. The results for this case are displayed in Fig. 5.8. Results for double edge cracked plate case are in good agreement with those obtained by extrapolation techniques, analytic solution and ANSYS.

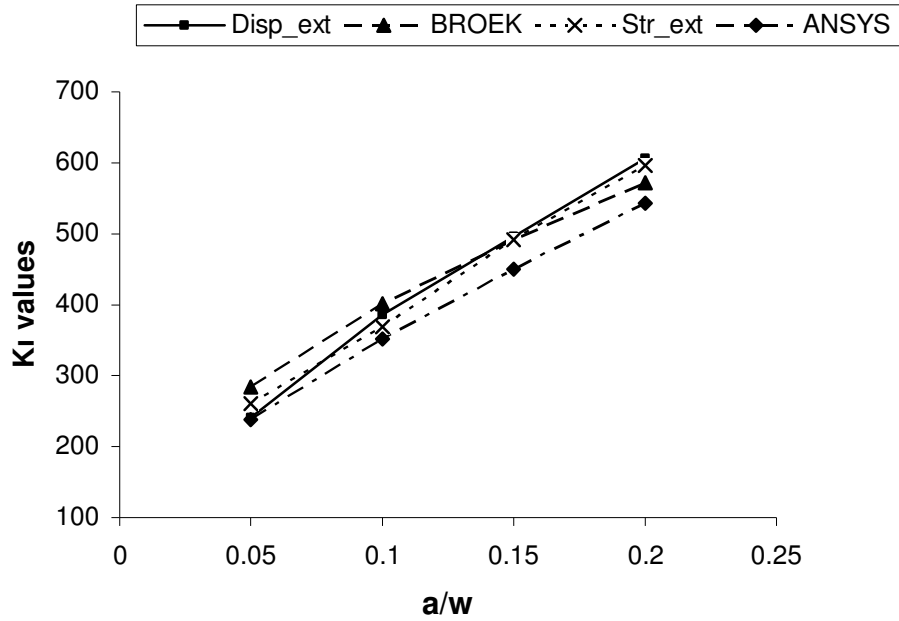


Fig. 5.8 Double edge cracked model SIF analysis

### 5.2.1.3 Single edge cracked model

The single edge cracked model geometry is shown in Fig.5.9. Due to symmetry, half model has been used (Fig.5.10) in the analysis. The SIF values can be calculated by **Broek (1986)** formulae.

$$K_I = \sigma \sqrt{\pi a} f\left(\frac{a}{w}\right) \quad (5.3)$$

where

$$f\left(\frac{a}{w}\right) = 1.99 - 0.41\left(\frac{a}{w}\right) + 18.7\left(\frac{a}{w}\right)^2 - 38.48\left(\frac{a}{w}\right)^3 + 53.85\left(\frac{a}{w}\right)^4$$

The other analytical formulas are applied and a graphical representation of  $f(a/w)$  correction factors with 2, 4, 6, and 8 mm crack lengths shown in Fig. 5.11 for the single edge cracked case.

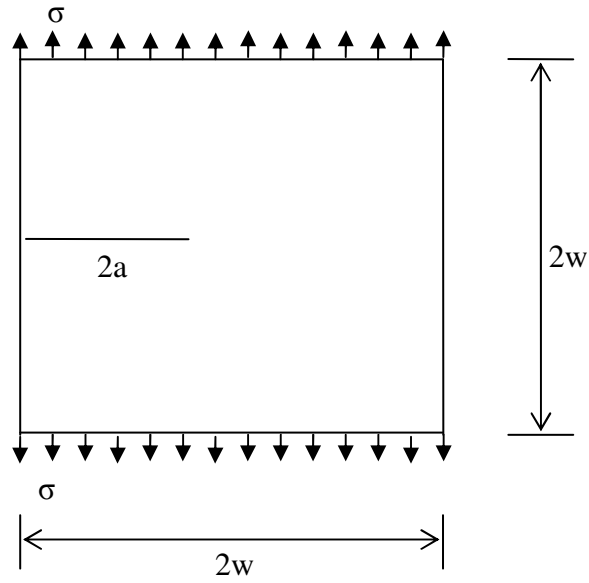


Fig. 5.9 Single edge cracked full geometry

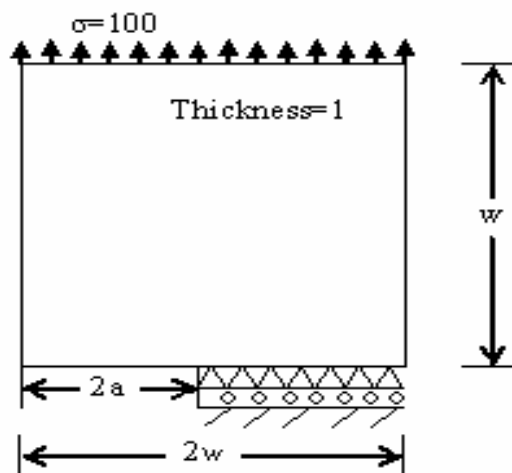


Fig. 5.10 Single edge cracked half geometry

***Comparison of correction factor conclusions***

The correction factors of single edge crack of **Broek (1986)**, **Anderson (1986)** and **Tada et al. (1986)** for  $a/w$  ratio of 0.2 are better than the center and double edge crack results as seen in Fig. 5.11.

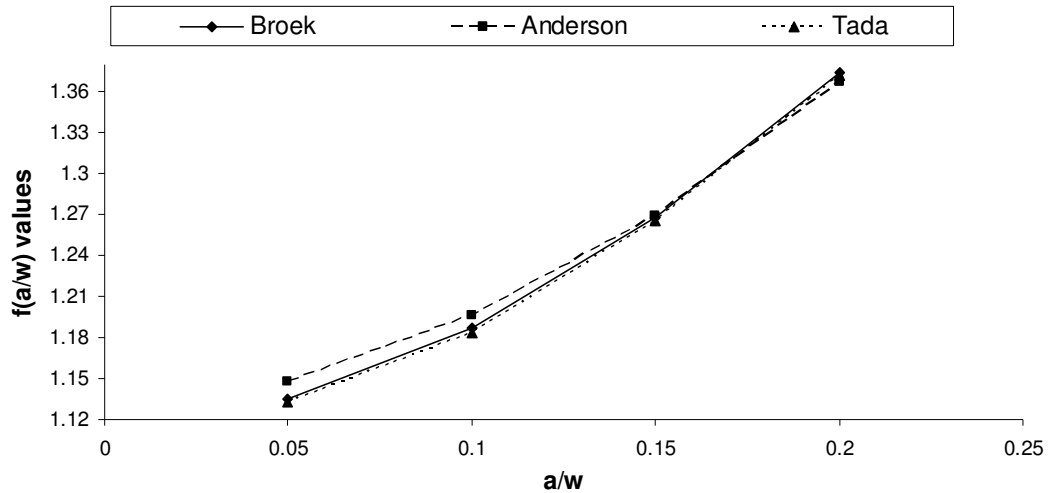


Fig. 5.11 Comparison of correction factors for the single edge cracked model

***Comparison of  $K_I$  values conclusions***

In the single edge cracked case following material properties are used:

- Young's modulus      $E = 80000 \text{ MPa}$
- Poisson's ratio      $\nu = 0.3$
- Applied stress      $\sigma = 100 \text{ MPa}$
- Plate width      $w = 20 \text{ mm}$
- Crack length      $a = 2, 4, 6 \text{ and } 8 \text{ mm.}$

The SIF for the range of crack lengths has been calculated using Eq. (5.3) and then compared with the analytical solution. The numerically calculated SIFs have been determined using the finite element program. The results for this case are presented in Fig. 5.12; inspection of these graphs reveals that the accuracy of the SIF values is acceptable up to  $a/w = 0.15$  for the single edge cracked plate case. After this ratio (0.15), the accuracy is violated and the difference reaches 20% at 0.2 ratios.

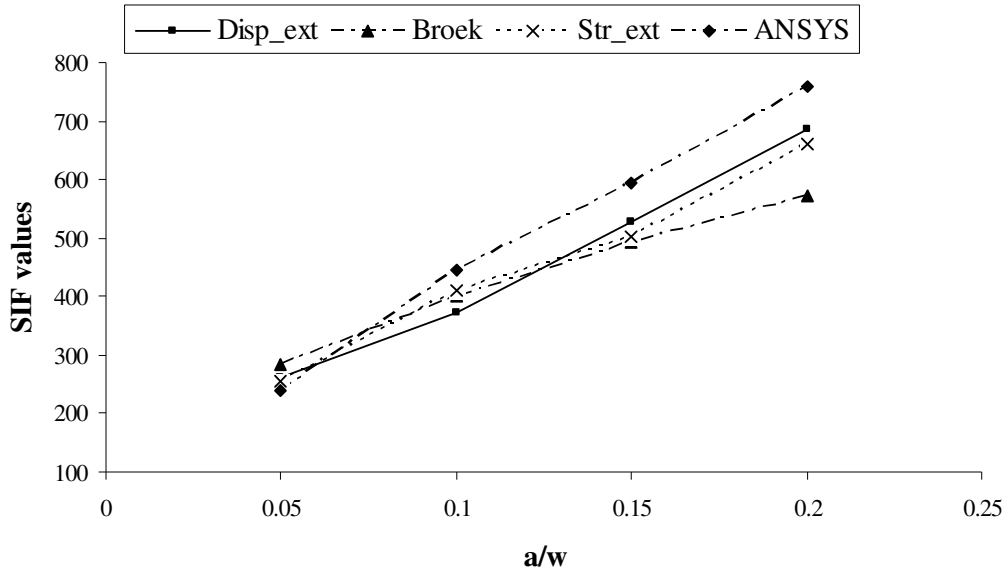


Fig. 5.12 Single edge cracked model SIF analysis

## 5.2.2 Mixed mode loading geometric models

The different cases of crack problems especially using mixed mode loading (single edge crack and off center crack) have been solved with the commercial finite element program ANSYS and with the DEM formulas given in Eqs. (3.31-3.36). Results of these different estimations have been compared with the results of literature [Guinea et al. (2000), Dechaumphai et al. (2003), Gray et al. (2003), Kanninen (1985) and Guzelbey et al. (2004)].

### 5.2.2.1 Single edge cracked model with mixed mode loading

Single edge cracked case with mixed mode loading full geometry and its FE mesh configuration are shown in Figs. 5.13 and 5.14. This single edge cracked case is subjected to a far field shear stress  $\tau = 1$  unit along the top edge and has a crack length  $a=3.5$  units. It is fixed at the bottom edge. Other geometric parameters studied are:  $W=7$  units and  $H=16$  units.

The FE analysis is performed using the modulus of elasticity and the Poisson's ratio values of  $30 \times 10^6$  and 0.25, respectively (Rao and Rahman, 2000). The plane strain and stress conditions are assumed separately in the analysis. The SIFs  $K_I$  and  $K_{II}$  for

this problem have been calculated 34.00 and 4.55 by reference **Rao and Rahman (2000)** respectively. These values are taken as reference values for comparisons.

Several mesh configurations around the crack tip are analyzed, as shown in Fig. 5.15. The mesh used in the analysis consists of 6-node triangular elements for crack region and 8-node quadrilateral elements for the remaining regions.

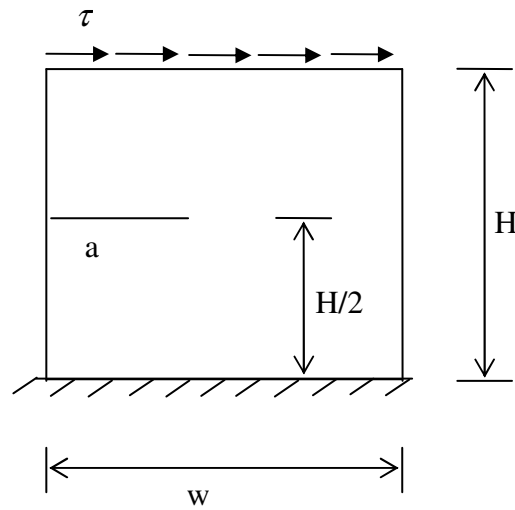


Fig. 5.13 Single edge cracked with mixed mode loading

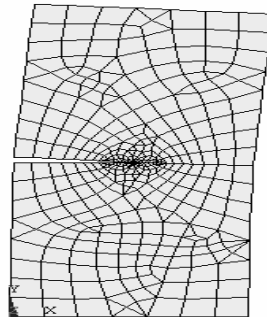


Fig. 5.14 Single edge cracked deformed FE mesh for  $a=3.5$ , (1240 nodes and 499 elements)

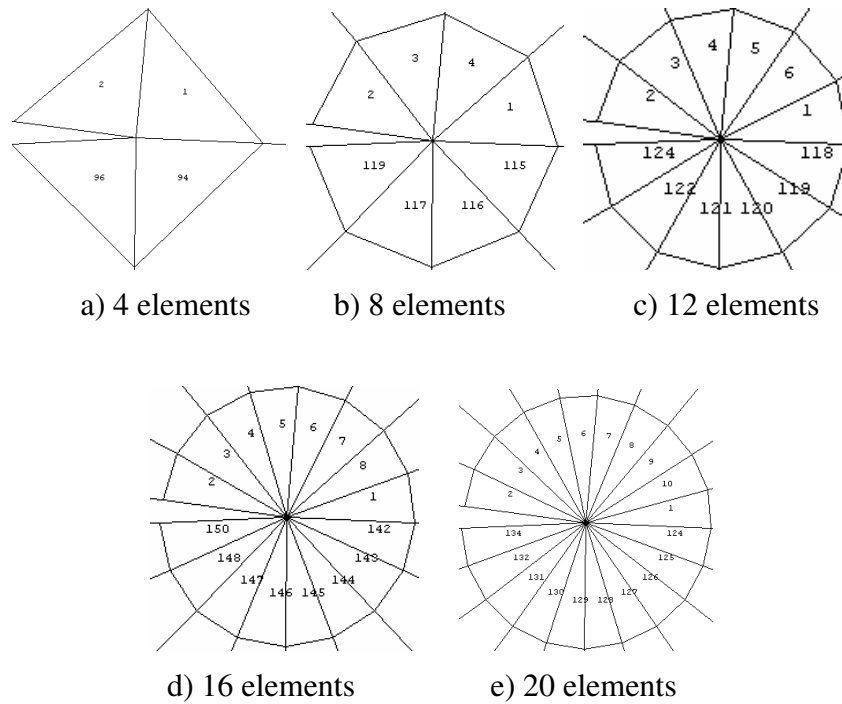


Fig. 5.15 Crack-tip modeling for single edge cracked model

***Influence of the size of the finite elements:***

Effect of the size of the elements on  $K_I$  and  $K_{II}$  are illustrated in Figs. 5.16-5.20 for the single edge cracked geometry. The figures show the results obtained with triangular meshes with element sizes ranging from 0.05 to 0.09  $l/W$  ratios, where  $l$  represents the distance between nodes at the crack tip,  $W$  is the width of the single edge cracked sample and  $n$  is the number of elements around the crack tip. The geometry and FE mesh configuration has been defined in Figs. 5.13 and 5.14.

In Fig. 5.16,  $K_I$  values are obtained using the Eqs. (3.12), (3.14) and (3.16). A regular increase of deviation is observed for  $K_I$  values with  $l/W$  ratio. Variation for Eq. (3.14) and (3.16) takes place at an increased rate compared to Eq. (3.12). Effect of  $n$  on the deviation values are observed to be minor compared to  $l/W$  ratio. Hence smaller  $l/W$  ratio is more suitable for Eqs. (3.14) and (3.16). Fig. 5.17 is used for analysis of effect of  $l/W$  ratio on Eq. (3.12) which is drawn at a decreased scale and only for  $n=12$ . From Fig. 5.17, deviation is nearly equal, about 0.35%, up to 0.07  $l/W$  ratio; after that point an increased deviation is observed.



$K_{II}$  value computed by **Rao and Rahman (2000)** seems to converge properly with the methods analyzed in this thesis. The procedure based on Eq. (3.12) gives rather good results with coarse meshes and simple angular discretizations for  $K_{II}$  values. Effect of mesh size on  $K_{II}$  is examined in Figs. 5.18-5.20.

From the Figs. 5.16-5.20,  $n$  seems to be selected greater than 8. If it is selected to be greater or equal to 12, deviation value observed at close values to each other. Hence, let us investigate figures only for  $n = 12$ . Eq. (3.17), in Fig. 5.20 seems to give exact result for  $l/W=0.05$ . Up to 0.07, error increases only by 0.05%. Beyond this point rapid increase of error is observed.

The largest differences in  $K_I$  and  $K_{II}$  are produced by Eqs. (3.15) and (3.16), where the  $K_I$  has been obtained forcing the  $r^{1/2}$  term of the interpolation function for the singular element to coincide with the theoretical asymptotic expansion and  $K_{II}$  is a first order estimation. In these situations, the accuracy of practical mesh configuration is typically between 2 and 5% for  $K_I$  and  $K_{II}$ .

A local refinement of the mesh in the crack tip zone improved the estimations of  $K_I$  and  $K_{II}$  up to a maximum value for an element size of  $l/W=0.07$ . Beyond this point a coarse mesh may give worse results for both  $K_I$  and  $K_{II}$ . This result may be the main conclusion from the analysis of the meshes for the single edge cracked case.

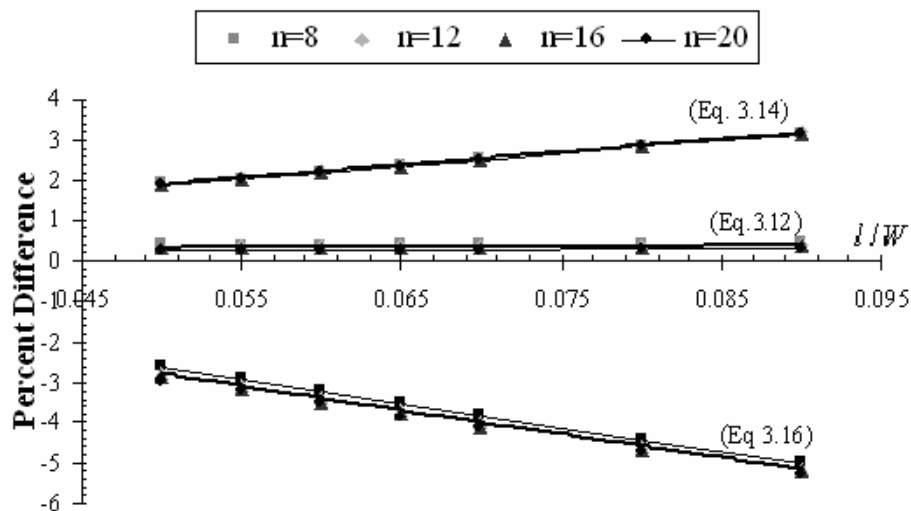


Fig. 5.16 Percent difference of  $K_I$  values for single-edge cracked model as a function of  $n=8, 12, 16$  and  $20$

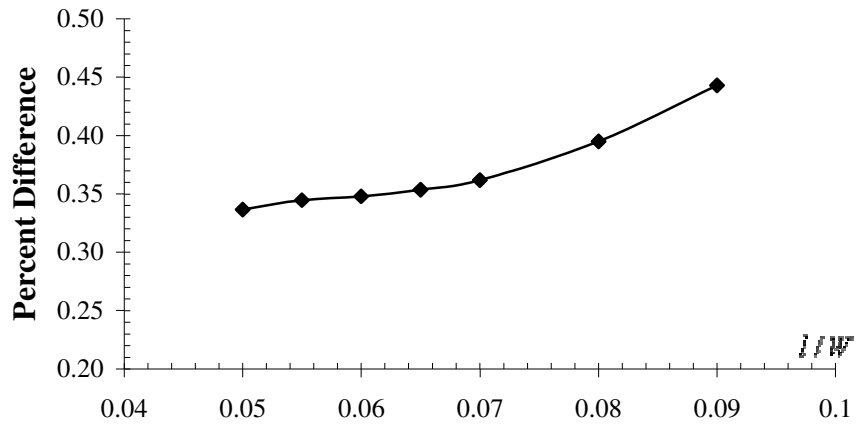


Fig. 5.17 Percent difference of  $K_1$  values for single-edge cracked model with the Eq. (3.12) as a function of  $n=12$

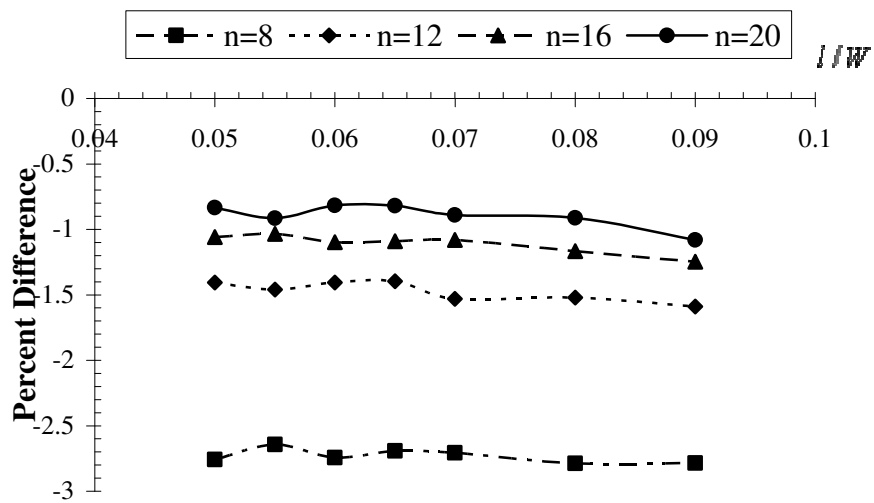


Fig. 5.18 Percent difference of  $K_{11}$  values for single-edge cracked model with the Eq. (3.13) as a function of  $n=8, 12, 16$  and  $20$

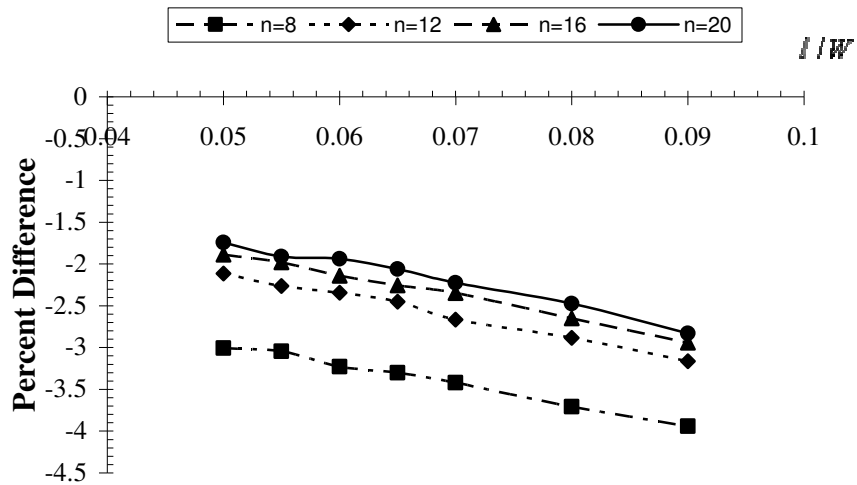


Fig. 5.19 Percent difference of  $K_{II}$  values for single-edge cracked model with the Eq. (3.15) as a function of  $n = 8, 12, 16$  and  $20$

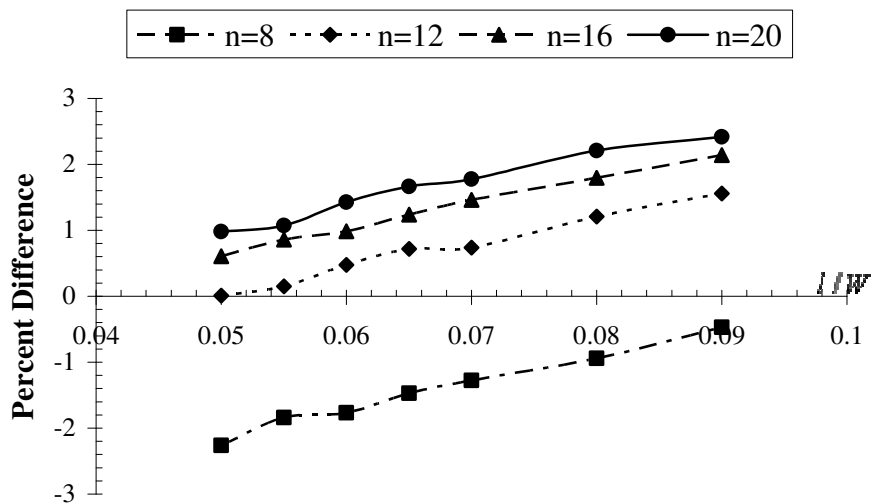


Fig. 5.20 Percent difference of  $K_{II}$  values for single-edge cracked model with the Eq.(3.17) as a function of  $n = 8, 12, 16$  and  $20$

***Influence of stress state and Poisson's ratio***

The stress state is a secondary variable for the mathematical equivalence between the stress field in plane stress and plane strain situations. The plane stress and plane strain's performance depends on the suitable representation of the elastic displacement field. The plane stress and plane strain states are not equivalent except in some very simple loading cases as a result of the numerical approximation.

Poisson's ratio influences can be seen in the computation of  $K_I$  and  $K_{II}$ , and its effect is greater for a plane strain condition from the Figs. 5.21~5.24. Investigating Figs. 5.21~5.24, it is observed that, whatever the stress state is, Eq. (3.12) for Mode I and Eq. (3.17) for Mode II gives the best results.  $n$  is taken as 8 and 12 in these calculations. Almost all cases give better results for  $n=12$ . Comparing Figs. 5.21 and 5.23 for the first mode and Figs. 5.22 and 5.24 for the second mode, in terms of stress state; close values are obtained for  $n=12$ . In Figs. 5.21 and 5.23 the deviation is about 0.25% for the first mode. The deviation value is about 0.5% for the second mode in Figs. 5.22 and 5.24. Another observation from the analyses may be about the effect of Poisson's ratio: Eqs. (3.12) and (3.17) give results with nearly constant deviations for plane stress case. In the case of plane strain again constant deviation is observed in a range of Poisson's ratio from 0 to 0.45. Beyond 0.45 up to 0.49 deviations in  $K_I$  value increases for Eq. (3.12) in Fig. 5.23, but for  $K_{II}$  value, it decreases in that range as observed in Fig. 5.24.

Stress state is another parameter to investigate its effect on the variation of SIF values. In the Fig. 5.25 variation of  $K_I$  and  $K_{II}$  is plotted for different stress states.

In the case of first mode, Fig. 5.25a indicates  $K_I$  value is independent of Stress State and up to Poisson's Ratio of 0.4, beyond this point plane strain situation deviates from plane stress. Hence, especially for metals, using a null Poisson's Ratio is advantageous during calculations. This conclusion was also stated by **Guinea et al. (2000)** for the first mode of fracture.

If Fig. 5.25b is investigated; in the case of second mode, when plane stress belong to the problem handled, again null Poisson's Ratio will give a correct result. But if the plane strain is the case then the exact value of Poisson's Ratio must be used.

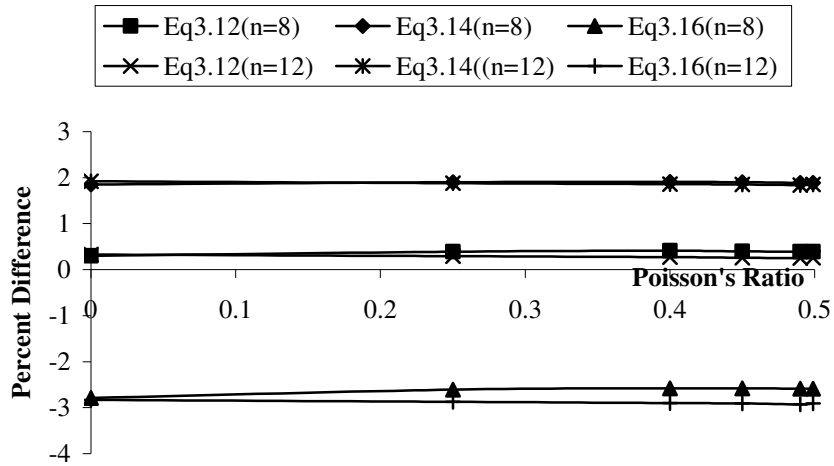


Fig. 5.21 Percent difference of  $K_I$  values for single-edge cracked model as a function of Poisson's ratio and *plane stress* state ( $n = 8$  and 12 elements around the crack tip)

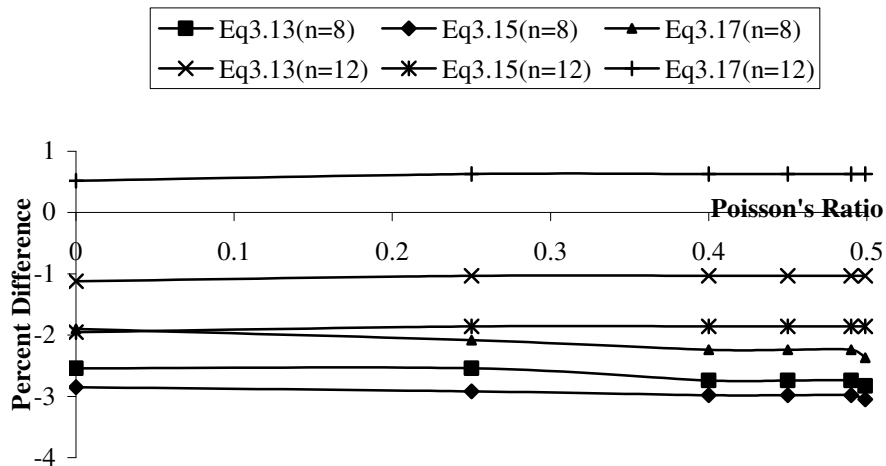


Fig. 5.22 Percent difference of  $K_{II}$  values for single-edge cracked model as a function of Poisson's ratio and *plane stress* state ( $n = 8$  and 12 elements around the crack tip)

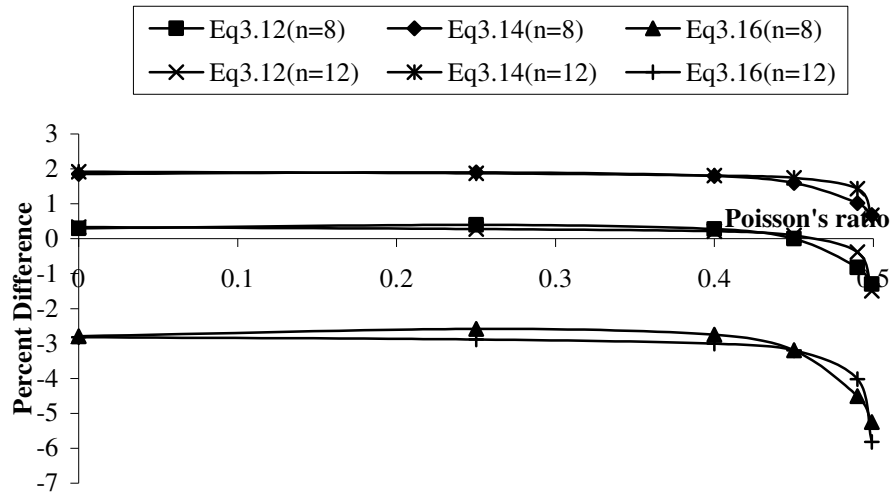


Fig. 5.23 Percent difference of  $K_1$  values for single-edge cracked model as a function of Poisson's ratio and *plane strain* state ( $n = 8$  and 12 elements around the crack tip)

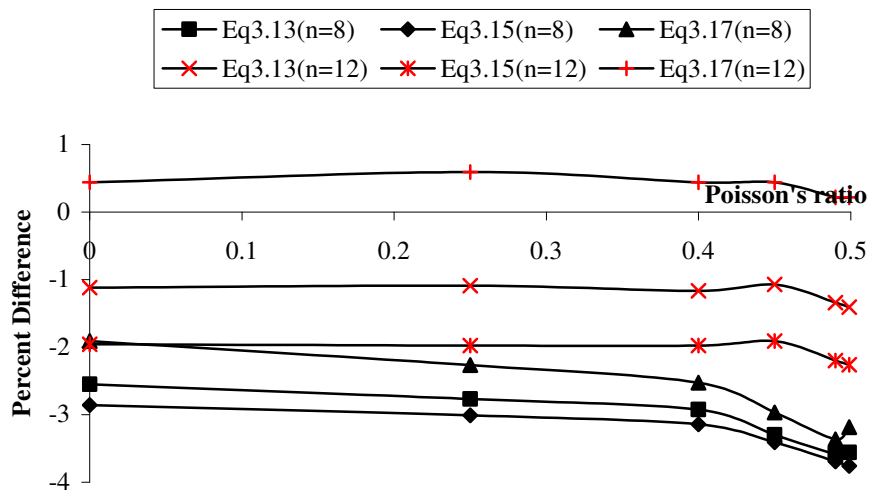
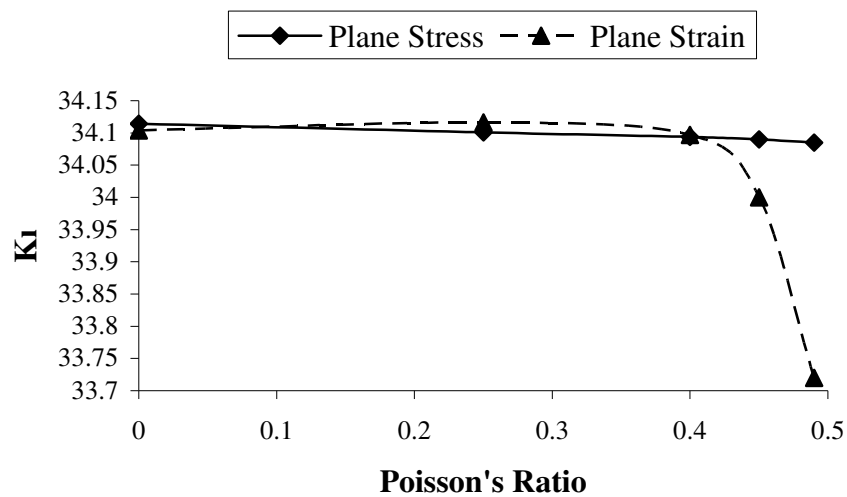


Fig. 5.24 Percent difference of  $K_{11}$  values for single-edge cracked model as a function of Poisson's ratio and *plane strain* state ( $n = 8$  and 12 elements around the crack tip)

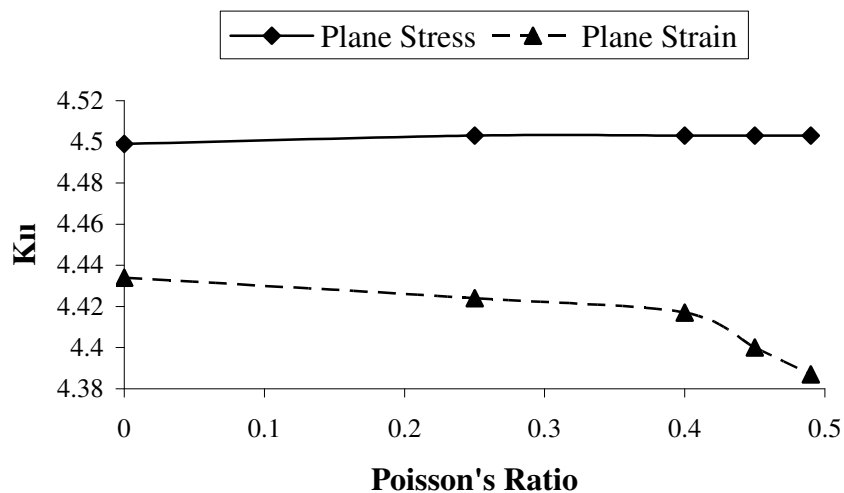
### 5.2.2.2 Off- center cracked model

Off-center cracked example is a mixed mode case in a finite body with a crack whose location and orientation are arbitrary. It has been subjected to the remote uniaxial tension  $\sigma$  applied along the y-axis as shown in Fig. 5.26.

The FE analysis is performed using the modulus of elasticity and the poisson's ratio 0.36 and 0.27 respectively (Gray et al. 2003). The plane strain and stress conditions are assumed separately in the analysis. Numerical results of SIFs, for mode-I and mode-II at both crack tips A and B has been given by reference Gray et al. (2003) for different crack angles with standard and modified crack tip quarter point. Several mesh configurations around the crack tip has been analyzed. The mesh used in the analysis consists of 6-node triangular elements for crack region and 8-node quadrilateral elements for the remaining regions. Some mesh configurations for  $\theta=0^\circ$ ,  $30^\circ$  and  $60^\circ$  can be seen in Figure 5.27.



a) Variation of  $K_I$



b) Variation of  $K_{II}$

Fig. 5.25 Effect of stress state and poisson's ratio on numerical SIF values

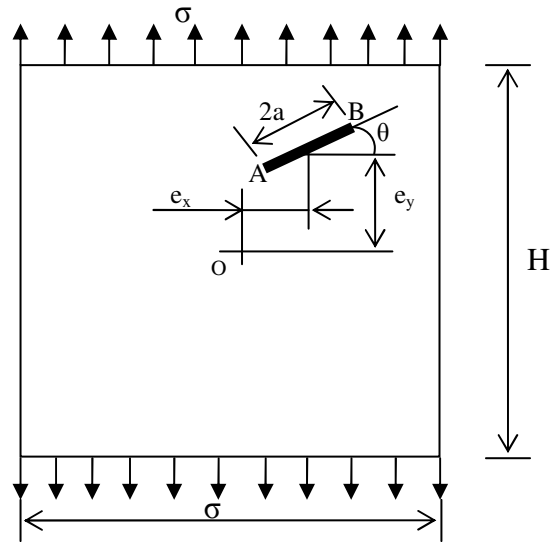


Fig. 5.26 Off-center crack model

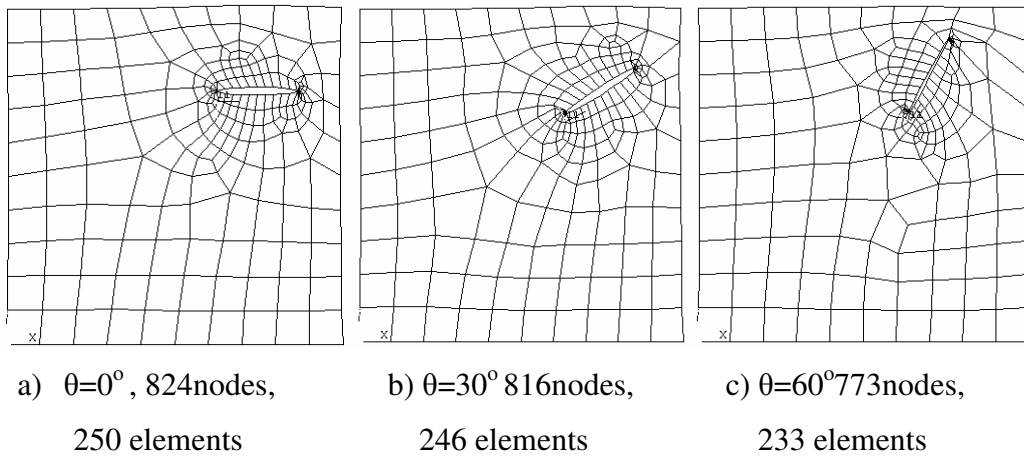


Fig. 5.27 Some FE mesh configurations of off-center crack geometry for  $a=0.5$

***Test calculation with off-center crack example***

A test calculation has been done by using off-center crack example. Its geometrical and some FE configurations can be seen in Figs. 5.26 and 5.27. According to the figures, following geometric data are studied:  $2W=2H=2$ ,  $2a=0.5$ ,  $\nu=0$  and  $e_x = e_y = 0.5$ . The SIFs provided by DEM Eqs. (3.12) and (3.17) and given by references **Gray et al. (2003)** and **Yuanhan (1991)** are compared with each other.



The  $K_I$  and  $K_{II}$  results given in Fig. 5.28 are consistent with the literature (**Gray et al., 2003** and **Yuanhan, 1991**) for the  $\theta=0^\circ, 30^\circ$  and  $60^\circ$  crack angles. The results are changing with a maximum difference of about 2% for  $K_I$  and 3% for  $K_{II}$ , compared to those of references. The differences in the results are considered to be reasonable because different numerical approaches are used in the compared studies.

In most studies,  $K_I$  is considered to be dominant in crack. This assumption is true if the crack is making an angle smaller than  $30^\circ$  with applied load. Fig. 5.28 indicates that, if the angle reaches  $30^\circ$  then  $K_{II}$  value reaches about half of the  $K_I$  which is not a negligible value. After  $60^\circ$ ,  $K_{II}$  becomes the dominant parameter for crack.

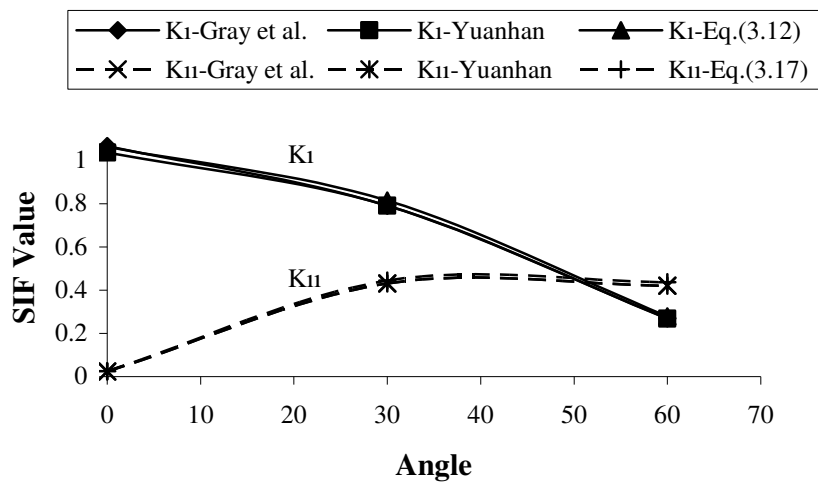


Fig. 5.28  $K_I$  and  $K_{II}$  values for off-center cracked model as a function of angle  $\theta$  ( $0^\circ, 30^\circ, 60^\circ$ )

### 5.3 J-Integral calculations

J integral calculations have been performed to determine the influence of the shape of the paths using center cracked model, to determine the influence of the node numbers on paths using single edge cracked model, to determine the effect of the obtained path shape and node numbers on it using three point bending beam and compact tension specimens.

### 5.3.1 Center cracked model

The center cracked model geometry and its quarter model were shown before in Fig.5.1 and Fig.5.2. But in this model we have used different dimensions to make a comparison with the reference values of **Isida (1971)**.

In this center cracked case, crack lengths are taken as 10, 20, 30, 40, and 50 units, the width,  $w$ , 100 units, and the thickness,  $t$ , 1 unit. Default values of elastic modulus,  $E$ , and poisson's ratio,  $\nu$  are 1 and 0 respectively. The plane stress state is assumed.

The SIF value has been calculated as (**Isida 1971**):

$$K_I = 1.334\sigma\sqrt{\pi a} \quad (5.4)$$

which is claimed to be accurate up to four significant figures.

Paths used in the analysis are shown in Figs. 5.29, 5.30 and 5.31 for  $a/w=0.5$ .

#### 5.3.1.1 Influence of the shape of the paths with center crack example

The effect of the shape of the path on the J-Integral values is illustrated in Tables 5.1-5.5. The tables show the results obtained with circular, rectangular and triangular meshes with crack lengths ranging from 0.1 to 0.5  $a/w$  ratios, where  $a$  represents crack length and  $w$  is the width of the center cracked example. The smallest errors have been observed for  $a/w=0.3$  except for PATH 5.

The results given in Table 5.1 showing that the PATH 1 J-Integral percentage error values for the rectangular and triangular values are on an acceptable level (0-4.7 %) but the circular path values are comparatively large (0-7.3 %).

In Tables 5.2, 5.3, 5.4 and 5.5, the percent errors of PATH 2, PATH 3, PATH 4 and PATH 5 are between 0-2 percent. All of them are smaller than PATH 1. Although

PATH 2 has the highest error among the PATH 2, 3, 4 and 5, it is still on an acceptable level.

The percent error,  $\epsilon_k$  is calculated as  $\epsilon_k (\%) = 100 \times \frac{K_I - K_{I,Isida}}{K_{I,Isida}}$

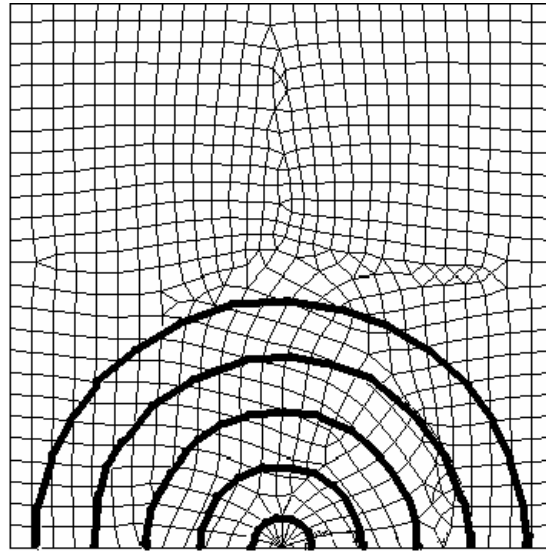


Fig. 5.29. Circular paths for center crack example with  $a/w=0.5$  ratio

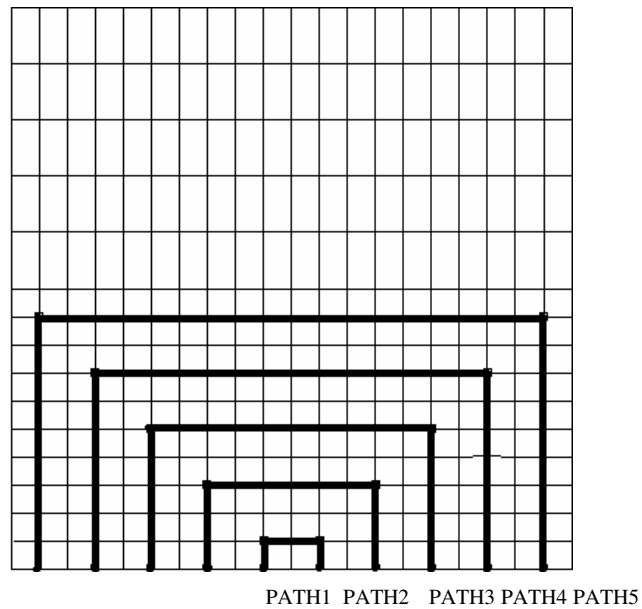


Fig. 5.30. Rectangular paths for center crack example with  $a/w=0.5$  ratio

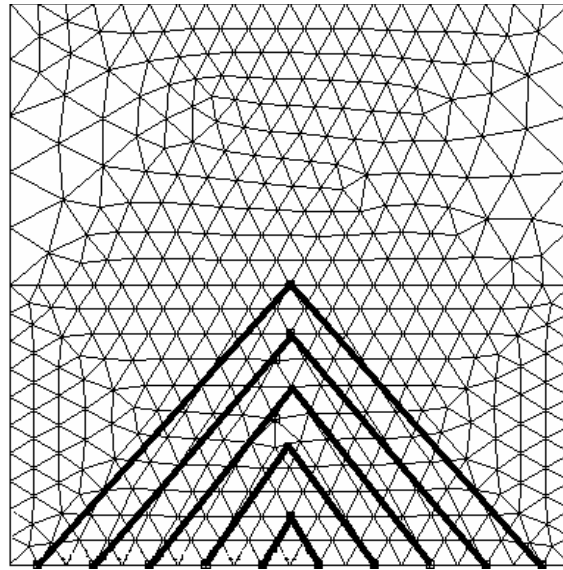


Fig. 5.31. Triangular paths for center crack example with  $a/w=0.5$  ratio

Table 5.1 Percent error of PATH 1 J-Integral values with different paths

a/w	ANSYS	circular	rectangular	Triangular
0.1	-0.55624	7.323857	2.719407	-1.48331
0.2	-0.3176	6.424137	-4.74953	-3.04605
0.3	0.312976	6.841482	-0.18609	3.535781
0.4	-0.15028	7.304637	-2.67819	-1.57793
0.5	0.296927	7.129825	-1.03388	-0.99381

Table 5.2 Percent error of PATH 2 J-Integral values with different paths

a/w	ANSYS	circular	rectangular	Triangular
0.1	-0.55624	-0.55624	-0.18541	-0.92707
0.2	-0.3176	0.014436	-1.45806	-1.68904
0.3	0.312976	0.135341	-0.38911	-0.52445
0.4	-0.15028	-0.20395	-1.57793	-2.0234
0.5	0.296927	0.003577	-0.92656	-1.35585

Table 5.3 Percent error of PATH 3 J-Integral values with different paths

a/w	ANSYS	circular	rectangular	Triangular
0.1	-0.55624	-0.74166	-1.23609	-1.3597
0.2	-0.3176	0.418652	-1.60243	-1.83341
0.3	0.312976	0.439858	-0.05921	-0.2876
0.4	-0.15028	-0.03757	-1.34178	-1.65307
0.5	0.296927	0.118055	-0.86216	-1.00812

Table 5.4 Percent error of PATH 4 J-Integral values with different paths

a/w	ANSYS	circular	rectangular	triangular
0.1	-0.55624	-0.86527	-0.74166	-0.92707
0.2	-0.3176	0.591887	-1.58799	-1.77566
0.3	0.312976	0.482152	-0.30452	-0.10151
0.4	-0.15028	-0.20395	-0.62258	-0.95535
0.5	0.296927	-0.09945	-0.28262	-0.61174

Table 5.5 Percent error of PATH 5 J-Integral values with different paths

a/w	ANSYS	circular	rectangular	Triangular
0.1	-0.55624	-0.55624	1.545117	0.185414
0.2	-0.3176	0.822867	-0.9961	-1.68904
0.3	0.312976	0.490611	-0.65979	-0.94739
0.4	-0.15028	-0.33276	-0.61185	-0.92314
0.5	0.296927	-0.08944	0.261153	-0.00358

### 5.3.2 Single edge cracked model

The single-edge cracked model geometry and its half model were shown before in Figs. 5.9 and 5.10. The dimensions used in this case are different to make a comparison with the reference of **Murakami (1987)**.

The single edge cracked case has a crack length,  $a$ , the width,  $b$  and the thickness  $t$ , 0.5, 1 and 1 respectively. As we said before the default values of  $E$  and  $\nu$ , 1 and 0 respectively with plane stress state assumption have been used.

The SIF has been calculated by **Murakami (1987)** as:

$$K_I = f\left(\frac{a}{w}\right)\sigma\sqrt{\pi a} \quad (5.5)$$

$$f\left(\frac{a}{w}\right) = 1.12 - 0.231\left(\frac{a}{w}\right) + 10.55\left(\frac{a}{w}\right)^2 - 21.72\left(\frac{a}{w}\right)^3 + 30.39\left(\frac{a}{w}\right)^4$$

### 5.3.2.1 Influence of the node numbers on paths with single edge crack example

The analyses have been repeated with 9-11-13-15-17-19 nodes on circular paths, 4-6-8-10-12-14 nodes on rectangular paths and 3-5-7-9-11-13 nodes on triangular paths (Figs. 5.32, 5.33, and 5.34). In these analyses  $a/w=0.3$  has been used.

Fig. 5.35 shows that the increase of node numbers on circular path has a slight positive effect up to 19 nodes. This positive effect is approximately 0.3 % and does not cause a significant change in J-Integral values. However the percent error is seriously decreasing with a decreasing number of nodes on rectangular (4 nodes) and triangular paths (3 nodes) (Figs. 5.36 and 5.37).

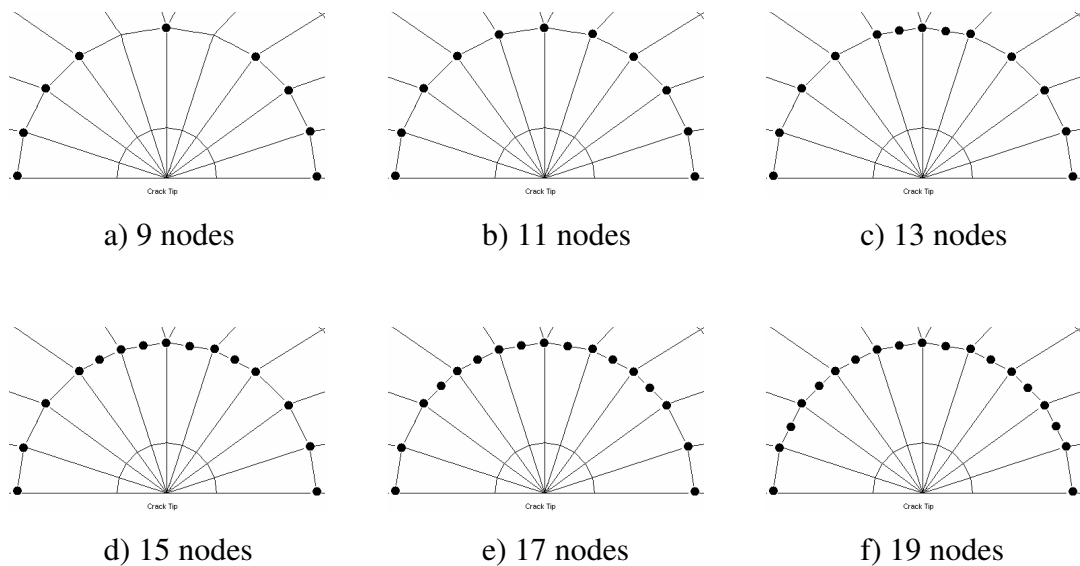


Fig.5.32 Number of nodes used in circular paths

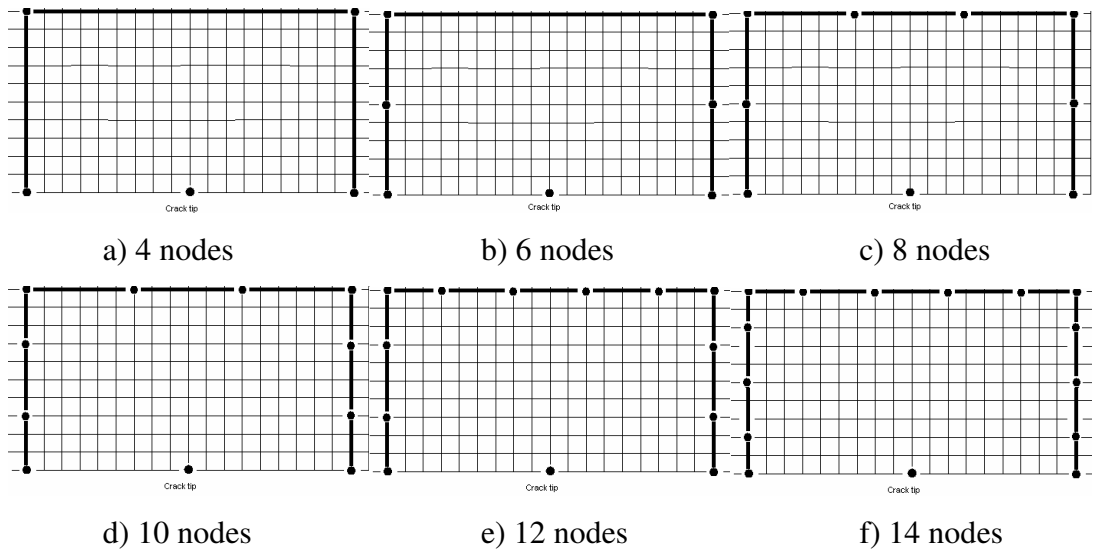


Fig.5.33 Number of nodes used in rectangular paths

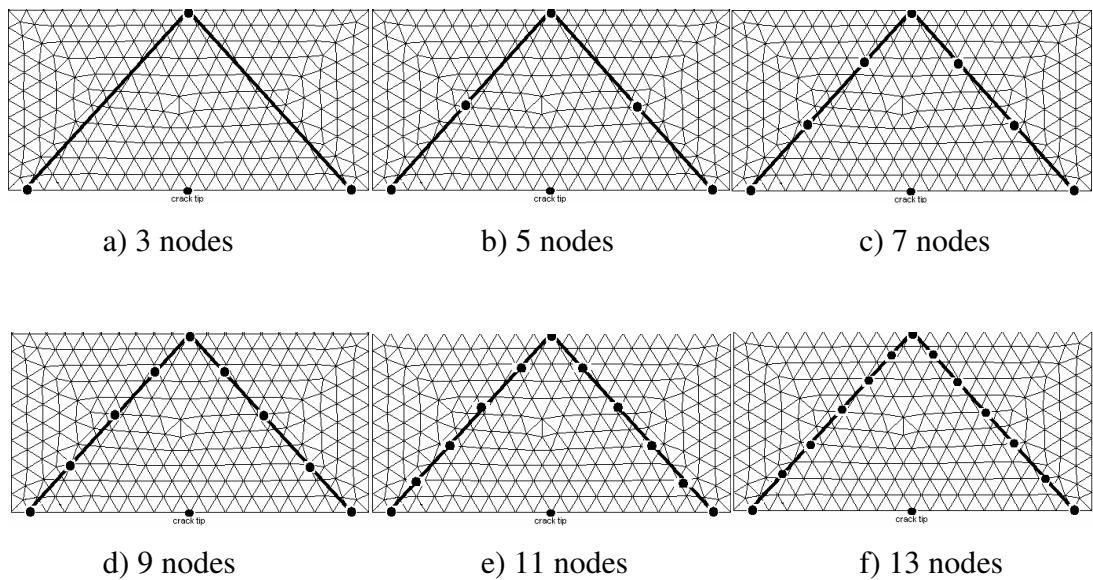


Fig.5.34 Number of nodes used in triangular paths

The analyses have been done with coarse and fine meshes for the same node numbers on paths. 943 nodes and 298 elements, 910 nodes and 280 elements and 811 nodes and 370 elements have been used with circular, rectangular and triangular paths respectively for coarse meshes. 3601 nodes and 1160 elements, 3497 nodes and 1120 elements and 6241 nodes and 3052 elements have been used with circular, rectangular and triangular paths respectively for fine meshes. The results are shown in Figs. 5.35, 5.36 and 5.37.

All the percent errors are on an acceptable level. But the finer mesh models give better results. The circular path is more accurate than triangular and rectangular paths.

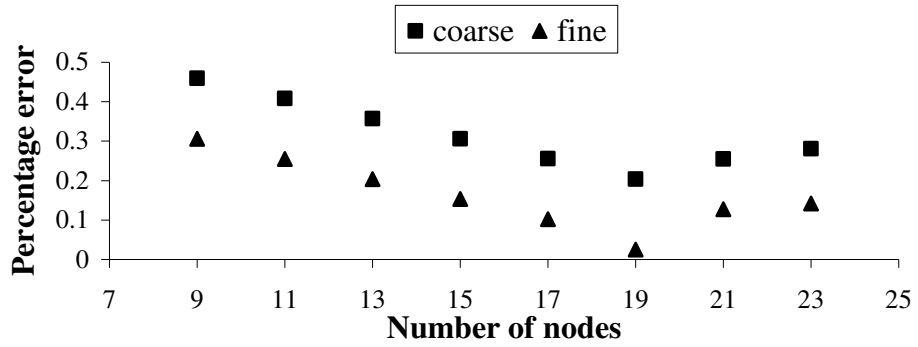


Fig.5.35 Percent error of J-Integral for circular path

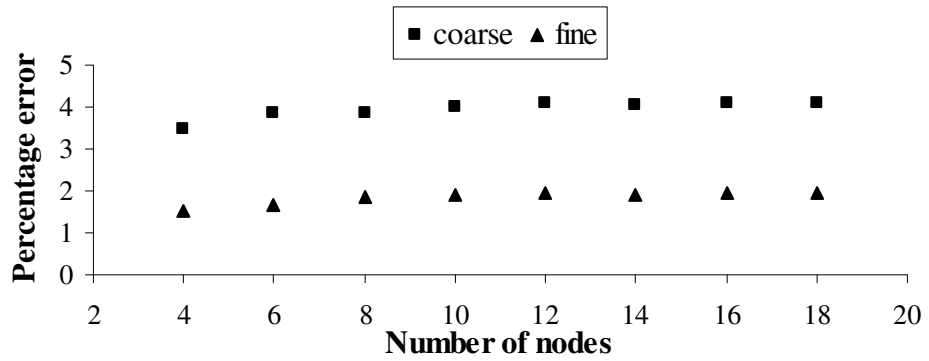


Fig.5.36 Percent error of J-Integral for rectangular path

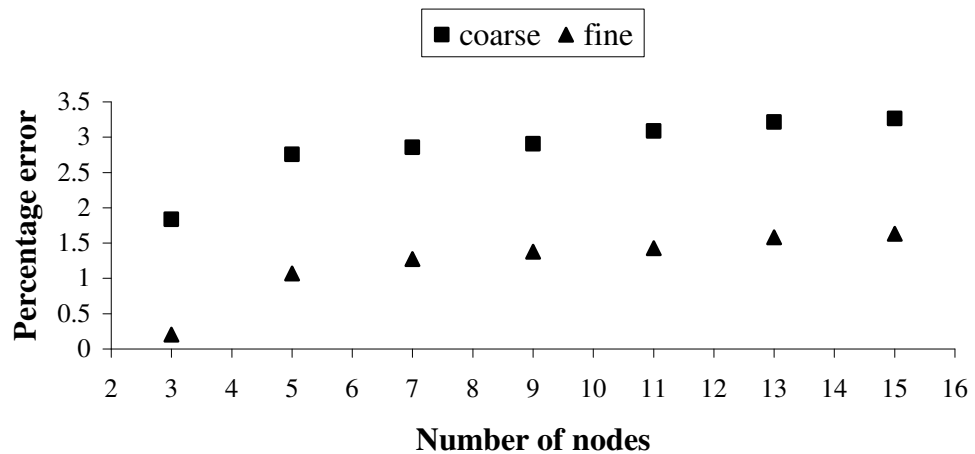


Fig.5.37 Percent error of J-Integral for triangular path



### 5.3.3 Three point bending beam

The three-point bending beam with a span-to-depth ratio of four is a test geometry shown in Fig.5.38. A half of the model was used (Fig. 5.39). The SIF was calculated by **Srawley (1976)** as:

$$K_1 = 1.775 \frac{6F}{B\sqrt{D}} \quad (5.6)$$

This case has a crack length,  $a$ , the width  $S$  and the height,  $D$ , 50, 400 and 100 respectively. An  $a/D$  ratio of 0.5 has been used with a unit thickness.

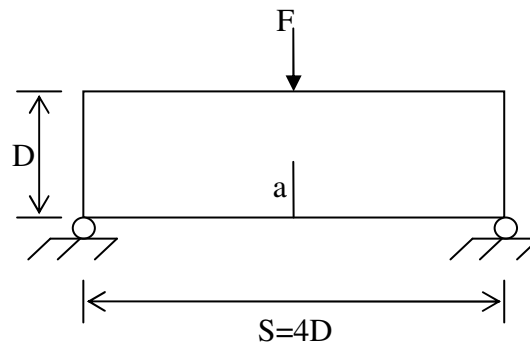


Fig.5.38 Three point bending beam; full model

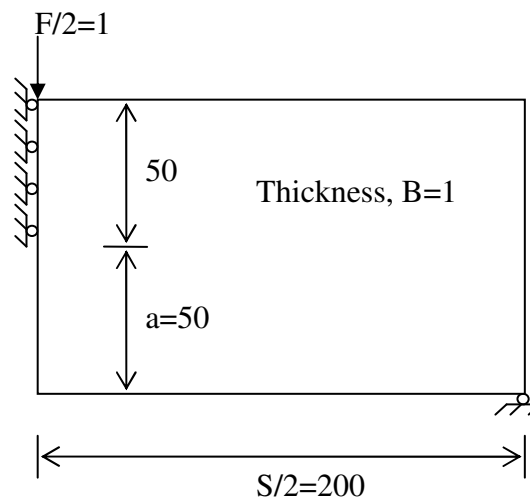


Fig.5.39 Three point bending beam; half model

### 5.3.4 Compact tension specimen

The compact tension specimen is the second test geometry shown in Fig.5.40. Half of the model has been used (Fig.5.41). The SIF was calculated by **Murakami (1987)** as:

$$K_I = P \left( 2 + \frac{a}{w} \right) \left( 0.886 + 4.64 \left( \frac{a}{w} \right) - 13.32 \left( \frac{a}{w} \right)^2 + 14.72 \left( \frac{a}{w} \right)^3 - 5.6 \left( \frac{a}{w} \right)^4 \right) / \sqrt{w} \left( 1 - \frac{a}{w} \right)^{3/2} \quad (5.7)$$

The specimen has a crack length,  $a$ , 3mm, the width,  $w$ , 50.8mm, and the thickness,  $t$ , 1 mm. Plane stress condition is used. The modulus of elasticity,  $E$  and Poisson's ratio,  $\nu$ , are chosen  $30 \times 10^6$  Pa and 0.25 respectively (**Murakami, 1987**).

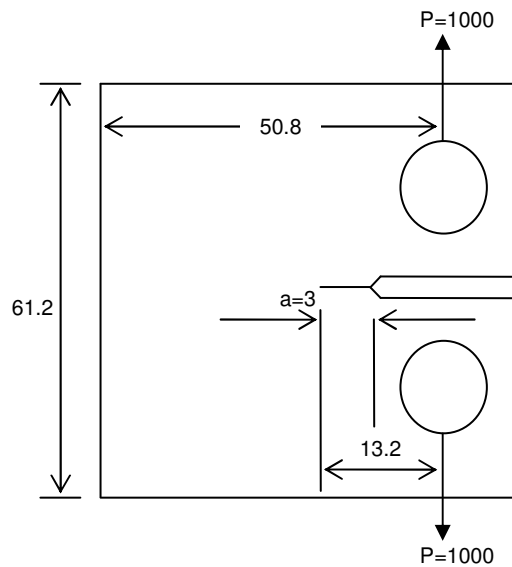


Fig.5.40 Compact tension specimen model

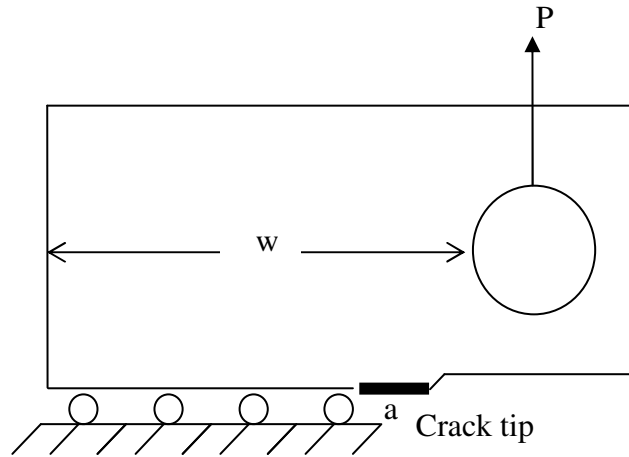


Fig.5.41 Compact tension specimen half model

### 5.3.5. J-Integral path effect on the test calculations

The obtained results for the convenient path (PATH 2 for circular paths with 19 nodes and PATH 2 for rectangular and triangular paths with 4 and 3 nodes respectively) are applied to two well known fracture problems: the compact tension and three point bending example. The geometrical and material properties are given in sections 5.3.3 and 5.3.4 and Figs. 5.38~5.41. The results are compared with ANSYS and literature.

It can be seen from tables 5.6 and 5.7 that the obtained results for circular path are in good agreement with the literature and ANSYS. The results of triangular and rectangular paths are also on an acceptable level.

Table 5.6 Compact tension specimen

J-Integral values of different paths				
Murakami (1987)	ANSYS	circular	rectangular	triangular
0.0156	0.0158	0.0159	0.0162	0.0169

Table 5.7 Three point bending specimen

J-Integral values of different paths(*10 <sup>-8</sup> )				
Srawley (1976)	ANSYS	circular	rectangular	triangular
3.544	3.467	3.455	3.426	3.398

#### 5.4. SIF formulations using artificial intelligence techniques

The prediction and formulation of  $K_I$  values for varying geometries using NNs and GP based FE (ANSYS) has been carried out.

Analytical solution and numerical analysis (DEM) have been applied to determine the SIF of the three well known geometries: the center cracked, the double edge cracked and the single edge cracked models. The crack geometries are given in Fig. 5.42.

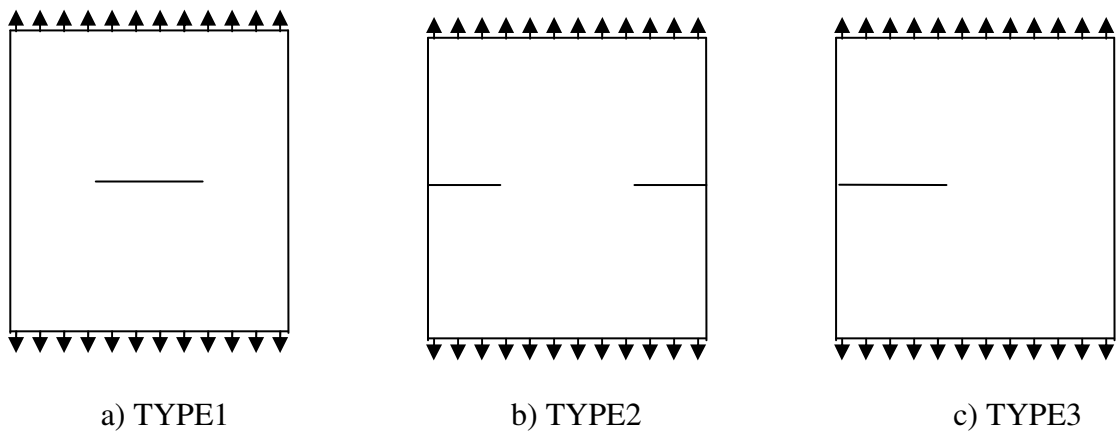


Fig. 5.42 Types of the crack geometries (Kutuk M.A. et al., 2007)

All of the three models have dimensions with [20\*20, 40\*40, 60\*60 and 80\*80] mm cross sections and 1mm thickness. The SIF values for a series of crack lengths are determined (for  $a=2, 3, 4, 5$  and 6 mm). Rectangular eight-node isoparametric and six-node elements are used for the configurations with the following material properties and loading:

$$E = 80000 \text{ N/mm}^2,$$

$$\nu = 0.3$$

$$\sigma = 60, 80, 100 \text{ and } 120 \text{ N/mm}^2.$$

Plane stress state is assumed and three-point Gaussian numerical integration has been used in the analysis.

The center cracked geometry is shown in Fig. 5.43a. Quarter symmetry is used in modeling as shown in Fig. 5.43b. The SIF for the opening mode  $K_I$  is calculated by the reference of **Broek (1986)** given in Eq. (5.1).

Finite element fine mesh configuration of the center cracked case is shown in Fig. 5.43c for 2mm crack length. In addition, 1477 nodes and 472 elements for 3mm crack length, 1516 nodes and 485 elements for 4mm crack length, 1530 nodes and 489 elements for 5mm crack length and 1470 nodes and 469 elements for 6mm crack length have been used in FE mesh configurations.

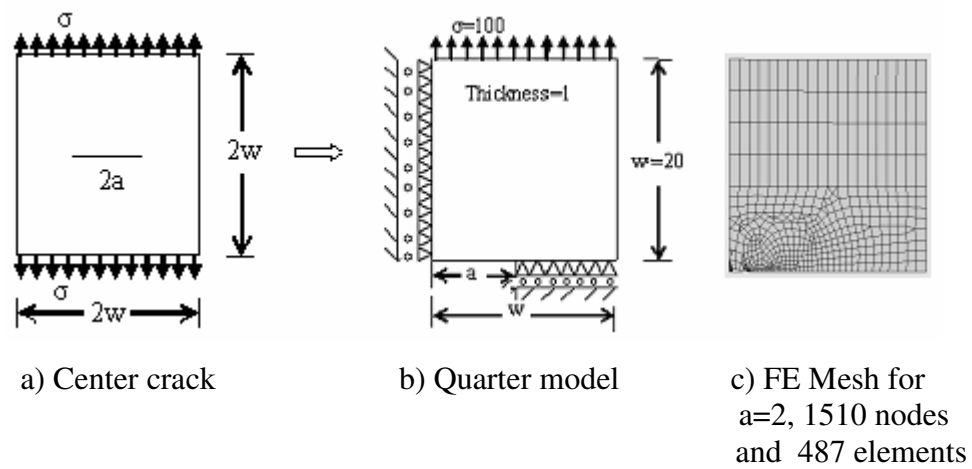


Fig. 5.43 Center cracked model geometry

The double cracked geometry is shown in Fig. 5.44a. Due to the symmetry, only a quarter of the geometry is used, as shown in Fig. 5.44b. SIF for the opening mode ( $K_I$ ) is given by **Broek (1986)** in Eq. (5.2)

Finite element fine mesh configuration of the double edge cracked case is shown in Fig. 5.44c for 2mm crack length. The same numbers of nodes and elements have been used in FE mesh configurations for 3, 4, 5, and 6mm crack lengths.

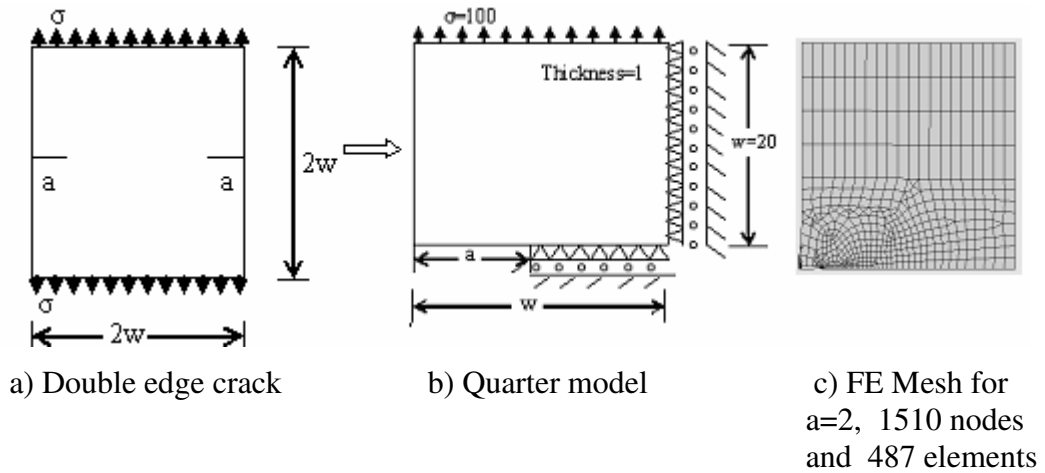


Fig. 5.44 Double edge cracked model geometry

In the single cracked case half symmetry was used for modeling, with only the displacement restrained in the x direction (shown in Fig. 5.45a and Fig.5.45b. The analytical solution is given by **Broek(1986)** in Eq. (5.3).

Finite element fine mesh configuration of the single cracked case is shown in Fig. 5.45c for 2mm crack length. In FE mesh configurations for 3mm crack length, 3384 nodes and 1093 elements, for 4mm crack length, 3465 nodes and 1124 elements, for 5mm crack length, 3247 nodes and 1048 elements, and for 6mm crack length, 3253 nodes and 1052 elements have been used.

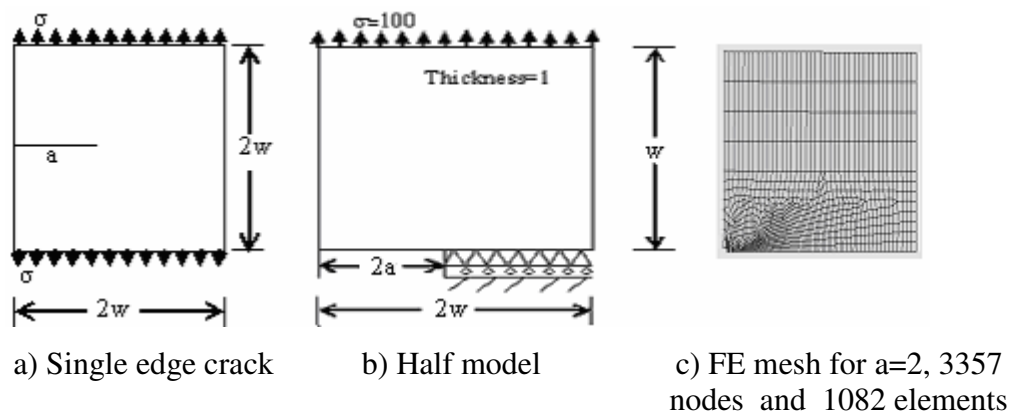


Fig. 5.45 Single cracked model geometry

The FE analysis is performed using the same material properties and mesh configurations given for the numerical analysis. The mesh used in the analysis

consists of triangular elements for crack region and 8-node quadrilateral elements for the remaining regions (i.e.PLANE82 type element in ANSYS).

#### 5.4.1 Neural Networks formulation of SIF

FE results are divided into train and test sets where patterns in the test set are randomly selected among the experimental database shown in bold characters given in Table A1. The training patterns for NNs have been obtained using ANSYS FE software package. A wide range of variables are chosen to represent a general model for NN with a data set of 167 training patterns and 25 testing patterns. The optimal NN architecture was found to be 4-11-1 architecture with hyperbolic tangent sigmoid transfer function (tansig). The training algorithm was quasi-Newton backpropagation (BFGS). All necessary neural procedures are performed by MATLAB NN Toolbox. The statistical parameters and performance of training and test sets for the  $K_I$  are given in Table 5.8 and Fig.5.46. It has been seen that the errors are quite satisfactory for each case for test set and training sets.

Table 5.8 Statistical parameters of the NN used for  $K_I$

	Training set	Test set
MAPE ( % ) (Mean absolute % Error)	2.5	3,8
Mean (Test/ FE)	1.0025	1.0052
$R$ (%)	99.98	99.92
COV	0.041	0,038

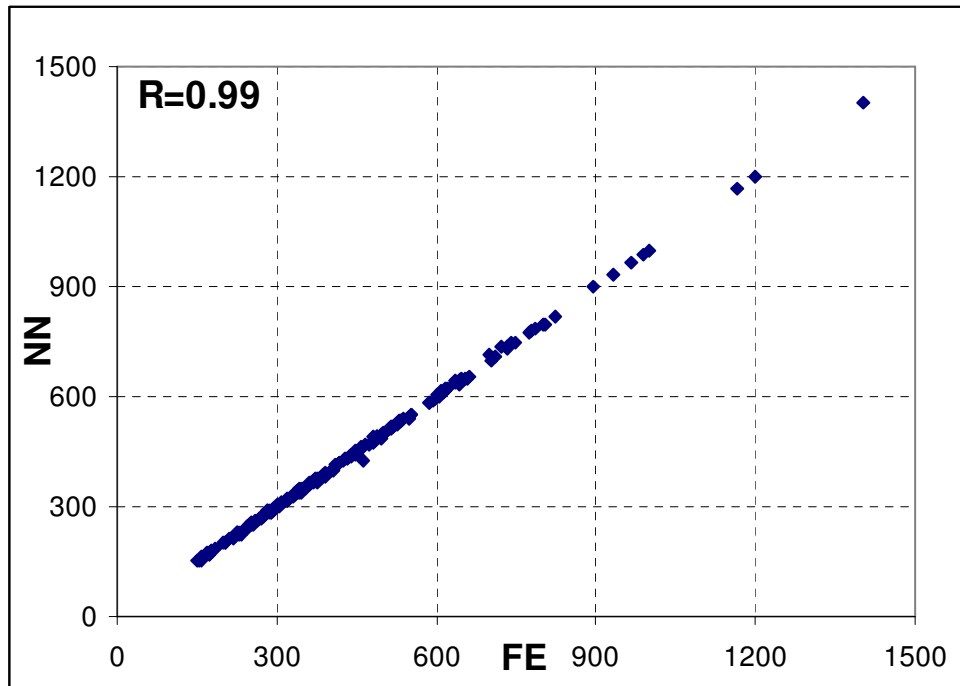


Fig. 5.46 Performance of NN results vs. FE results

The trained NN in the present study does not serve as a black box anymore as it is considered in most of the NN . It is an independent program to compute  $K_I$  values for three different geometries for a given set of  $\sigma_{applied}$  ,  $a$  ,  $w$  , and  $Type$  values as shown in Fig.5.47.

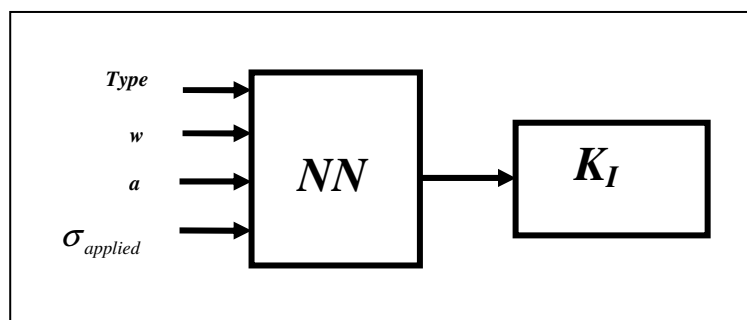


Fig.5.47 NN Model for  $K_I$  calculation

Furthermore it is actually an explicit formulation that computes directly the SIF for three different geometries which is given as a function of some fracture parameters:



$$K_I = f(\sigma_{\text{applied}}, a, w, \text{Type}) \quad (5.8)$$

where,  $\sigma_{\text{applied}}$  is the applied stress,  $a$  is the crack length,  $w$  is the plate width. *Type 1* is for the Center cracked geometry, *Type 2* is for the Double cracked geometry and *Type 3* is for the Single cracked geometry which was shown in Fig.5.42.

It should be noted that the input parameters have been normalized by  $\sigma^*/120$ ;  $a^*/10$ ;  $w^*/80$ ;  $\text{type}^*/3$ , where  $\sigma^*$ ,  $a^*$ ,  $w^*$  and  $\text{type}^*$  are the initial values of applied stress, crack length, plate width and type of the geometry respectively. The output in the NN model is normalized by 5.

$K_I$  values of the three types of geometries can be obtained as the final output given as:

$$\text{SIF} = \frac{1500}{1 + e^{(A+B+C+D+E+F+G+H+I+J-4.605)}} \quad (5.9)$$

where

$$A = \left[ \frac{-0.244}{1 + e^{(-1.8\sigma - 11.9316a + 7.9829w - 3.2604\text{Typ} - 0.4924)}} \right]$$

$$B = \left[ \frac{-9.0276}{1 + e^{(0.3481\sigma + 0.5379a + 2.003w - 4.2190\text{Typ} - 4.554)}} \right]$$

$$C = \left[ \frac{-3.6166}{1 + e^{(2.043\sigma + 4.299a - 6.5471w + 3.4896\text{Typ} - 5.1108)}} \right]$$

$$D = \left[ \frac{6.9278}{1 + e^{(-0.37091\sigma + 4.4105a + 1.1457w - 0.8999\text{Typ} + 1.9105)}} \right]$$

$$E = \left[ \frac{-2.0821}{1 + e^{(-2.5539\sigma - 1.6284a - 1.453w + 0.8030\text{Typ} + 4.2783)}} \right]$$

$$F = \left[ \frac{2.9283}{1 + e^{(4.2693\sigma - 0.18729a + 0.25676w - 0.2219\text{Typ} - 0.6339)}} \right]$$

$$G = \left[ \frac{14.7994}{1 + e^{(1.5389\sigma + 2.6326a - 4.0914w + 2.3096\text{Typ} - 4.8723)}} \right]$$

$$H = \left[ \frac{3.7636}{1 + e^{(0.97228\sigma + 5.1834a - 13.0414w - 19.4780\text{Typ} + 1.5278)}} \right]$$

$$I = \left[ \frac{1.8144}{1 + e^{(0.16825\sigma + 3.1168a + 1.0347w + 10.249Typ - 1.1797)}} \right]$$

$$J = \left[ \frac{-0.44753}{1 + e^{(2.6006\sigma - 6.936a + 17.0891w - 8.6196Typ + 4.9684)}} \right]$$

Using Eq. (5.9) it is now possible to calculate the exact SIF values for a crack of any of the three types existing on a plate of finite dimensions.

The center, double and single edge crack cases are solved with the commercial finite element program ANSYS, DEM developed in this study and the explicit formulation (Eq. 5.9) obtained using ANN (**Kutuk M.A. et al., 2007**). The results of the three different methods are compared with the results of analytical formula proposed by **Broek (1986)** in Figs. 5.48, 5.49 and 5.50.

#### 5.4.2 Genetic Programming formulation of SIF

FE results are divided into train and test sets where patterns in test set are randomly selected among the experimental database shown in bold characters given in Table A2. The training patterns for GP formulation have been obtained using ANSYS FE software package. A wide range of variables are chosen to represent a general model for GP with a data set of 167 training patterns and 25 testing patterns. The statistical parameters and performance of training and test sets for the  $K_I$  are given in Table 5.9 and Fig.5.51. It has been seen that the errors are quite satisfactory for each case for test set and training sets.

Table 5.9 Statistical parameters of the GP Model used for  $K_I$

	Training set	Test set
MAPE ( % ) (Mean absolute % Error)	5	8.8
Mean (Test/ FE)	1.008	0.982
R ( % )	0.986	0.979
COV	0.058	0.095

Explicit formulation of SIF is obtained as a function of stress, crack width, plate width and crack type from Fig. 5.47 which is the expression tree of GP formulation given as follows (in MATLAB CODE):

$$\mathbf{SIF} = ((G1C11 / ((d(1) * G1C11) - G1C16)) + d(1)) * ((d(3) - (d(3) / (G2C13 / d(1)))) + d(3)) * (d(0) / (((d(3) - G3C11) / (G3C11 / d(1))) + d(2)));$$

Where constants are

$$G1C11 = -79.7; G1C16 = -40.7; G2C13 = 20.3; G3C11 = -65.8$$

It should be noted that parameters in the formulation stand for the following:

$$d(0) = \sigma$$

$$d(1) = a$$

$$d(2) = w$$

$$d(3) = \text{Crack Type}$$

After substituting the corresponding values, the final equation becomes:

$$\mathbf{SIF} = \left( \frac{79.7}{79.7a - 40.7} + a \right) \left( w + \text{TYPE} - \frac{a * w}{20.3} \right) \left( \frac{\sigma}{w + \frac{a(\text{TYPE} + 65.8)}{-65.8}} \right) \quad (5.10)$$

### 5.4.3 Conclusions for SIF with Neural Networks

The outcomes from different solution procedures of the center crack, double crack and single crack geometries are compared in Figs. 5.48, 5.49 and 5.50 respectively.

Investigating Figs. 5.48, 5.49 and 5.50, it is clear that the outcomes of all three methods, ANSYS, DEM and Eq.(5.9) are in good agreement for all types of cracks. Similarity among the figures is also observed for separation of analytical results from the others. The models used in ANSYS and DEM are real models of the crack problems, while the analytical formulations are approximations for the present problems. Hence deviation of the analytical values is considered to be the main result of approximation.

As the equation is obtained after training of NN using the outcomes of ANSYS, the results of the equation will be very close to that of numerical methods.

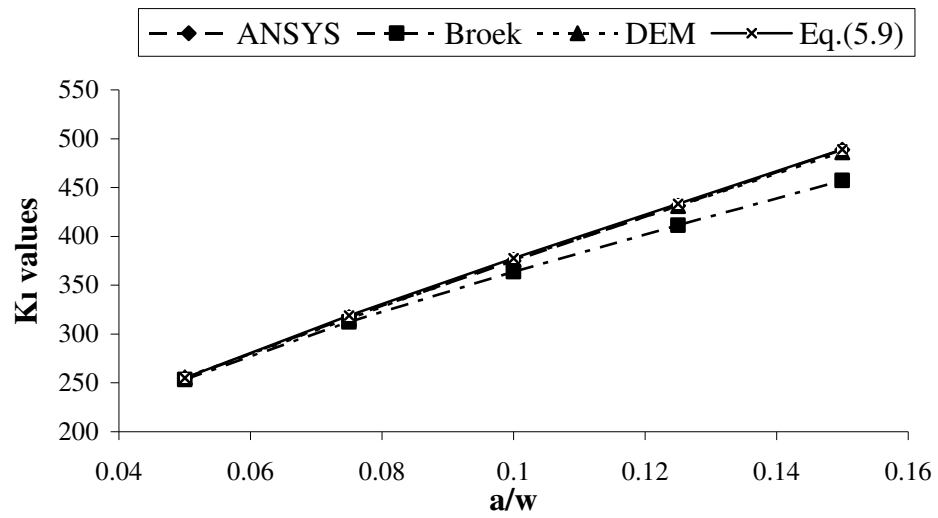


Fig. 5.48 Center cracked model analysis

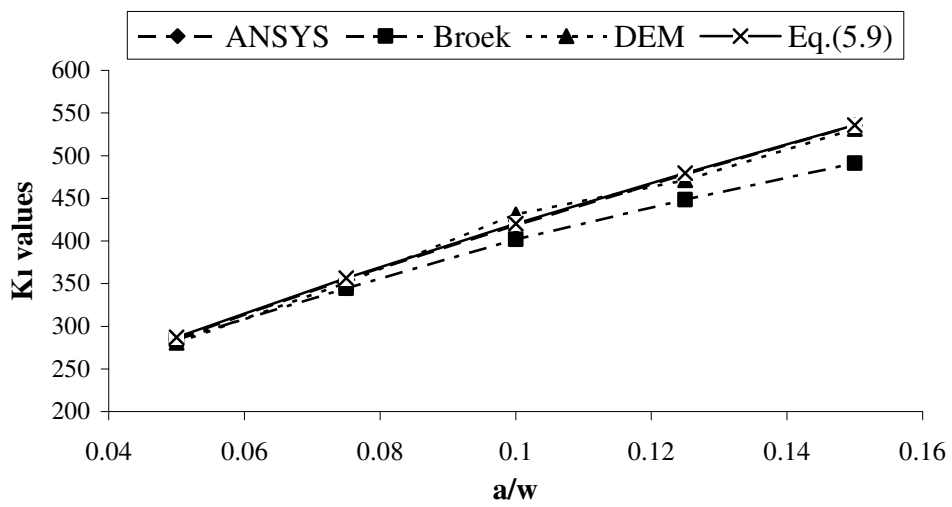


Fig. 5.49 Double edge cracked model analysis

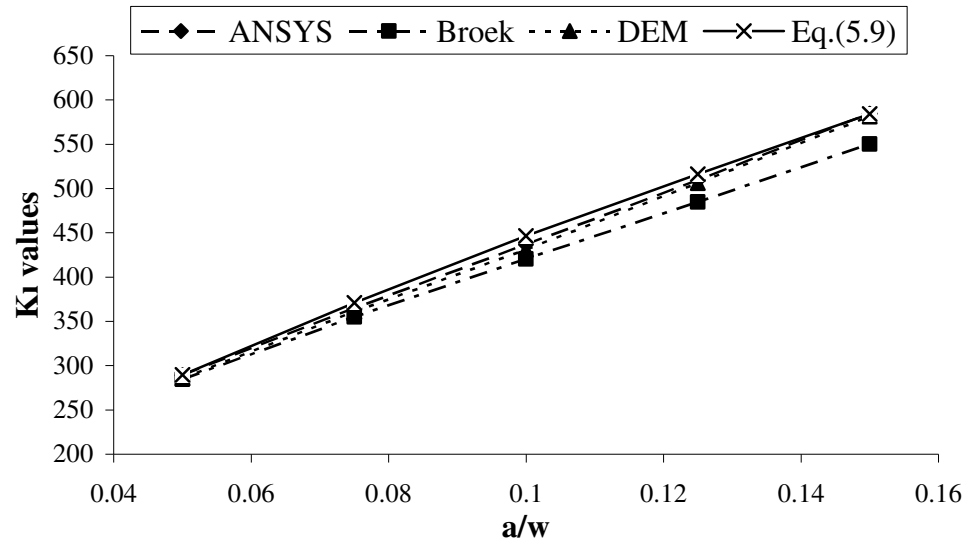


Fig. 5.50 Single edge cracked model analysis

#### 5.4.4 Conclusions for SIF with Genetic Programming

As a result, the proposed GP formulation is quite accurate, fast and of practical use compared to design codes and existing models. It should be noted that empirical formulations in fracture mechanics are mostly based on predefined functions where regression analyses of these functions are later performed. However, in the case of GP approach there is no predefined function to be considered i.e. GP creates randomly formed functions and selects the one that best fits the experimental results. Moreover, there is no restriction in the complexity and structure of the randomly formed functions, either.

The statistical parameters and performance of training and test sets for the  $K_I$  are given in Table 5.9 and Fig.5.51. It has been seen that the errors are quite satisfactory for each case for test set and training sets.

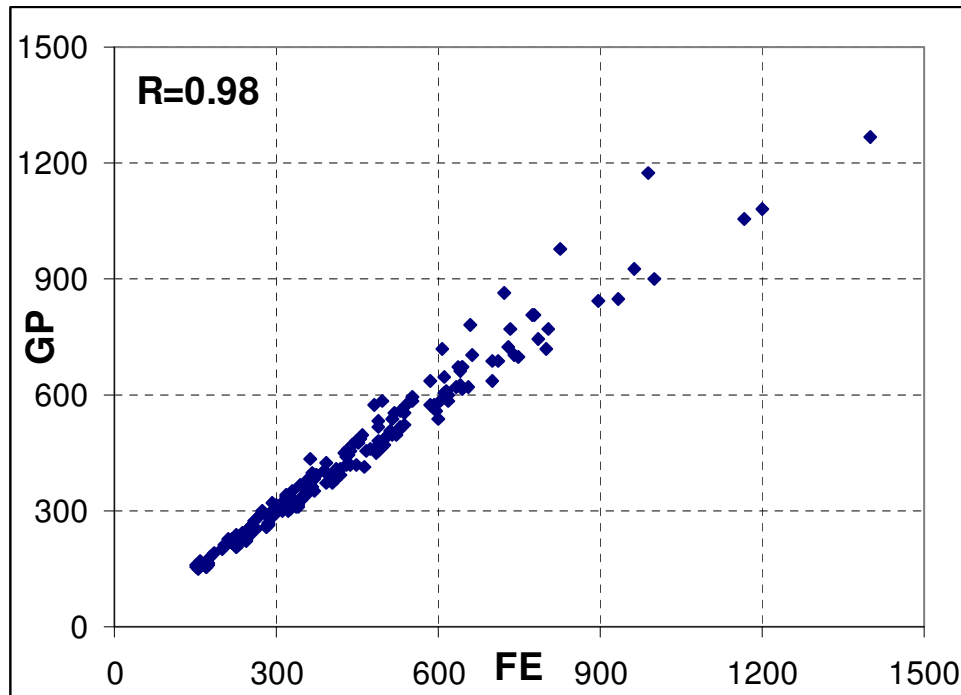


Fig. 5.51 Performance of GP results vs. FE results

### 5.5. J-integral formulations using artificial intelligence techniques

The prediction and formulation of J-integral values for varying geometries using NNs and GP based FE (ANSYS) results is another new area in fracture mechanic problems.

J-Integral calculations have been done with an ANSYS macro. For this purpose, a Fortran subroutine has been developed for ANSYS which reads the results from stress analysis and computes the appropriate line integral along a path through the integration points. The obtained J-integral values using ANSYS have been used for NN's and GP training and formulation.

The crack geometries were given before in Fig. 5.42. The same material properties and loading conditions used in the SIF calculations have taken in J-integral analysis.

### 5.5.1 Neural Networks formulation of J-Integral

The computation of J-integral for three different geometries has been done with an independent program for given set of  $\sigma_{applied}$ ,  $a$ ,  $w$ , and  $Type$  values as shown in Fig.5.52.

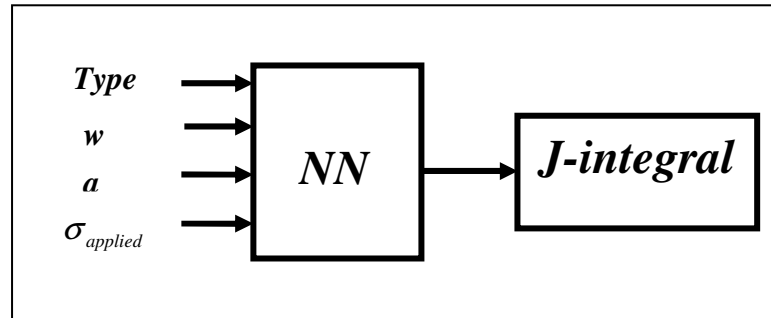


Fig.5.52 NN Model for J-integral calculation.

Furthermore it is actually an explicit formulation that computes directly stress intensity factor for three different geometries which is given as a function of some fracture parameters which are defined before:

$$J\text{-integral} = f(\sigma_{applied}, a, w, Type) \quad (5.11)$$

The explicit formula is obtained using the weights of the trained network given as follows:

$$Net_j = \sum_{i=1}^n w_{ij} x_i \quad (5.12)$$

where  $Net_j$  is the weighted sum of the  $j$ th neuron for the input received from the preceding layer with  $n$  neurons,  $w_{ij}$  is the weight between the  $j$ th neuron and the  $i$ th neuron in the preceding layer,  $x_i$  is the output of the  $i$ th neuron in the preceding layer. The output of the  $j$ th neuron  $out_j$  is calculated with a sigmoid function as follows:

$$\text{out}_j = f(\text{Net}_j) = \frac{1}{1 + \exp(-k\text{Net}_j)} \quad (5.13)$$

where,  $k$  is a constant used to control the slope of the semi-linear region.

Recalling Eqs. (5.11) and (5.12) the explicit formula is obtained by using the weights of the trained network given step by step as follows:

$$\mathbf{u}_i = \sum_{j=1}^N w_{ij} X_j + \mathbf{b}_i \quad \text{and} \quad Y_i = f(\mathbf{u}_i) \quad (5.14)$$

where  $\mathbf{u}_i$  is the summation of the  $i$ th node and  $Y_i$  the output of transfer function of this summation. It should be noted that the input parameters have been normalized by  $\sigma^*/120$ ;  $a^*/10$ ;  $w^*/80$ ;  $\text{type}^*/3$ , where  $\sigma^*$ ,  $a^*$ ,  $w^*$  and  $\text{type}^*$  are the initial values of applied stress, crack length, plate width and type of the geometry respectively. The output in the NN model is normalized by 5.

J-integral values of the three types of geometries can be obtained as the final output given as:

$$\text{J - integral} = \left[ \frac{2}{1 + e^{-2(A+B+C+D+E+F+G+H+I+J+K+3.443)}} - 1 \right] * 5 \quad (5.15)$$

where;

$$A = \left[ \frac{-0.46405}{1 + e^{(-2.6408 \sigma - 2.2589 a + 0.13524 w - 0.87134 \text{Typ} + 5.8804)}} \right]$$

$$B = \left[ \frac{-0.03106}{1 + e^{(-3.1708 \sigma - 0.29585 a + 3.6756 w - 1.7084 \text{Typ} + 2.5017)}} \right]$$

$$C = \left[ \frac{-0.02843}{1 + e^{(-0.00758 \sigma - 1.7096 a + 0.44385 w - 7.0648 \text{Typ} + 3.3699)}} \right]$$

$$D = \left[ \frac{2.3925}{1 + e^{(1.8116 \sigma + 3.0799 a - 4.6103 w + 2.3179 \text{Typ} - 5.7426)}} \right]$$

$$E = \left[ \frac{-0.01627}{1 + e^{(-10.283\sigma + 1.4449a + 0.43135w - 1.1258\text{Typ} + 5.2284)}} \right]$$



$$F = \left[ \frac{0.021426}{1 + e^{(3.1397 \sigma + 1.9112 a + 0.31462 w - 9.2923 \text{Typ} + 2.6032)}} \right]$$

$$G = \left[ \frac{0.004407}{1 + e^{(8.0378 \sigma + 5.6773 a - 1.6958 w - 10.979 \text{Typ} - 2.4535)}} \right]$$

$$H = \left[ \frac{-0.96294}{1 + e^{(1.5529 \sigma - 0.67697 a - 0.49757 w + 0.36692 \text{Typ} - 2.2822)}} \right]$$

$$I = \left[ \frac{0.41914}{1 + e^{(2.2066 \sigma + 0.98552 a - 0.34465 w + 0.43413 \text{Typ} - 2.8048)}} \right]$$

$$J = \left[ \frac{0.013253}{1 + e^{(5.6031 \sigma + 0.91457 a + 1.5444 w - 6.1405 \text{Typ} + 1.913)}} \right]$$

$$K = \left[ \frac{1.0617}{1 + e^{(2.0078 \sigma + 4.2115 a - 6.2548 w - 7.555 \text{Typ} - 1.2849)}} \right]$$

The calculation of the J-integral values for any three crack types existing on a plate of finite dimensions can be done using Eq. (5.15).

### 5.5.1.1 Parametric studies on J-integral calculations

It is obvious from statistical results ( $R=0.99$ ) above that the proposed NN model accurately learned to map the relationship between the J-integral value and varying parameters. Thus the trained NN proposed in this study has been used to conduct an extensive parametric study to investigate the effect of varying parameters on J-integral value. The response surface of each parametric study is also obtained for a comprehensive investigation. Interesting outcomes are observed on the graphs of trends. The trend of J-integral value for various parameters is shown in Figs. 5.53, 5.54 and 5.55. As seen from Fig. 5.53 a sharp increase in J-integral value is observed for increasing values of applied stress “ $\sigma$ ”. This increase is drastically observed after applied stress value exceeds 35 particularly for Type 3 crack type. As seen from Fig. 5.54 the increase is relatively less for increasing crack length “ $a$ ” with all Types. Regarding Fig. 5.55, sudden decrease is observed in J-integral values particularly for values of plate widths ( $w$ )s ranging from 35 to 45. Type 2 is less affected in this situation as compared with Type 1 and 3. For increasing values of plate width J-integral values show almost the same smooth linear trend.

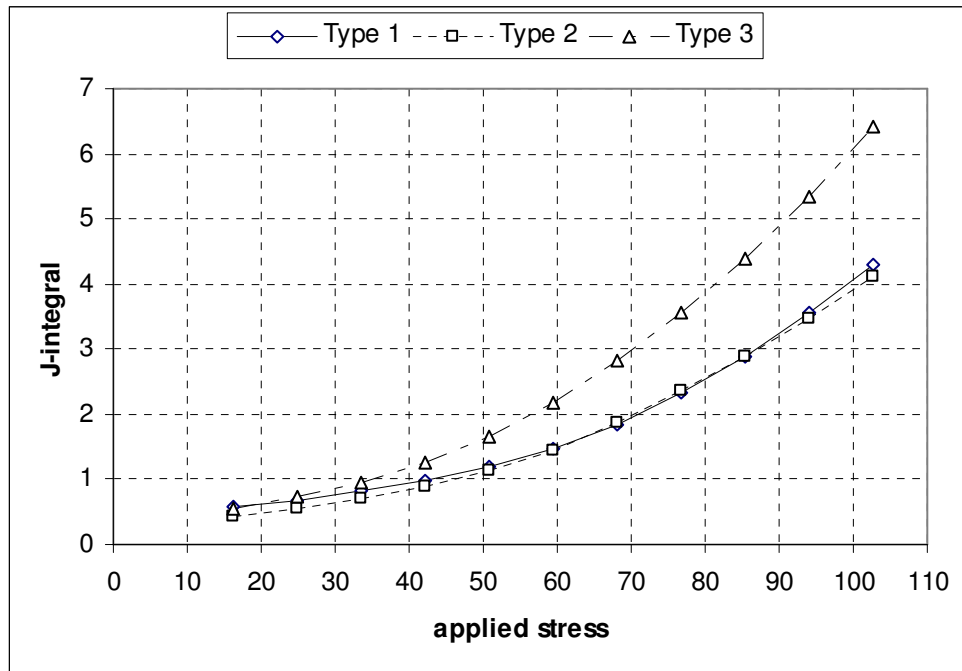


Fig. 5.53 Trend of J-integral vs  $\sigma$  ( $a=10$  mm,  $w=40$  mm)

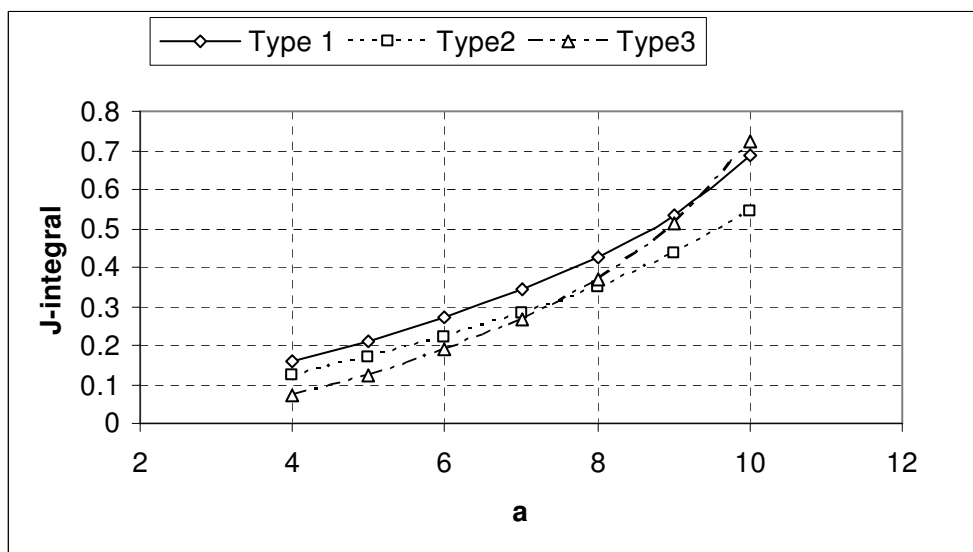


Fig. 5.54 Trend of J-integral vs  $a$  ( $\sigma=25$  MPa,  $w=40$  mm)

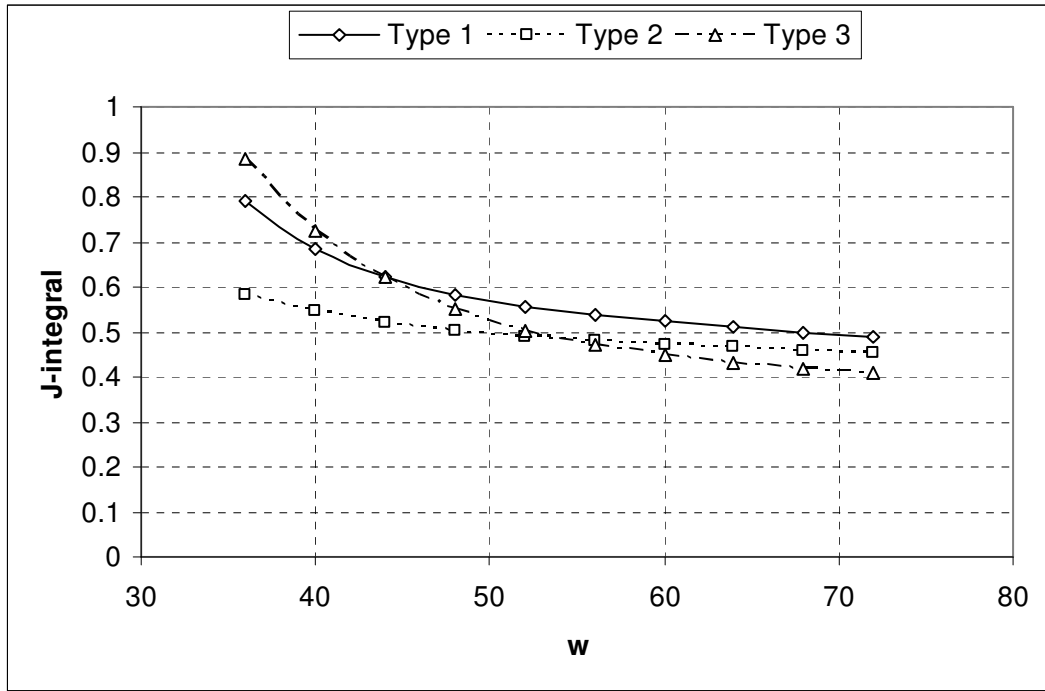


Fig. 5.55 Trend of J-integral vs w ( $\sigma=25$  MPa,  $a=10$  mm)

### 5.5.2 Genetic Programming formulation of J-integral

FE results are divided into train and test sets where patterns in test set are randomly selected among the experimental database shown in bold characters given in Table A2. The training patterns for GP formulation have been obtained using ANSYS FE software package. A wide range of variables are chosen to represent a general model for NN with a data set of 167 training patterns and 25 testing patterns. The statistical parameters and performance of training and test sets for the J-integral are given in Table 5.10 and Fig.5.56. It has been seen that the errors are quite satisfactory for each case for test set and training sets.

Explicit formulation of J-integral is obtained as a function of stress, crack width, plate width and crack type from Fig 5.57 which is the expression tree of GP formulation given as follows (in MATLAB CODE):

$$J = ((d(2)+d(0)-G1C0)/((d(2)*G1C11)-(d(2)*d(1)))) * (\exp(((d(3)^3)-d(2))/(d(2)+d(2)))) * d(1) * (d(1)+\ln(((G3C16+d(0))/d(3)))));$$

Where constants are

$$G1C0 = 52.35; \quad G1C11 = 50.15; \quad G3C16 = -57.79;$$

It should be noted that parameters in the formulation stand for the following:

$$d(0) = \sigma$$

$$d(1) = a$$

$$d(2) = w$$

$$d(3) = \text{Crack Type}$$

After putting the corresponding values, the final equation becomes:

$$J = \left( \frac{w + \sigma - 52.35}{50.15w - a * w} \right) \left( a * e^{\frac{\text{Type}^3 - w}{2w}} \right) \left( a + \ln \left( \frac{\sigma - 57.79}{\text{Type}} \right) \right) \quad (5.16)$$

### 5.5.3 Conclusions for J-integral with Neural Networks

The NN models are chosen to be the same as in SIF calculations. (single, double and center crack cases). The data obtained by FE for these 3 cases were combined together and formed the unified database for the training set of the NN model. The NN results are compared with FE results and are found to be quite accurate. Thus parametric studies are performed by the use of the proposed NN model to investigate the effect of varying parameters on the J-integral value.

It is obvious from Table 5.10 that statistical results (R=0.99) that the proposed NN model accurately learned to map the relationship between the J-integral value and varying parameters. Thus the trained NN proposed in this study was used to conduct an extensive parametric study to investigate the effect of varying parameters on J-integral value

The proposed NN model is also presented in explicit form in Eq. (5.15) which is derived by the weights and biases of the trained NN. The obtained explicit formulation is shown to be valid for common three cases of crack. Parametric studies are also performed to prove the generalization capability of the explicit formulation obtained by NNs.

#### 5.5.4 Conclusions for J-integral with Genetic Programming

The data obtained by FE for the 3 cases (single, double and center) have been combined together and formed the unified database for the training set of the GP model. The GP results are compared with FE results and are found to be quite accurate. Thus parametric studies are later performed by the use of the proposed GP formulation to investigate the effect of varying parameters on the J-integral value. The obtained GP formulation is shown to be valid for common three cases of crack.

The statistical parameters and performance of training and test sets for the J-integral are given in Table 5.10 and Fig. 5.56. It has been seen that the errors are again quite satisfactory for each case for test and training sets.

Table 5.10 Statistical parameters of the GP Model used for J-integral

	Training set	Test set
MAPE ( % ) (Mean absolute % Error)	36.2	43.5
Mean (Test/ FE)	1.22	1.30
<i>R</i> (%)	0.961	0.96
COV	0.41	0.49

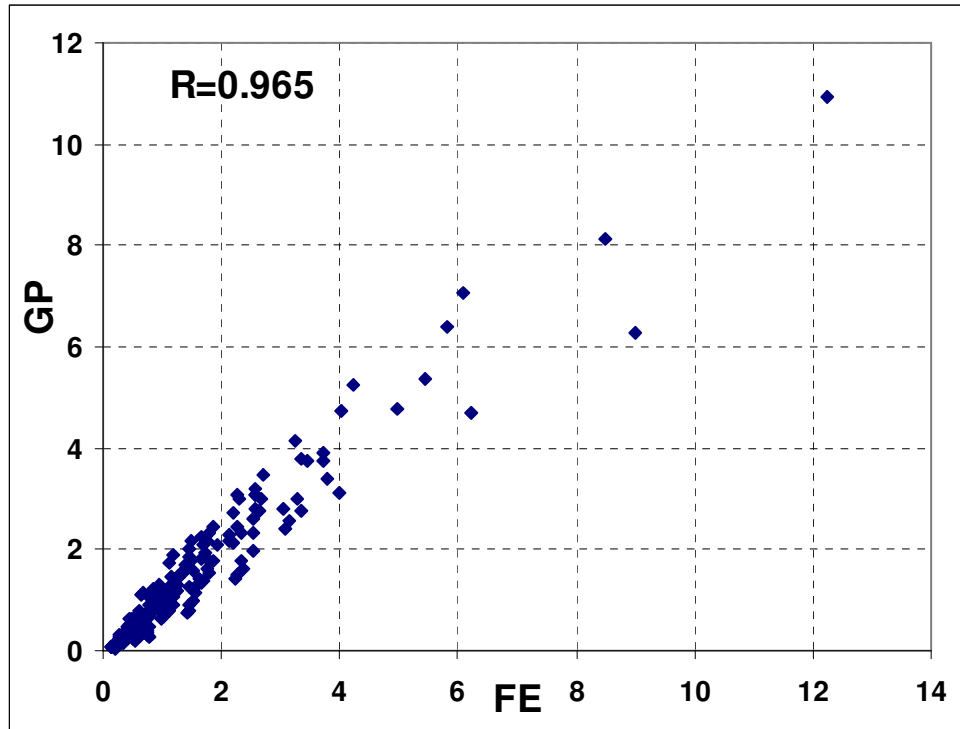


Fig. 5.56 Performance of GP results vs. FE results

### 5.5.5 General conclusions

Approximate equations are available in literature for calculation of SIF. The approximate equations for finite sized specimens need to be modified prior to use. On the other hand, numerical methods are much more flexible than analytical solutions but numerical approach requires much time for modeling and solution of the problem to determine SIF. NN and GP are considered to be a tool for generating an analytical equation for SIF calculations.

The explicit formulations [Eqs. (5.9), (5.10), (5.15) and (5.16)] are obtained as the outcome of NN's and GP. The proposed models are valid for the ranges of the training set of common three cases of crack. Thus NN and GP results are comparable in accuracy to the results of numerical methods due to in Figs. 5.46-5.56. As a result, the proposed models and the formulation of SIF and J-integral values of common three cases of crack are quite accurate, fast and practical for special type problem solutions.

## 5.6 The crack path prediction

The FEM is used to get the SIF values with displacement extrapolation method and the crack path. The flow chart of procedure used to predict the crack path is given before in Fig. 3.9. The procedure is used to simulate the crack growth path of a center edge cracked and single edge cracked plate under Mode-I loading; single edge cracked plate and off-center cracked example under a mixed mode loading. The geometrical and material properties are given in previous sections on SIF calculations.

The predicted crack paths can be seen from Figs. 5.57 and 5.58 for Mode I loading and Figs. 5.59 and 5.60 for mixed mode loading. The crack propagates straight ahead for Mode I loading. It is an expected result because of zero  $K_{II}$  values. The results for the single edge cracked with mixed mode loading example show the predicted crack paths that closely resemble the solution given in reference **Rao BN. and Rahman S. (2000)**.

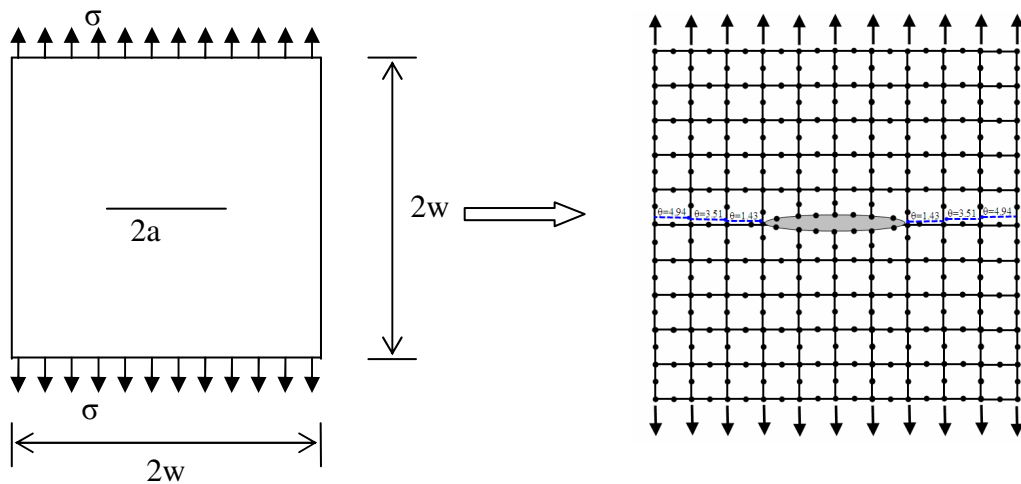


Fig 5.57 Crack path predictions of center edge cracked model

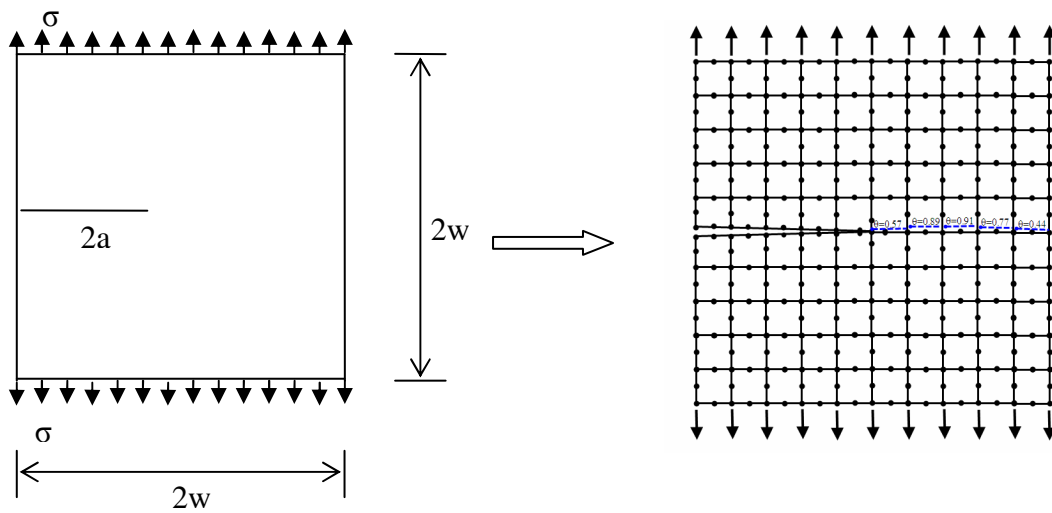


Fig 5.58 Crack path predictions of single edge cracked model

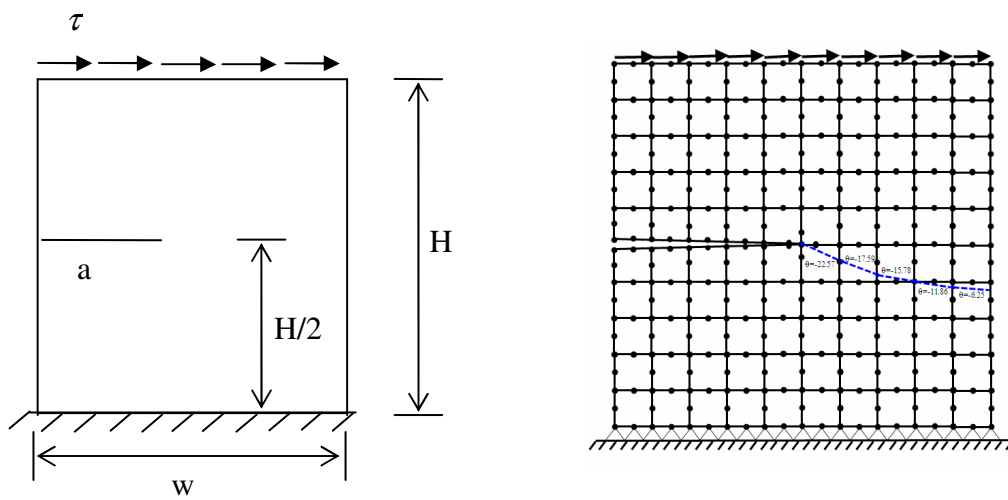


Fig 5.59 Crack path predictions of single edge cracked with mixed mode loading model



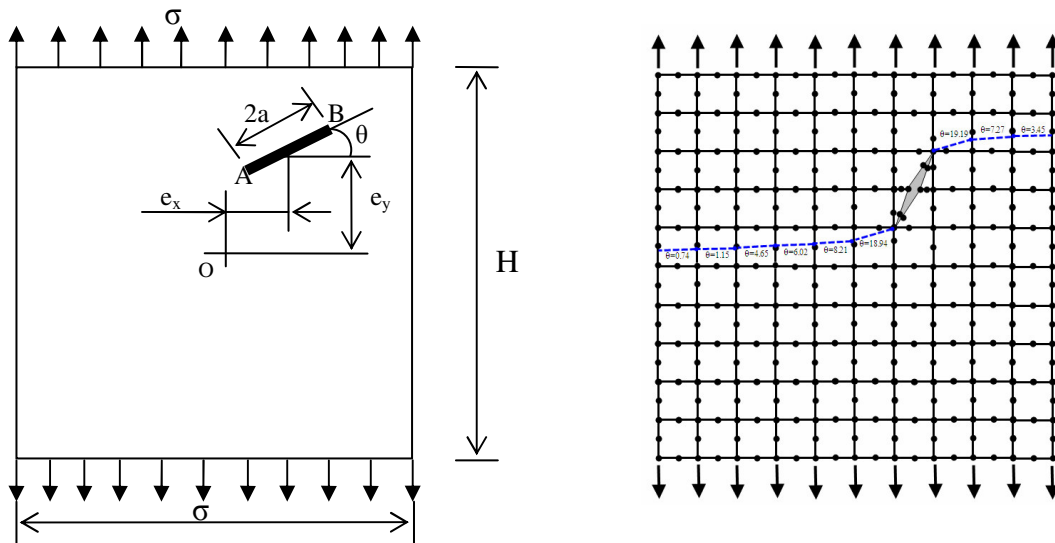


Fig 5.60 Crack path predictions of off-center cracked model

Case studies prove that the developed program has a stable algorithm. The program can be used safely to calculate the SIF, J-integral values and crack path prediction for mixed mode loadings.

## CHAPTER 6

### CONCLUSIONS

This thesis presents an attempt to develop the formulations and computer programs for two-dimensional fracture mechanics problems. It is quite clear from previous chapters that most of the research objectives have been achieved, and the following original contributions have been made to the subject:

- (i) An existing finite element elasto-plastic algorithm has been improved for fracture parameters analysis.
- (ii) DEM and SEM have been compared successfully
- (iii) The developed algorithms for SIF and J-integral calculations and crack path prediction are capable of performing a wide range of applications.
- (iv) NN and GP have been applied to fracture problems successfully.
- (v) Prediction of crack path has been applied to Mode I and mixed mode loading cases.

Several programs have been developed in FORTRAN 90, a number of case studies have been analysed using those programs, and the results were compared with those obtained either from analytical solutions or by means of ANSYS. The developed computer program has been validated for the models given below:

- (i) Center cracked model for SIF calculations
- (ii) Double edge cracked model for SIF calculations
- (iii) Single edge cracked model for SIF calculations
- (iv) Single edge cracked model with mixed mode loading for SIF calculations
- (v) Off-center cracked model for SIF calculations
- (vi) Center cracked model for J-integral calculations
- (vii) Single edge cracked model for J-integral calculations
- (viii) Three point bending beam

- (ix) Compact tension specimen
- (x) Center cracked model for crack path prediction
- (xi) Single edge cracked model for crack path prediction
- (xii) Single edge cracked model with mixed mode loading for crack path prediction
- (xiii) Off-center cracked model for crack path prediction

The results showed good agreement with analytical results, related references and ANSYS.

Considering the results of SIF calculations in this work, the following conclusions can be drawn:

- (i) The comparison of displacement and stress extrapolation method is in good agreement for the calculation of Mode I SIF values for crack tip element.
- (ii) DEM gives very accurate predictions, even for coarse meshes, if a good angular discretization is made around the crack tip.
- (iii) SEM is not used for Mode II SIF calculations. Stresses have lower precision because they are computed from the nodal displacement solutions.
- (iv) The geometry of the selected case, crack size, element type and mesh discretization are important factors for the Mode I and Mode II SIF results.
- (v) NN and GP are considered as alternative tools for generating an analytical equation using numerical data.
- (vi) It should be noted that soft computing techniques are only valid for the range of parameters used for NN or GP training.

Considering the results of J-integral calculations in this work, the following conclusions can be extracted:

- (i) J-Integral values can give very accurate predictions, even for coarse meshes. If a suitable path with the optimum number of nodes and a suitable mesh are used around the crack tip, it will give a very accurate result.
- (ii) The explicit formulation of J-integral can give very accurate results for the given geometric models and training sets.

## **RECOMMENDATIONS FOR FUTURE WORK**

- i. The developed program may be converted to a three-dimensional fracture mechanics program.
- ii. This study may be extended to fatigue analysis.
- iii. It can be combined with impact analysis for plates.
- iv. Viscoelastoplastic problems may be considered for plates
- v. Thermoplastic analysis may be studied.
- vi. Penetration of plates can be studied considering fracture and impact analysis.
- vii. Crack propagation for EPFM
- viii. Multi-crack propagation

## REFERENCES

- Anderson T. L., (1986). *Fracture Mechanics Fundamentals and Applications*, CRC Pres, London
- Ahmad, J., Barnes, C. R., Kanninen, M. F., (1983). An elasto-plastic finite element investigation of crack initiation under mixed-mode static and dynamic loading, *Elastic Plastic Fracture:Second symposium*, Vol.1, Inelastic Crack analysis, ASTM, STP 803, I-214-I239.
- Aoki, S. Kishimoto, K., Sakata M., (1981). Energy Release rate in elastic-plastic fracture problems, *Trans. of the ASME, J. of Applied Mechanics*, Vol. 48, pp 825-829.
- Atluri, S. N., Nishioka, T., (1984). Incremental Path-Independent Integrals in inelastic and dynamic fracture mechanics, *Eng. Fracture Mechanics*, Vol. 20, No. 2, pp209-244.
- Banks Sills, L. Sherman, D., (1986). Comparison of methods for calculating stress intensity factors with quarter-point elements", *Int. J. of Fracture*, Vol.32, pp127-140.
- Banks-Sills L., (1991) Application of the Finite Element Method to Linear Elastic Fracture Mechanics, *Applied Mechanics Reviews*, 44: 447-461.
- Barsoum RS. (1974). Application of quadratic isoparametric finite elements in linear fracture mechanics, *International Journal of Fracture*, 10: 603-5
- Broberg K.B., (1984). What happens at fast crack growth, *Fundamentals of Deformation and Fracture*, April, Sheffield

Broek D., (1986). Elementary Engineering Fracture Mechanics, Kluwer Academic Publishers Group.

Burdekin F.M. Stone D.E.W. (1966). The crack opening displacement approach to fracture mechanics in yielding, *J. of Strain Analysis*, Vol.1, pp-145-153

Cartwright, D.J., Rook, D.P., (1976). Compendium of stress intensity factors, HMSO, London.

Chambers L., (2001). The Practical Handbook of Genetic Algorithms Applications, 2nd Ed., Chapman and Hall/CRC

Courtin S., Gardin C., Bezine G., and Hamouda H.B.H (2005). Advantages of the J-integral approach for calculating stress intensity factors when using the commercial finite element software ABAQUS, *Engineering Fracture Mechanics*, 72:2174-2185.

Cruse T.A. (1986). Two-Dimensional BIE fracture mechanics analysis, *Applied Math Modelling*, Vol.2, pp287-293

Cruse T.A., Raveendra S.T., (1988). A Comparison of long and short crack elasto-plastic response using the BEM, *Eng. Fracture Mechanics*, Vol.30, No.1, pp59-75

Dechaumphai P, Phongthanapanich S, Sricharoenchai T. (2003). Combined delaunay triangulation and adaptive finite element method for crack growth analysis. *Acta Mechanica Sinica*, 19-2: 162-171

Erdogan F., (2000). *Fracture mechanics*, International Journal of Solids and Structures, 37: 171-183.

Eshelby, J.D., (1969). Energy relations and the energy-momentum tensor in continuum mechanics, *Inelastic behaviour of solids*, Editor Kanninen, M. et al, McGraw-Hill, Newyork

Ewalds,H.L.,Wanhill,R.J.H, (1986). Fracture Mechanics, Edward Arnold Pub., London.

Fenner R.T., (1986). Engineering Elasticity Application of Numerical and Analytical Techniques, John Wiley and Sons, New York

Ferreira C., (2002). Gene Expression Programming: Mathematical Modelling by an Artificial Intelligence

Ferreira C., (2001). Gene Expression Programming in Problem solving, *invited tutorial of the 6th Online World Conference on Soft Computing in Industrial Applications*, September 10-24

Ferreira C., (2001). Gene Expression Programming: A New Adaptive Algorithm for Solving Problems. *Complex Systems*, Vol. 13, issue 2: 87-129.

Goldberg D.E., (1989). Genetic Algorithms in Search, Optimization, and Machine Learning. Reading, MA: Addison-Wesley

Gray LJ, Phan AV, Paulino GH, Kaplan T., (2003). Improved quarter-point crack tip element, *Engineering Fracture Mechanics*, 70: 269-283.

Griffith, A.A., (1921). The Phenomena of rupture and flow in Solids, *Phil. Trns. R. Soc.* A221, 163-198.

Guinea GV, Planas J, Elices M , (2000). K-I evaluation by the displacement extrapolation technique. *Engineering Fracture Mechanics*, 66 (3): 243-255.

Guzelbey, I.H. (1992). Finite and Boundary Element Analysis of Elasto-plastic Finite Strain Contact Problems, PhD Thesis, Cranfield Institute of Technology

Guzelbey I. H., Atmaca N. and Kanber B., (2004). Comparison of Displacement and Stress Extrapolation Techniques for Stress Intensity Factor, *CMES<sup>1</sup>-04, Proceedings of the First Cappadocia International Mechanical Engineering Symposium*, 14-16 July, Cappadocia, Turkey, 684-691

Haupt R.L., Haupt S.E., (2004)., Practical Genetic Algorithms, 2nd Edition, Wiley-Interscience.

Haykin S., (2000). Neural Networks – A Comprehensive Foundation, Macmillan College Publ. Co.

Hebb, D.O.(1949). The Organization of Behavior, Wiley, New York

Hertzberg R., (1996). Deformation and Fracture Mechanics of Engineering Materials. John Wiley and Sons, New York.

Holland J. H., (1975). Adaptation in Natural and Artificial Systems Ann Arbor: University of Michigan Pres

Hopfield J.J.,(1982). Neural networks and physical systems with emergent collective computational abilities", *Proceedings of the National Academy of Sciences of the USA*, vol. 79 no. 8 pp. 2554-2558

Horvath A., (1994). Higher-order singular isoparametric elements for crack problems, *Comm. Num. Mech. Engng.*, 10:73-80

Hsu-I-Min (1989). Crack Problems for elastic-plastic materials under anti-plane shear loadings, PhD Thesis, Ohio State Univ., pp1-468, order No. 8913652, UMI

Inglis, C. E., (1913). Stress in a plate due to the presence of cracks and sharp corners, *proced. Inst. Naval architects*, vol.60.

Irwin, G.R., (1957). Analysis of stresses and strains near the end of a crack traversing a plate, *Trans., ASME, J. of Appl. Mech.*

IrwinG.R., (1960). Plastic zone near a crack and fracture toughness. *In: Proc. 7th Sagamore Conference*, p. IV-63.



Isida M., (1971). Effect of width and length on stress intensity factors of internally cracked plates under various boundary conditions, *International Journal of Fracture*, 7, 301-16.

Kanninen M. F., (1985). *Advanced Fracture Mechanics*, Oxford University Press NY, Oxford

Karami G., Fenner R.T., (1986). Analysis of mixed mode fracture and crack closure using the boundary integral equation method, *Int. J. of fracture*, Vol.30, pp13-29

Keyvanfar F., (1985). Effects of residual stresses on fatigue crack propagation, PhD thesis, Stanford Univ., pp 1-224

Koza J.R. (1992). *Genetic Programming: On the Programming of Computers by Means of Natural Selection*, Cambridge, MA: MIT Press

Kutuk M.A., Atmaca N., and Guzelbey I.H., (2007). Explicit formulation of SIF using neural networks for opening mode of fracture. *Engineering Structures*, doi:10.1016/j.engstruct.2006.11.008

Miller K.J., Kfoury, A.P. (1979). A comparison of elastic-plastic fracture parameters in biaxial stress states, *Elastic-plastic Fracture Symposium sponsored by ASTM*, pp214-228

Minsky M., Seymour P., (1969). *Perceptrons: An introduction to Computational Geometry*, MIT Press, Cambridge, MA

Murakami Y., (1987). *Stress Intensity Factors Handbook*, Oxford: Pergamon Press.

Nguyen Q.S., Stolz, C. and Debryne G., (1990). Energy methods in fracture mechanics: stability, bifurcations and second variations. *European Journal of Mechanics, A/Solids* 9, pp. 157–173.

Pan E. (1997). A general boundary element analysis of 2-D linear elastic fracture mechanics, *International Journal of Fracture*, 88:41-59.

Pilcer S., Ohlson N.G., (1983). An elastic-plastic analysis of relationships between  $K_x$ ,  $J$ , and CTOD, *4th Int. Conf. of Mechanical Behaviour of Materials*, Vol.2, pp959-965

Rao BN. and Rahman S., (2000). An efficient meshless method for fracture analysis of cracks, *Computational Mechanics*, 26:398 ~ 408.

Rice J.R.(1968). A path independent integral and the appropriate analysis of strain concentration by notches and cracks, *Journal of Applied Mechanics* 379-386.

Richard H.A., Kuna M., (1990). Theoretical and experimental study of superimposed fracture modes I,II, and III, *Eng. Fracture Mechanics*, Vol.35, No.6, pp949-960

Richard H.A., Fulland M. and Sander M., (2005). Theoretical crack path prediction, *Fatigue and Fracture of Engineering Materials and Structures*, Vol.28 (1-2), pp3–12.

Rook D.P., Hutchins, S.M., (1984). Stress intensity factors for cracks at loaded holes – effect of load distribution” , *J. of Strain Analysis*, Vol.19, No.2, pp81-96.

Rosenblatt, F., (1958). The Perceptron: A Probabilistic Model for Information Storage and Organization in the Brain, Cornell Aeronautical Laboratory, *Psychological Review*, v65, No. 6, pp. 386-408.

Rumelhart D.E., Hinton G.E., Williams R.J., (1986). Learning internal representation by error propagation Parallel Distributed Processing: Exploration in the Microstructure of Cognition, Vol. 1. MIT Press, Cambridge, MA, Chapter 8

Sakata, M. Aoki, S. Kishimoto, K., (1979). Extension of J-Integral and its application to the estimation of structural strength, *Proc. of the USA-Japan Joint Seminar*, pp23-34.

Saouma V.E., Zatz I.J., (1984). Numerical evaluation of the quarter-point-tip element, *Int. J. for Numerical Methods in Eng.* Vol.20, 1629-1641

Shanyi Du., Lee J.D., (1982). Finite element analysis of slow crack growth, *Eng. Fracture Mechanics*, Vol.16, No.2, pp229-245

Sih G.C., Mcdonald B., (1974). Fracture Mechanics Applied to Engineering Problems- Strain-Energy Density Fracture Criterion, *Eng. Fracture Mechanics*, Vol.6, pp361-386

Srawley J.E., (1976). Wide range stress intensity factor expressions for ASTM E399 standart fracture toughness specimens, *International Journal of Fracture*, 12: 475-6.

Tracey, D.M., (1971). Finite elements for determination of crack tip stress intensity factors, *Eng. Fracture Mechanics*, Vol. 3, 255-265.

Tracey D.M., (1976). Finite element solution for crack tip behaviour in small-scale yielding, *Trans. of the ASME*, pp146-150

Turner C.E. (1975). Yielding Fracture Mechanics, *Journal of Strain Analysis*, Vol.10, pp207-215.

Vainshtok, V. A., (1980). Virtual Crack variation method for determination of stress intensity factors for cracks of mixed analysis for the Eng. *Science Proc. of the 2<sup>nd</sup> Int. Symposium*, pp797-803.

Wells A. A.(1962). Unstable crack propagation in metal: Damage and fast fracture, *Proceed. of the Crack Propagation Symposium Cranfield*, The College of Aeronautics, Vol.1, pp210-230

Westergaard, H.M., (1939). Bearing pressure and cracks, *Journal of Applied Mechanics*, Vol. 66, A49-A52.

Widrow B., and Hoff M.E., (1960). Adaptive Switching Circuits, *1960 IRE WESCON Convention Record*, New York: IRE pp. 96-104

Wu W.L., (2004). *Boundary Element Formulations for Fracture Mechanics Problems*, PhD Thesis, University of Wollongong

Xie Y.J., Wang X.H., Lin Y.C. (2004). Stress intensity factors for cracked rectangular cross-section thin-walled tubes, *Engineering Fracture Mechanics*, 71:1501-1513

Yishu Z., (1989). Experimental study on mixed mode crack propagation, *Eng. Fracture Mechanics*, Vol.34, No.4, pp891-899

Yuanhan W., (1991). Asymmetric crack problems calculated by the boundary collocation method, *Engineering Fracture Mechanics*, 40:133-43.

Zehnder A.T., (2007). Lecture notes on fracture mechanics, *Cornell University*.

Zien H. M., (1983). Fracture Mechanics J-integral calculation in Thermo-elastic plasticity, *Computers and Structures*, Vol.17, No.5-6, pp775-781.

Zienkiewicz O.C., Valliappan S., King I.P. (1969). Elasto-plastic solutions of engineering problems initial stress , finite element approach, *Int. J. for Numerical Methods in Eng.*, Vol. 1, pp75-100.

Zupan J., Gasteiger J., (1993). *Neural Networks for Chemists - An Introduction*; VCH: Weinheim

## APPENDIX

**Table A1. FE results vs. NN results for SIF**

\*Bold cases are test sets.

$\Sigma$	a	w	type	FE	NN	FE/NN
<b>60</b>	<b>2</b>	<b>20</b>	<b>1</b>	<b>159.11</b>	<b>161.16</b>	0.99
60	2	20	2	177.48	177.59	1.00
60	2	20	3	185.23	187.5	0.99
<b>60</b>	<b>2</b>	<b>40</b>	<b>2</b>	<b>174.5</b>	<b>173.41</b>	1.01
60	2	40	1	152.86	152.67	1.00
60	2	40	3	173.52	171.22	1.01
<b>60</b>	<b>2</b>	<b>60</b>	<b>2</b>	<b>170.14</b>	<b>173.03</b>	0.98
60	2	60	1	151.63	152.57	0.99
60	2	60	3	171.13	170.03	1.01
<b>60</b>	<b>2</b>	<b>80</b>	<b>2</b>	<b>169.1</b>	<b>174.38</b>	0.97
60	2	80	1	157.01	153.69	1.02
60	2	80	3	169.7	171.83	0.99
60	4	20	1	259.16	259.89	1.00
60	4	20	2	273.56	272.18	1.01
60	4	20	3	316.84	317.57	1.00
60	4	40	1	225.05	227.3	0.99
60	4	40	2	251.1	254.46	0.99
60	4	40	3	262.04	264.2	0.99
60	4	60	1	218.57	217.5	1.00
60	4	60	2	244.94	246.92	0.99
60	4	60	3	250.08	253.28	0.99
60	4	80	1	216.5	212.05	1.02
60	4	80	2	242.81	239.7	1.01
60	4	80	3	245.72	245.5	1.00
<b>60</b>	<b>6</b>	<b>20</b>	<b>2</b>	<b>361.47</b>	<b>365.94</b>	0.99
60	6	20	1	389.85	384.54	1.01
60	6	20	3	482.2	475.01	1.02
60	6	40	1	293.3	292.81	1.00
60	6	40	2	321.28	322.15	1.00
60	6	40	3	350.78	348.28	1.01
60	6	60	1	275.78	276.95	1.00
60	6	60	2	307.72	310.62	0.99
60	6	60	3	321.11	323.75	0.99
60	6	80	1	269.5	266.94	1.01
60	6	80	2	301.83	300.32	1.01
60	6	80	3	309.63	312.8	0.99
60	8	20	1	600.08	606.93	0.99
60	8	20	2	494.48	486.28	1.02

60	8	20	3	700.19	714.28	0.98
<b>60</b>	<b>8</b>	<b>40</b>	<b>1</b>	<b>366.64</b>	<b>364.38</b>	1.01
60	8	40	2	387.05	387.17	1.00
60	8	40	3	448.22	443.58	1.01
<b>60</b>	<b>8</b>	<b>60</b>	<b>1</b>	<b>331.16</b>	<b>328.79</b>	1.01
60	8	60	2	365.7	365.53	1.00
60	8	60	3	392.65	389.22	1.01
60	8	80	1	318.4	318.15	1.00
60	8	80	2	355.28	354.88	1.00
60	8	80	3	370.98	373.14	0.99
<b>80</b>	<b>2</b>	<b>20</b>	<b>1</b>	<b>212.14</b>	<b>212.39</b>	1.00
80	2	20	2	236.64	234.57	1.01
80	2	20	3	246.97	250.69	0.99
80	2	40	1	203.81	201.64	1.01
80	2	40	2	228.53	228.75	1.00
80	2	40	3	231.36	225.41	1.03
80	2	60	1	202.18	202.28	1.00
80	2	60	2	226.86	230.09	0.99
80	2	60	3	228.18	225.75	1.01
<b>80</b>	<b>2</b>	<b>80</b>	<b>2</b>	<b>225.47</b>	<b>230.3</b>	0.98
80	2	80	1	200.74	202.77	0.99
80	2	80	3	226.26	227.7	0.99
<b>80</b>	<b>4</b>	<b>20</b>	<b>3</b>	<b>464.23</b>	<b>426.63</b>	1.09
80	4	20	1	345.55	346.78	1.00
80	4	20	2	374.49	365.87	1.02
80	4	40	1	300.07	300.22	1.00
80	4	40	2	334.8	336.72	0.99
80	4	40	3	349.38	351.03	1.00
80	4	60	1	291.42	290.98	1.00
80	4	60	2	326.59	326.9	1.00
80	4	60	3	333.43	333.68	1.00
80	4	80	1	288.66	285.4	1.01
80	4	80	2	323.74	319.88	1.01
80	4	80	3	327.63	326.16	1.00
80	6	20	1	515.36	515.14	1.00
80	6	20	2	481.96	493.06	0.98
80	6	20	3	642.93	633.09	1.02
<b>80</b>	<b>6</b>	<b>40</b>	<b>2</b>	<b>428.38</b>	<b>432.42</b>	0.99
80	6	40	1	392.75	393.27	1.00
80	6	40	3	467.71	468.09	1.00
<b>80</b>	<b>6</b>	<b>60</b>	<b>1</b>	<b>367.36</b>	<b>369.66</b>	0.99
80	6	60	2	410.29	412.19	1.00
80	6	60	3	428.15	430.59	0.99
80	6	80	1	359.33	359.56	1.00
80	6	80	2	404.75	399.44	1.01
80	6	80	3	412.85	413.85	1.00
<b>80</b>	<b>8</b>	<b>20</b>	<b>2</b>	<b>659.3</b>	<b>648.39</b>	1.02
80	8	20	1	800.11	796.76	1.00

80	8	20	3	933.58	931.88	1.00
80	8	40	1	488.85	491.34	0.99
80	8	40	2	516.06	520.5	0.99
80	8	40	3	597.63	594.65	1.01
80	8	60	1	441.55	441.47	1.00
80	8	60	2	487.6	489.67	1.00
80	8	60	3	523.54	522.39	1.00
80	8	80	1	424.53	425.05	1.00
80	8	80	2	473.71	471.53	1.00
80	8	80	3	494.64	496.85	1.00
100	2	20	1	265.18	265.71	1.00
100	2	20	2	295.8	293.79	1.01
100	2	20	3	308.72	313.34	0.99
100	2	40	1	254.76	253.44	1.01
100	2	40	2	285.66	288.08	0.99
100	2	40	3	289.2	283.51	1.02
<b>100</b>	<b>2</b>	<b>60</b>	<b>2</b>	<b>283.57</b>	<b>289.27</b>	0.98
100	2	60	1	252.72	254.29	0.99
100	2	60	3	285.22	283.85	1.00
<b>100</b>	<b>2</b>	<b>80</b>	<b>2</b>	<b>281.84</b>	<b>288.2</b>	0.98
100	2	80	1	250.92	253.68	0.99
100	2	80	3	282.83	284.99	0.99
<b>100</b>	<b>4</b>	<b>20</b>	<b>2</b>	<b>455.94</b>	<b>453.57</b>	1.01
100	4	20	1	431.93	431.6	1.00
100	4	20	3	528.07	531.49	0.99
<b>100</b>	<b>4</b>	<b>40</b>	<b>1</b>	<b>375.09</b>	<b>376.98</b>	0.99
100	4	40	2	418.5	420.58	1.00
100	4	40	3	438.66	436.81	1.00
100	4	60	1	364.28	366.72	0.99
100	4	60	2	408.23	410.74	0.99
100	4	60	3	416.79	418.37	1.00
100	4	80	1	360.83	359.23	1.00
100	4	80	2	404.68	401.83	1.01
100	4	80	3	409.54	409.3	1.00
100	6	20	1	644.2	643.4	1.00
100	6	20	2	607.52	615.75	0.99
100	6	20	3	803.66	795.8	1.01
100	6	40	1	488.84	489.16	1.00
100	6	40	2	535.47	536.14	1.00
100	6	40	3	584.64	582.44	1.00
100	6	60	1	459.63	463.76	0.99
100	6	60	2	512.86	515.03	1.00
100	6	60	3	535.19	536.75	1.00
100	6	80	1	449.16	452.47	0.99
100	6	80	2	503.05	501.58	1.00
100	6	80	3	516.06	519.2	0.99
<b>100</b>	<b>8</b>	<b>20</b>	<b>2</b>	<b>824.13</b>	<b>817.41</b>	1.01
100	8	20	1	1000.1	996.14	1.00

100	8	20	3	1167	1164.7	1.00
<b>100</b>	<b>8</b>	<b>40</b>	<b>3</b>	<b>747.04</b>	<b>747.95</b>	1.00
100	8	40	1	611.06	611.92	1.00
100	8	40	2	645.08	649.99	0.99
<b>100</b>	<b>8</b>	<b>60</b>	<b>1</b>	<b>551.94</b>	<b>549.17</b>	1.01
100	8	60	2	609.5	608.88	1.00
100	8	60	3	654.42	651.54	1.00
100	8	80	1	530.66	533.03	1.00
100	8	80	2	592.14	590.3	1.00
100	8	80	3	618.3	621.53	0.99
120	2	20	1	318.21	317.16	1.00
120	2	20	2	354.95	351.05	1.01
120	2	20	3	370.46	376.64	0.98
120	2	40	1	305.71	302.46	1.01
120	2	40	2	342.79	344.5	1.00
120	2	40	3	347.04	338.6	1.02
120	2	60	1	303.27	304.27	1.00
120	2	60	2	340.29	346.74	0.98
120	2	60	3	342.27	339.34	1.01
<b>120</b>	<b>2</b>	<b>80</b>	<b>2</b>	<b>338.2</b>	<b>345.32</b>	0.98
120	2	80	1	301.11	303.41	0.99
120	2	80	3	339.39	340.44	1.00
120	4	20	1	518.32	517.94	1.00
120	4	20	2	547.13	542.39	1.01
120	4	20	3	633.68	641.33	0.99
120	4	40	1	450.1	449.53	1.00
120	4	40	2	502.2	502.45	1.00
120	4	40	3	526.4	523.1	1.01
120	4	60	1	437.14	437.97	1.00
120	4	60	2	489.88	491.51	1.00
120	4	60	3	500.15	500.7	1.00
120	4	80	1	432.99	429.45	1.01
120	4	80	2	485.61	481.11	1.01
120	4	80	3	489.6	489.63	1.00
<b>120</b>	<b>6</b>	<b>20</b>	<b>2</b>	<b>722.93</b>	<b>738.55</b>	0.98
120	6	20	1	773.04	776.47	1.00
120	6	20	3	964.39	963.51	1.00
<b>120</b>	<b>6</b>	<b>40</b>	<b>1</b>	<b>586.61</b>	<b>583.61</b>	1.01
120	6	40	2	642.57	641.27	1.00
120	6	40	3	701.57	700.49	1.00
<b>120</b>	<b>6</b>	<b>60</b>	<b>1</b>	<b>551.56</b>	<b>552.6</b>	1.00
120	6	60	2	615.44	616.34	1.00
120	6	60	3	642.23	644.54	1.00
120	6	80	1	538.99	539.25	1.00
120	6	80	2	603.66	599.99	1.01
120	6	80	3	619.27	622.61	0.99
120	8	20	1	1200.2	1202.5	1.00
120	8	20	2	988.96	988.17	1.00



120	8	20	3	1400.4	1402.1	1.00
120	8	40	1	733.28	734.3	1.00
120	8	40	2	778.8	779.14	1.00
120	8	40	3	896.44	900.23	1.00
120	8	60	1	662.32	656.42	1.01
120	8	60	2	731.4	731.3	1.00
120	8	60	3	785.31	783.62	1.00
<b>120</b>	<b>8</b>	<b>80</b>	<b>3</b>	<b>739.88</b>	<b>748.48</b>	0.99
120	8	80	1	636.79	636.24	1.00
120	8	80	2	710.57	708.86	1.00

**Table A2. FE results vs. GP results for SIF**

\*Bold cases are test sets.

$\sigma$	a	w	TYPE	FE	GP	FE/GP
<b>60</b>	<b>2</b>	<b>20</b>	<b>1</b>	<b>159.11</b>	<b>171.53</b>	<b>0.93</b>
60	2	20	2	177.48	180.85	0.98
60	2	20	3	185.23	190.20	0.97
60	4	20	1	259.16	275.64	0.94
60	4	20	2	273.56	292.92	0.93
60	4	20	3	316.84	310.32	1.02
60	6	20	1	389.85	402.67	0.97
<b>60</b>	<b>6</b>	<b>20</b>	<b>2</b>	<b>361.47</b>	<b>432.18</b>	<b>0.84</b>
60	6	20	3	482.20	462.09	1.04
60	8	20	1	600.08	539.32	1.11
60	8	20	2	494.48	586.41	0.84
60	8	20	3	700.19	634.49	1.10
<b>80</b>	<b>2</b>	<b>20</b>	<b>1</b>	<b>212.14</b>	<b>228.70</b>	<b>0.93</b>
80	2	20	2	236.64	241.13	0.98
80	2	20	3	246.97	253.60	0.97
80	4	20	1	345.55	367.52	0.94
80	4	20	2	374.49	390.55	0.96
<b>80</b>	<b>4</b>	<b>20</b>	<b>3</b>	<b>464.23</b>	<b>413.76</b>	<b>1.12</b>
80	6	20	1	515.36	536.89	0.96
80	6	20	2	481.96	576.24	0.84
80	6	20	3	642.93	616.12	1.04
80	8	20	1	800.11	719.09	1.11
<b>80</b>	<b>8</b>	<b>20</b>	<b>2</b>	<b>659.30</b>	<b>781.88</b>	<b>0.84</b>
80	8	20	3	933.58	845.99	1.10
100	2	20	1	265.18	285.88	0.93
100	2	20	2	295.80	301.41	0.98
100	2	20	3	308.72	317.00	0.97
100	4	20	1	431.93	459.41	0.94
<b>100</b>	<b>4</b>	<b>20</b>	<b>2</b>	<b>455.94</b>	<b>488.19</b>	<b>0.93</b>
100	4	20	3	528.07	517.20	1.02
100	6	20	1	644.20	671.12	0.96
100	6	20	2	607.52	720.31	0.84

100	6	20	3	803.66	770.15	1.04
100	8	20	1	1000.1	898.86	1.11
<b>100</b>	<b>8</b>	<b>20</b>	<b>2</b>	<b>824.13</b>	<b>977.35</b>	<b>0.84</b>
100	8	20	3	1167.0	1057.49	1.10
120	2	20	1	318.21	343.06	0.93
120	2	20	2	354.95	361.69	0.98
120	2	20	3	370.46	380.39	0.97
120	4	20	1	518.32	551.29	0.94
120	4	20	2	547.13	585.83	0.93
120	4	20	3	633.68	620.64	1.02
120	6	20	1	773.04	805.34	0.96
<b>120</b>	<b>6</b>	<b>20</b>	<b>2</b>	<b>722.93</b>	<b>864.37</b>	<b>0.84</b>
120	6	20	3	964.39	924.18	1.04
120	8	20	1	1200.2	1078.63	1.11
120	8	20	2	988.96	1172.82	0.84
120	8	20	3	1400.4	1268.98	1.10
60	2	40	1	152.86	158.09	0.97
<b>60</b>	<b>2</b>	<b>40</b>	<b>2</b>	<b>174.50</b>	<b>162.49</b>	<b>1.07</b>
60	2	40	3	173.52	166.89	1.04
60	4	40	1	225.05	237.33	0.95
60	4	40	2	251.10	244.91	1.03
60	4	40	3	262.04	252.52	1.04
60	6	40	1	293.30	319.39	0.92
60	6	40	2	321.28	331.23	0.97
60	6	40	3	350.78	343.13	1.02
<b>60</b>	<b>8</b>	<b>40</b>	<b>1</b>	<b>366.64</b>	<b>386.61</b>	<b>0.95</b>
60	8	40	2	387.05	403.46	0.96
60	8	40	3	448.22	420.44	1.07
80	2	40	1	203.81	210.79	0.97
80	2	40	2	228.53	216.65	1.05
80	2	40	3	231.36	222.52	1.04
80	4	40	1	300.07	316.44	0.95
80	4	40	2	334.80	326.55	1.03
80	4	40	3	349.38	336.69	1.04
80	6	40	1	392.75	425.86	0.92
<b>80</b>	<b>6</b>	<b>40</b>	<b>2</b>	<b>428.38</b>	<b>441.64</b>	<b>0.97</b>
80	6	40	3	467.71	457.50	1.02
80	8	40	1	488.85	515.47	0.95
80	8	40	2	516.06	537.94	0.96
80	8	40	3	597.63	560.58	1.07
100	2	40	1	254.76	263.48	0.97
100	2	40	2	285.66	270.81	1.05
100	2	40	3	289.20	278.15	1.04
<b>100</b>	<b>4</b>	<b>40</b>	<b>1</b>	<b>375.09</b>	<b>395.56</b>	<b>0.95</b>
100	4	40	2	418.50	408.19	1.03
100	4	40	3	438.66	420.86	1.04
100	6	40	1	488.84	532.32	0.92
100	6	40	2	535.47	552.05	0.97

100	6	40	3	584.64	571.88	1.02
100	8	40	1	611.06	644.34	0.95
100	8	40	2	645.08	672.43	0.96
<b>100</b>	<b>8</b>	<b>40</b>	<b>3</b>	<b>747.04</b>	<b>700.73</b>	<b>1.07</b>
120	2	40	1	305.71	316.18	0.97
120	2	40	2	342.79	324.97	1.05
120	2	40	3	347.04	333.78	1.04
120	4	40	1	450.10	474.67	0.95
120	4	40	2	502.20	489.83	1.03
120	4	40	3	526.40	505.03	1.04
<b>120</b>	<b>6</b>	<b>40</b>	<b>1</b>	<b>586.61</b>	<b>638.79</b>	<b>0.92</b>
120	6	40	2	642.57	662.46	0.97
120	6	40	3	701.57	686.25	1.02
120	8	40	1	733.28	773.21	0.95
120	8	40	2	778.80	806.91	0.97
120	8	40	3	896.44	840.87	1.07
60	2	60	1	151.63	153.92	0.99
<b>60</b>	<b>2</b>	<b>60</b>	<b>2</b>	<b>170.14</b>	<b>156.80</b>	<b>1.09</b>
60	2	60	3	171.13	159.68	1.07
60	4	60	1	218.57	226.42	0.97
60	4	60	2	244.94	231.27	1.06
60	4	60	3	250.08	236.14	1.06
60	6	60	1	275.78	297.91	0.93
60	6	60	2	307.72	305.31	1.01
60	6	60	3	321.11	312.73	1.03
<b>60</b>	<b>8</b>	<b>60</b>	<b>1</b>	<b>331.16</b>	<b>351.64</b>	<b>0.94</b>
60	8	60	2	365.70	361.90	1.01
60	8	60	3	392.65	372.20	1.05
80	2	60	1	202.18	205.23	0.99
80	2	60	2	226.86	209.07	1.09
80	2	60	3	228.18	212.91	1.07
80	4	60	1	291.42	301.89	0.97
80	4	60	2	326.59	308.36	1.06
80	4	60	3	333.43	314.85	1.06
<b>80</b>	<b>6</b>	<b>60</b>	<b>1</b>	<b>367.36</b>	<b>397.21</b>	<b>0.92</b>
80	6	60	2	410.29	407.08	1.01
80	6	60	3	428.15	416.98	1.03
80	8	60	1	441.55	468.85	0.94
80	8	60	2	487.60	482.53	1.01
80	8	60	3	523.54	496.27	1.05
100	2	60	1	252.72	256.54	0.99
<b>100</b>	<b>2</b>	<b>60</b>	<b>2</b>	<b>283.57</b>	<b>261.33</b>	<b>1.09</b>
100	2	60	3	285.22	266.13	1.07
100	4	60	1	364.28	377.36	0.97
100	4	60	2	408.23	385.45	1.06
100	4	60	3	416.79	393.56	1.06
100	6	60	1	459.63	496.51	0.93
100	6	60	2	512.86	508.85	1.01

100	6	60	3	535.19	521.22	1.03
<b>100</b>	<b>8</b>	<b>60</b>	<b>1</b>	<b>551.94</b>	<b>586.07</b>	<b>0.94</b>
100	8	60	2	609.50	603.16	1.01
100	8	60	3	654.42	620.34	1.05
120	2	60	1	303.27	307.85	0.99
120	2	60	2	340.29	313.60	1.09
120	2	60	3	342.27	319.36	1.07
120	4	60	1	437.14	452.83	0.97
120	4	60	2	489.88	462.54	1.06
120	4	60	3	500.15	472.27	1.06
<b>120</b>	<b>6</b>	<b>60</b>	<b>1</b>	<b>551.56</b>	<b>595.82</b>	<b>0.93</b>
120	6	60	2	615.44	610.62	1.01
120	6	60	3	642.23	625.47	1.03
120	8	60	1	662.32	703.28	0.94
120	8	60	2	731.40	723.79	1.01
120	8	60	3	785.31	744.40	1.05
60	2	80	1	157.01	151.90	1.03
<b>60</b>	<b>2</b>	<b>80</b>	<b>2</b>	<b>169.10</b>	<b>154.03</b>	<b>1.10</b>
60	2	80	3	169.70	156.17	1.09
60	4	80	1	216.50	221.25	0.98
60	4	80	2	242.81	224.82	1.08
60	4	80	3	245.72	228.40	1.08
60	6	80	1	269.50	288.05	0.94
60	6	80	2	301.83	293.43	1.03
60	6	80	3	309.63	298.83	1.04
60	8	80	1	318.40	336.13	0.95
60	8	80	2	355.28	343.50	1.03
60	8	80	3	370.98	350.90	1.06
80	2	80	1	200.74	202.53	0.99
<b>80</b>	<b>2</b>	<b>80</b>	<b>2</b>	<b>225.47</b>	<b>205.38</b>	<b>1.10</b>
80	2	80	3	226.26	208.23	1.09
80	4	80	1	288.66	295.00	0.98
80	4	80	2	323.74	299.76	1.08
80	4	80	3	327.63	304.53	1.08
80	6	80	1	359.33	384.07	0.94
80	6	80	2	404.75	391.24	1.03
80	6	80	3	412.85	398.44	1.04
80	8	80	1	424.53	448.18	0.95
80	8	80	2	473.71	458.00	1.03
80	8	80	3	494.64	467.87	1.06
100	2	80	1	250.92	253.16	0.99
<b>100</b>	<b>2</b>	<b>80</b>	<b>2</b>	<b>281.84</b>	<b>256.72</b>	<b>1.10</b>
100	2	80	3	282.83	260.29	1.09
100	4	80	1	360.83	368.75	0.98
100	4	80	2	404.68	374.70	1.08
100	4	80	3	409.54	380.66	1.08
100	6	80	1	449.16	480.08	0.94
100	6	80	2	503.05	489.06	1.03

100	6	80	3	516.06	498.05	1.04
100	8	80	1	530.66	560.22	0.95
100	8	80	2	592.14	572.51	1.03
100	8	80	3	618.30	584.83	1.06
120	2	80	1	301.11	303.79	0.99
<b>120</b>	<b>2</b>	<b>80</b>	<b>2</b>	<b>338.20</b>	<b>308.07</b>	<b>1.10</b>
120	2	80	3	339.39	312.34	1.09
120	4	80	1	432.99	442.50	0.98
120	4	80	2	485.61	449.64	1.08
120	4	80	3	489.60	456.80	1.07
120	6	80	1	538.99	576.10	0.94
120	6	80	2	603.66	586.87	1.03
120	6	80	3	619.27	597.66	1.04
120	8	80	1	636.79	672.26	0.95
120	8	80	2	710.57	687.01	1.03
<b>120</b>	<b>8</b>	<b>80</b>	<b>3</b>	<b>739.88</b>	<b>701.80</b>	<b>1.05</b>
					Mean	<b>1.00</b>
					Std dev.	<b>0.06</b>
					R	<b>0.98</b>
					MAPE	<b>0.06</b>

## CURRICULUM VITAE

### PERSONAL INFORMATION

Surname, Name: ATMACA, Nihat  
Nationality: Turkish (TC)  
Date and Place of Birth: 23 October 1971 , İstanbul  
Marital Status: Married  
Phone: 90 342 3171777  
Fax: 90 342 3601107  
email: atmaca@gantep.edu.tr

### EDUCATION

Degree	Institution	Year of Graduation
MS	ÇUKUROVA UNI.-Civil Engineering (Mechanic)	1999
BS	GAZİANTEP UNI.-Civil Engineering	1994
High School	Kayseri Fevzi Çakmak High School	1987

### WORK EXPERIENCE

Year	Place	Enrollment
1999- Present	GAZÜ- Gaziantep Vocational High School	Instructor
1995-1997	MKÜ- İskenderun Vocational High School	Instructor

### FOREIGN LANGUAGES

English

### PUBLICATIONS

1. Kutuk M.A., Atmaca N., Guzelbey İ.H., Explicit formulation of SIF using neural networks for opening mode of fracture, *Engineering Structures* (2007), doi:10.1016/j.engstruct.2006.11.008

2. Guzelbey I. H., Atmaca N. and Cevik A., (2006). Unified formulation of J-integral for common crack types using Genetic Programming, *Sakarya Üniversitesi Fen Bilimleri Enstitüsü Dergisi* (in press), 2006
3. Atmaca N., Guzelbey İ.H. and Kutuk M.A., The effect of mesh size, poisson's ratio and stress state on numerical  $K_I$  and  $K_{II}$  values, *Kahramanmaraş Sütçü İmam Üniversitesi Fen Bilimleri Enstitüsü Dergisi* (in press), 2007
4. Guzelbey I. H., Atmaca N. and Kanber B., (2004). Comparison of Displacement and Stress Extrapolation Techniques for Stress Intensity Factor, *CMES<sup>1</sup>-04, Proceedings of the First Cappadocia International Mechanical Engineering Symposium*, 14-16 July, Cappadocia, Turkey, 684-691
5. Guzelbey I. H., Atmaca N. ve Erklig A., (2003). Serbest Ucundan Tekil Yüke Maruz Bir Kirişin Elasto Plastik Çözümü, *Teorik ve Uygulamalı Mekanik Türk Milli Komitesi XIII. Ulusal Mekanik Kongresi*, 8-12 Eylül, Gaziantep, 891-895.